(2)

Tunable cw single-frequency source for injection seeding 2-μm lasers

Final Technical Report
Office of Naval Research Contract
N00014-88-K-0576
July 1, 1988 to December 31, 1988

Robert L. Byer
Principal Investigator

Ginzton Laboratory Report No. 4697
June, 1990

Edward L. Ginzton Laboratory
Stanford University
Stanford, California 94305-4085

Tunable CW single-frequency source for injection seeding 2-μm lasers

Robert L. Byer
Principal Investigator

Abstract

The objective of this program was development of stable, single-frequency, continuous-wave (CW) optical parametric oscillators (OPOs) for the application of injection seeding pulsed lasers. Progress has been made in the demonstration and performance characterization of doubly resonant optical parametric oscillators (DROs) operating near degeneracy pumped by 532-nm CW radiation obtained from second harmonic generation of diode-array-pumped Nd:YAG lasers. It was observed that the OPO reproduced the coherence of the pump radiation with little additional noise. A detailed analysis of the tuning and control properties of the DRO helpful for development of active stabilization techniques has been completed. Design considerations for a 2-μm DRO based on this analysis are presented. Stabilization of the DRO requires synchronized control of at least three parameters; temperature, pump frequency, and applied potential for electro-optic tuning are considered. Research on this topic is continuing motivated by a the exceptional coherence and tuning properties of the OPO and applications involving optical frequency synthesis that will extend far beyond injection seeding.

Table of Contents

Tunable CW single-frequency source for injection seeding 2-μm lasers

N00014-88-K-0576

Personnel Associated with the Program

Robert L. Byer — Principal Investigator

Robert C. Eckardt — Senior Research Associate

Eric Gustafson — Research Associate

William J. Kozlovsky — Ph.D., November 1988

Charles D. Nabors — Ph.D., December 1989

Alan Nilsson — Ph.D., August 1989

Timothy Day — Graduate student

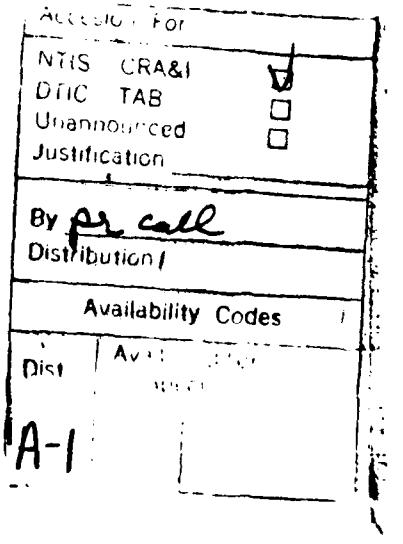

Tunable CW single-frequency source for injection seeding 2-μm lasers

I. Introduction

The objective of this program has been to develop stable, single-frequency optical parametric oscillators that can be used for injection seeding pulsed lasers to obtain reproducible single-mode operation. The Thulium and Holmium laser systems operating near 2.0 μm are of particular interest. There are a number of applications for single-frequency lasers at this wavelength including eye-safe transmitters for LIDAR and communications systems, and sources of pump radiation for nonlinear optical frequency conversion to other regions of the infrared spectrum. The research results of this program will allow the construction of optical parametric oscillators for the injection seeding application. More importantly, however, these results are leading toward the more general use of optical parametric oscillation as a precise and versatile technique for optical frequency synthesis.

Optical parametric oscillators have not been widely considered for the generation for injection seeding or injection locking radiation. Because of the complexity of their operation,[1] doubly resonant parametric oscillators (DROs) were often assumed to be so unstable and difficult to control that there use should be avoided. Singly resonant optical parametric oscillators (SROs) are much simpler, but they have much higher thresholds for oscillation and have only been operated in the pulsed mode. Even pumped with long

---

[1] R. G. Smith, "A study of factors affecting the performance of a continuously pumped doubly resonant optical parametric oscillator," IEEE J. Quantum Electron. **QE-9**, pp. 530-542, (May, 1973).

pulses, however, simple SROs typically operate with a multimode output.[2] If careful measures are taken in the operation of an SRO, it is possible to force single mode oscillation and allow continuous tuning[3,4] , but this quickly leads to very elaborate systems. The central conclusion presented here is that the DRO can be made to operate with single-mode output with reasonable active stabilization techniques. The double resonance condition provides additional frequency selectivity forcing single mode operation even in pulsed DROs.[5] We have extended the operation of the diode-laser-pumped monolithic DRO to continuous-wave (CW) operation and, in addition, find that the DRO essentially reproduces the coherence of the pump. Based on characterization of the pulsed and CW operation, the DRO theory is extended to allow analysis of techniques for continuous tuning and active stabilization.

The properties of the CW DRO are particularly well suited for injection seeding of pulsed lasers. The output of a DRO is widely tunable, and a single OPO could be used to injection seed a variety of laser systems. Ring geometry parametric oscillators have gain in only one direction, and for this reason offer high resistance to optical feedback. Recent advances in solid-state lasers combined with improvements in nonlinear optical materials

---

2 W. J. Kozlovsky, E. K. Gustafson, R. C. Eckardt and R. L Byer, "An efficient monolithic MgO:$LiNbO_3$ singly resonant optical parametric oscillator," *Opt. Lett.* **13**, pp. 1102-1104 (December 1988).

3 S. J. Brosnan and R. L. Byer, "Optical Parametric Oscillator Threshold and Linewidth Studies," IEEE J. Quantum Electron. **QE-15**, 415 (June 1979).

4 T. K. Minton, S. A. Reid, H. L. Kim and J. D. McDonald, "A scanning, single-mode, LiNbO3, optical parametric oscillator, Opt. Comm. **69**, pp. 289-293, (Jan. 1, 1989).

5 W. J. Kozlovsky, C. D. Nabors, R. C. Eckardt and R. L Byer, "Monolithic MgO:$LiNbO_3$ doubly resonant optical parametric oscillator pumped by a frequency-doubled diode-laser-pumped Nd:YAG laser," *Opt. Lett.* **14**, pp. 66-68 (Jan. 1, 1989).

now offer the opportunity of highly stable CW single-mode operation. We have investigated ring-geometry, $LiNbO_3$ OPOs pumped at a wavelength of 532 nm. The pump radiation was produced by semiconductor-diode-laser-pumped, nonplanar-ring-oscillator, Neodymium lasers operating at 1.064 μm. The laser output was converted to 532 nm by externally resonant second harmonic generation.[6] The two-step nonlinear optical process of harmonic generation followed by parametric oscillation was chosen because noncritical phase matching was possible in each stage with the result of relatively high overall efficiency at low power levels.

Research on optical parametric oscillators draws on a number of fields that are rapidly evolving. It is quite possible that new nonlinear optical materials will allow other schemes for parametric generation of specific wavelengths. Periodically poled nonlinear optical materials,[7,8] for example, could revolutionize many of the techniques of nonlinear optical frequency conversion. Quasi-phasematching[9] and tailored periodicity can provide noncritical phase matching for nonlinear optical processes at wavelengths where it is not possible with existing materials. The techniques of integrated optics can also be applied to

---

6 W. J. Kozlovsky, C. D. Nabors and R. L. Byer, "Efficient Second Harmonic Generation of a Diode-Laser-Pumped cw Nd:YAG Laser Using Monolithic MgO:$LiNbO_3$ External Resonant Cavities," IEEE J. Quantum Electron. **24**, 913 (June, 1988).

7 E. J. Lim, M. M. Fejer, and R. L. Byer, "Second harmonic generation of green light in periodically poled planar lithium niobate waveguide," *Electron. Lett.* **25**, pp. 174-175 (Feb. 2, 1989).

8 G. A. Magel, E. J. Lim, M. M. Fejer, and R. L. Byer, "Second harmonic generation in periodically-poled $LiNbO_3$," Optics News **15**, pp. 20-21, (Dec. 1989).

9 M. M. Fejer, G. A. Magel, and E. J. Lim, "Quasi-phase-matched interactions in lithium niobate," Proc. SPIE **1148** *Nonlinear Optical Properties of Materials*," pp. 213-224 (1989).

parametric oscillators.[10] It is possible in the future that the nonlinear optical use of single-domain, bulk, inorganic crystals may be limited to applications such as those involving high power or perhaps very high optical coherence. There is also rapid development in lasers which are used to generate the pump radiation. With the materials and lasers available now, monolithic DROs fabricated from $LiNbO_3$ and diode-laser-pumped Nd:YAG lasers are good choices for a CW 2-μm DRO, but better choices could become available. The basic theory and technology developed in this program, however, will be easily adapted to the new systems.

The detailed results of this program are presented in three appendices to this report. Two of these appendices are reprints of journal publications, and the third is a copy of a manuscript which has been submitted for publication. Appendix A describes the operation of the near-degeneracy DRO with output tunable between 1007 to 1129 nm.[11] Appendix B describes the characterization of the coherence properties of this DRO.[12] The work described in the second appendix was performed after the completion of this contract, and it was supported by a subsequent contract. The theoretical development[13] in Appendix C was performed over a period of time that spanned the performance period of both contracts. A discussion of these results is presented in the next section. The theory and

---

10 H. Suche and W. Sohler, "Integrated optical parametric oscillators," *Optoelectronic - Devices and Techniques* (Tokyo) **4**, pp.1-20, (June 1989).

11 C. D. Nabors, R. C. Eckardt, W. J. Kozlovsky, and R. L. Byer, "Efficient, Single-axial-mode operation of a monolithic optical parametric oscillator," Opt. Lett. **14**, pp. 1134-1136, (Oct. 15, 1989).

12 C. D. Nabors, S. T. Yang, T. Day, and R. L. Byer, "Coherence properties of a doubly resonant monolithic optical parametric oscillator," J. Opt. Soc. Am. B, **7**, pp. 815-820, (May 1990).

13 R. C. Eckardt, C. D. Nabors, W. J. Kozlovsky, and R. L. Byer, "Optical parameteric oscillator frequency tuning and control," submitted to *J. Opt. Soc. Am.* B.

analysis is applied to design considerations for a 2-μm DRO in section III. A summary and discussion of continuing research related to this program is given in the final section.

II. Research Progress

a. CW-pumped, near-degeneracy DRO

The DRO with which we demonstrated CW operation was similar in construction to the pulsed pumped DRO with which we worked earlier. The major difference was that the coatings of the CW DRO had higher reflectivity. Both monolithic DROs employed ring paths formed by reflections from two high-reflectivity multilayer-dielectric-coated surfaces near normal incidence and an uncoated total internal reflection surface at a grazing incidence. The coated reflecting surfaces had 10-mm radius of curvature, and the length of the MgO:$LiNbO_3$ resonators was 12.5 mm. The calculated beam waist for these cavities was $w_0 = 27$ μm. Temperature tuned noncritical phase matching was used. A variable potential was also applied to metal electrodes on crystal surfaces perpendicular for the crystalline b-axis to permit fine tuning of the cavity resonances and phase matching.

We had 30 mW of single-frequency 532-nm CW radiation available to pump the DROs. The experimentally observed threshold for the higher-finesse DRO was 12 mW. The lower-finesse DRO had a CW threshold of 35 mW which was later observed with a higher power laser that could generate up to 150 mW at the 532-nm second harmonic. Initially, however, it was possible to reach threshold of the lower-finesse DRO only by pulsing the diode-laser-pumped Nd:YAG laser.

The added frequency selection of the double resonance condition resulted in single-mode-pair oscillation for both the pulsed and CW DROs. Output frequency distributions

were measured with a 300-MHz-free-spectral-range scanning interferometer and a one-meter grating monochromator. The pulsed DRO was remarkable constant both temporally and spectrally from shot to shot at 320 kHz repetition rate, but did have a tendency to drift on longer time scales. Stable CW operation was attained for periods up to a couple of minutes. Initial attempts at dither-and-lock operation of the CW oscillator were only partially successful.

The CW DRO is capable of very high efficiency with optimization of parameters and displayed good efficiency even with the constraints of the initial observations. A pump depletion of 78% was achieved at twice threshold. At this level of deletion, 39% of the transmitted pump energy was contained in the DRO signal and idler outputs. This shows that there was approximately 0.37% round-trip internal power loss and 0.37% output coupling for the finesse $\mathcal{F} = 960$ DRO operating near degeneracy with 1035- and 1096-nm signal and idler outputs. Projections from earlier experiments had placed internal losses at 0.4%, and output coupling was specified to be 0.5% both in reasonable agreement with observation. It is customary in such experiments to first demonstrate the operation desired, and then to optimize performance. Increased pump power and adjusted output coupling and cavity geometry could increase overall conversion efficiency, but the efficiencies achieved are satisfactory.

Both the pulsed and CW DROs were used to characterize temperature and voltage tuning. Tuning on the broadest scale is centered around the temperature tuned phase-matching tuning curve. On a more detailed scale, tuning of the DRO consists of superimposed series of discontinuous wavelength changes of hops between adjacent axial modes. Each of these series of mode hops is centered on a cluster curve which intersects the phase-matching curve. The larger wavelength change between separate series of mode

hops is referred to as cluster jump and involves a change of typically a hundred or more axial modes. Cluster jumps are more numerous when cavity finesse is higher.

DRO tuning was observed by incrementally changing temperature and ramping applied potential. The full extent of tuning of the CW DRO was 1007 to 1129 nm limited by the high-reflectivity region of the dielectric coatings. The greatest wavelength extent of electric field tuning was plus or minus 19 nm centered on degeneracy. The extent of electric field tuning decreases with detuning from degeneracy. In preliminary servo control experiments, the DRO was able to follows tuning of the pump laser but only for 90 MHz. The mode spacing of the DRO cavity was 5.1 GHz, and the theoretical analysis described in section IIc and Appendix C shows that continuous tuning can extend through an extent greater than the mode spacing. The tuning measurements described above and the coherence measurements described in the next section provide the experimental basis for the theoretical modeling.

b. Coherence properties

The coherence properties of the DRO are remarkable and have recently been the subject of a number of investigations in quantum optics and squeezed state generation. A property that is important in the generation of radiation for injection seeding is that DROs have the capability to provide highly coherent output reproducing the statistical properties of the pump with very little additional noise. This has been shown theoretically by Graham and Haken [14] in a quantum mechanical analysis of the DRO, and it has been demonstrated in experimental measurements of the coherence properties of the DRO. The

---

14 R. Graham and H. Haken, "The Quantum-Fluctuations of the Optical Parametric Oscillator. I," Z. Phys. **210**, pp. 276-302, (1968).

quantum mechanical analysis showed that the diffusion of the sum of the signal and idler wave phases follow the phase diffusion of the pump wave adiabatically. Although the phase difference of the signal and idler may diffuse in an undamped manner, the statistical properties of a DRO are basically the same as those of an ideal laser. A result of these properties is the addition of only a small amount of phase noise in the output of the DRO above that present in the pump.

It has been confirmed that the DRO essentially reproduces the pump frequency stability in coherence measurements of the output of a cw DRO. [ref. 12 and Appendix B] For periods of approximately one minute, the free-running DRO which was not servo locked would oscillate on a single mode pair without a mode hop. Measurement of beating between the DRO output and an independent diode-laser-pumped solid-state laser during the periods between mode hops demonstrated the frequency stability. The beatnote linewidth was 13 kHz, which was the expected value for the typically 10-kHz linewidths of the pump laser and independent reference laser. The scanning interferometer measurements described earlier were limited to the instrument resolution of a few megahertz.

Additional coherence measurements showed that the signal and idler were phase-anticorrelated when referenced to the pump laser. Also, the width of the signal-idler beatnote with the DRO near but not at degeneracy was 500 Hz. The signal-idler beatnote indicates the frequency fluctuations added to the DRO output in addition to those present on the pump. The resolution of this beatnote measurement was approximately 300 Hz, indicating addition frequency jitter of a few 100 Hz in the individual DRO outputs. This is well below the 10 kHz short term frequency stability of the pump laser.

c. Tuning and control

The combined requirements of double resonance, conservation of energy, and phase matching result in complicated tuning behavior for the DRO. An analysis of tuning that considers temperature dependent dispersion, thermal expansion, and the electro-optical and piezoelectric effects is presented in detail in Appendix C and summarized here. Earlier analyses[15,1] are extended to provide a quantitative description of spectral hops between adjacent axial modes and the larger discontinuous frequency changes of cluster jumps in agreement with experimental observations.

Control of three parameters such as pump frequency, temperature, and applied electric field is required to attain optimum phase matching and frequency matching of the cavity resonances for DRO operation. If mode hops are prevented, the pump frequency change is divided between the DRO signal and idler Temperature change can be used to maintain phase matching and applied potential to maintain frequency matching through feedback techniques. DROs should find application for slowly tuned, incrementally tuned, and fixed frequency operation, whereas singly resonant optical parametric oscillators (SROs) have advantages for rapidly tuned and transient pulse operation.

With at least three partially independent control parameters, the operation of the DRO is becoming difficult to understand on an intuitive basis. The extended theory provides explanation useful for devising control techniques and provides information on tolerances required for stable operation. Considering the parameters individually, stable operation of the monolithic MgO:$LiNbO_3$ DRO described above requires pump frequency

---

15 J. A. Giordmaine and R. C. Miller, "Optical parametric oscillation in $LiNbO_3$," in *Physics of Quantum Electronics*, P. L. Kelley, B. Lax and P. E. Tannenwald, eds. (McGraw, New York, 1966), pp. 31-42.

be held constant within 5 or 10 MHz, applied potential to a volt or so, and temperature to approximately 0.001 °C. The pump frequency control could be realized with good temperature control of a monolithic solid-state laser. The voltage tolerance is also reasonable. Temperature control to a millidegree, particularly at a temperature near 270 °C would pose a problem. It would be better to consider temperature control and voltage control together. Applied potential could be used to maintain frequency matching of the cavity modes compensating for temperature drift outside of the fixed parameter operating range. The extent of voltage change required to maintain stable operation could then serve as an error signal for correcting temperature to reach the best phase matching. The tuning and control theory is applied to the 2-μm monolithic MgO:$LiNbO_3$ DRO in section IIIb. First some more basic questions of threshold are considered.

III. Design considerations for a 2-μm DRO

a. Threshold

The pump power threshold for parametric oscillation is an important parameter in design considerations. Obviously it is desirable to have threshold well below the available pump power. If pump power greatly exceeds threshold, conversion efficiency will be reduced by conversion of the signal and idler radiation back to the pump by the inverse parametric process. Threshold power and cavity parameters will also indicate if the proposed operation is within the power handling capability of the nonlinear optical material and other cavity components.

Threshold calculations are presented for monolithic $LiNbO_3$ DROs pumped at 532 nm. Operation near degeneracy with MgO:$LiNbO_3$ is considered for comparison with

demonstrated DROs, and thresholds are projected for operation with congruent $LiNbO_3$ at signal and idler outputs near 2.1 μm and 700 nm. These calculations are compared with other materials and SRO cavities. The threshold relationship used here is that given by Boyd and Kleinman[16] and considers focused Gaussian beams with diffraction and birefringent walkoff. The equation as used here is restated in MKS units.[17] This equation and definition of the parameters involved are given in Table I. Perfect phase matching and perfect frequency matching of the cavity modes is assumed.

In calculating thresholds for the near degeneracy MgO:$LiNbO_3$ DROs, a nonlinear coefficient of -4.7 pm/V is used. This value was obtained by phase-matched second harmonic generation[18] , and it it slightly smaller than the value for congruent lithium niobate obtained by the parametric fluorescence measurement technique.[19] The parametric fluorescence value is still used in calculations for congruent $LiNbO_3$. The calculated value for the finesse = 360 near-degeneracy DRO is 31 mW good agreement with the observed value of 35 mW. The calculated value for the finesse = 960 DRO is about one-third of the observed value. This difference could be due to errors in mode matching or transient effects which would occur as the high finesse DRO was scanned through resonances.

---

16 G. D. Boyd and D. A. Kleinman, "Parametric interaction of focused Gaussian light beams," J. Appl. Phys. **39**, pp. 3597-3639 (July 1968).

17 R. L. Byer, "Optical parametric oscillators," in *Quantum Electronics: A Treatise*, vol. 1, part B, H. Rabin and C. L. Tang, eds. (Academic, New York, 1975) pp. 588-702.

18 R. C. Eckardt, H. Masuda, Y. X. Fan, and R. L. Byer, "Absolute and relative nonlinear optical coefficients of KDP, KD*P, BaB_2O_4, $LiIO_3$, MgO:$LiNbO_3$, and KTP measured by phase-matched second harmonic generation," to be published, IEEE J. Quantum Electron. **26**, (May 1990).

19 M. M. Choy and R. L. Byer, "Accurate Second- Order Susceptibility Measurements of Visible and Infrared Nonlinear Crystals," Phys. Rev. B **14**, 1693 (15 Aug. 1976).

Table I. Equations for DRO and SRO threshold pump powers and description of terms.

$$P_{3,\mathrm{DRO}} = \frac{\pi\,\varepsilon_0\,c^4\,n_0^2\,\alpha_1\,\alpha_2}{2\,\omega_0^3 d^2\,(1-\gamma^2)^2\,l\,\overline{h_m}(B,\xi)}, \qquad P_{3,\mathrm{SRO}} \approx \frac{\pi\,\varepsilon_0\,c^4\,n_0^2\,\alpha_2}{\omega_0^3 d^2\,(1-\gamma^2)^2\,l\,\overline{h_m}(B,\xi)}$$

P_3 threshold pump power in Watts

$\varepsilon_0 = 8.85 \times 10^{-12}$ Coulomb^2 / Newton-m^2

$c = 3 \times 10^8$ m/sec

$n_0 = (n_1 + n_2)/2$ where n_1 and n_2 are the indices of refraction at the signal and idler wavelengths λ_1 and λ_2, and $1/\lambda_1 + 1/\lambda_2 = 1/\lambda_3$ where λ_3 is the pump wavelength.

$2\alpha_1$ = cavity round trip power loss at λ_1.

$2\alpha_2$ = cavity round trip power loss at λ_2.

$\omega_0 = (\omega_1 + \omega_2)/2$, average angular frequency in radians per sec. $\omega_1 = 2\pi c/\lambda_1$ and $\omega_2 = 2\pi c/\lambda_2$

d, nonlinear optical coefficient

$\gamma = (\omega_1 - \omega_2)/(\omega_1 + \omega_2)$, a factor that determines increase in threshold when tuned away from degeneracy.

l crystal length in meters

B double refraction parameter, $B = 0$ for 90° phasematching. In other cases $B = \rho\,(l\,\omega_0 n_0/c)^{1/2}/2$, where ρ is the birefringent walkoff angle.

$\xi = l/b_0$, ξ is the focusing parameter and b_0 is the confocal parameter given by $b_0 = (2Rl - l^2)^{1/2}$ where R is the radii of curvature of the two OPO cavity mirrors.

$\overline{h_m}(B,\xi)$ OPO gain reduction factor (see reference 10 or 13 for a complete explanation.) For $B = 0$ there is a broad maximum of $h_m = 1.068$ at $\xi = 2.84$. In the case which is described here $l = 0.0125$ m, $\xi = 1.29$ and $\overline{h_m} = 0.89$. A second example which is used for comparison of some angle tuned crystals is $\overline{h_m}(B=4,\xi=0.1) \approx 0.04$.

Table II. Temperature-tuned, noncritically-phase-matched OPO thresholds, l = 1.25 cm, B = 0, ξ = 1.29

Material	$MgO:LiNbO_3$		congruent $LiNbO_3$	
oscillator	DRO	DRO	DRO	SRO
T_{PM}	107°C		263°C	
Finesse	$\mathcal{F}$ = 960	$\mathcal{F}$ = 360	$\mathcal{F}$ = 500	$\mathcal{F}_2$ = 500
λ_1	1064 nm		2128 nm	
λ_2			709 nm	
λ_3	532 nm			
n_1	2.232		2.194	
n_2			2.272	
n_3			2.253	
d_{eff}	4.7 pm/V		5.6 pm/V	
$P_{Th,calc}$	4.4 mW	31 mW	20 mW	6.4 W
$P_{Th,obs}$	12 mW	35 mW	—	—

Table III. Thresholds for some angle-tuned DROs, $\mathcal{F}$ = 500, B = 4, ξ = 0.1.

Material	congruent $LiNbO_3$	KTP	$KNbO_3$
Phase matching	Type-I	Type-II	Type-I
θ_{PM}	45.4°	53.9°	39.8°
ϕ	30°	0°	90°
ρ	1.98°	-2.74°	3.58°
λ_1	2128 nm		2128 nm
λ_2			709 nm
λ_3	1064 nm		532 nm
n_1	2.193	1.772	2.198
n_2		1.722	
n_3		1.747	
l	0.83 cm	0.54 cm	0.20 cm
d_{eff}	5.1 pm/V	2.7 pm/V	5.2 pm/V
$P_{Th,calc}$	3.6 W	13 W	2.9 W

A finesse of 500 is assumed for the 2-μm DRO. Congruent $LiNbO_3$ is used in the calculation because it phase matches at a temperature about 100 °C lower than $MgO:LiNbO_3$. The calculated threshold for the 532-nm-pumped, 2-μm DRO is 20 mW. This level of pump radiation is easily produced by externally resonant second harmonic generation of diode-laser-pumped Nd:YAG lasers. The threshold for a 532-nm-pumped, 2-μm SRO is more than two orders of magnitude larger. Some of the details of these calculations are given in Table II. For comparison, the results of threshold calculations for three angle tuned DROs are given in Table III. Birefringent walkoff greatly increases these thresholds, which are also a couple of orders of magnitude higher than the threshold for the noncritically-phase-matched DRO. Two noncritically-phase-matched steps of nonlinear optical frequency conversion, second harmonic generation followed by parametric oscillation, are easily achieved using existing diode-pumped solid-state lasers as sources of pump radiation.

b. Tuning and control projections

The DRO tuning and control theory described in Appendix C is applied to the 532-nm-pumped, 2-μm DRO in this section. The same monolithic ring geometry is assumed as used for the near-degeneracy DROs. The nonlinear optical material is congruent $LiNbO_3$ which will phase match at about 263°C. The phase-matching tuning curve is shown in Fig. 1a. The temperature range is restricted to above 180°C and below 300°C. Operating above the lower limit avoids any problem with photorefractive changes in the material when pumped with intense green light. The higher limit is chosen to avoid thermal damage to the dielectric coatings. The multilayer SiO_2-TiO_2 coatings are applied at 275°C; the upper temperature limit for their use is unknown, but 300°C should be safe.

Test coatings on a congruent $LiNbO_3$ wafer had minimum transmission of 0.14% at 2090 nm and 712 nm. The coating, which is a quarter wave stack at 2.1 μm, is a three-

quarter wave stack at 0.7 μm where it also has high reflectivity. Transmission was less than 0.5% (indicating greater than 99.5% reflectivity) from 1980 - 2090 nm and from 695 - 729 nm. Coating reflectivity is expected to limit the tuning range.

The phase-matching requirement and the conservation of energy condition that signal and idler frequencies sum to the pump frequency specify the phase-matching curve. In addition the DRO must have the signal and idler resonances coincide in satisfying the conservation of energy condition. The result of this additional constraint is seen in high-resolution examination of DRO tuning which shows the output occurring near one of the three cluster curves closest to phase matching. Calculated cluster curves for temperature tuning at constant applied potential are shown in Fig. 1b, and for electric-field tuning at constant temperature are shown in Fig. 2a . The cluster curves are displayed with the phase-matching curve and the gain-bandwidth limit in these figures.

Examining the tuning along an individual cluster curve in even greater detail will show the DRO output occurring in a series of mode hops. Dispersion becomes significantly larger for signal and idler when the DRO is tuned far from degeneracy as is the case for a 532-nm-pumped OPO with outputs at 709 and 2128 nm. The result will be that the cavity resonance widths will limit tuning to a smaller range than the tuning range between mode hops. The widths of the cavity resonances are related to the cavity finesse. A finesse of 500 is again assumed for these calculations. This finesse also corresponds to a round trip power loss of 1.13%, well within what is possible with the reflectivity of the test coating. A detailed calculation of electric field tuning along a cluster curve at constant temperature and constant pump frequency is shown in Fig. 2b. Three calculations of single parameter tuning for electric field, temperature, and pump frequency are shown in Figs. 3a, b, and c.

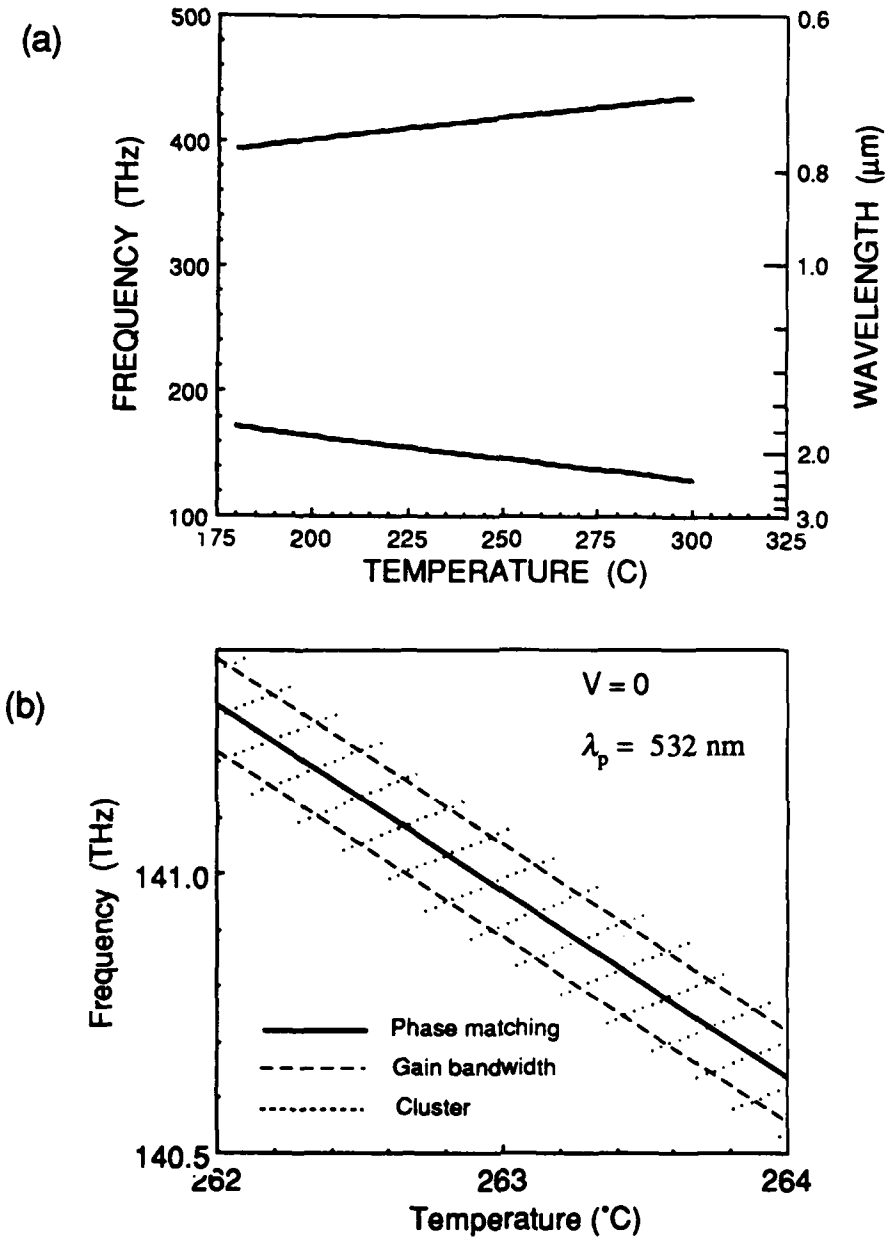

Fig. 1. (a) Phase-matching curve for a temperature-tuned congruent $LiNbO_3$ OPO pumped at 532 nm. (b) A more detailed calculation on an expanded scale shows the cluster curves and gain-bandwidth limits it addition to the phase-matching curve. DRO output follows the cluster curves but is restricted to the regions near phase matching.

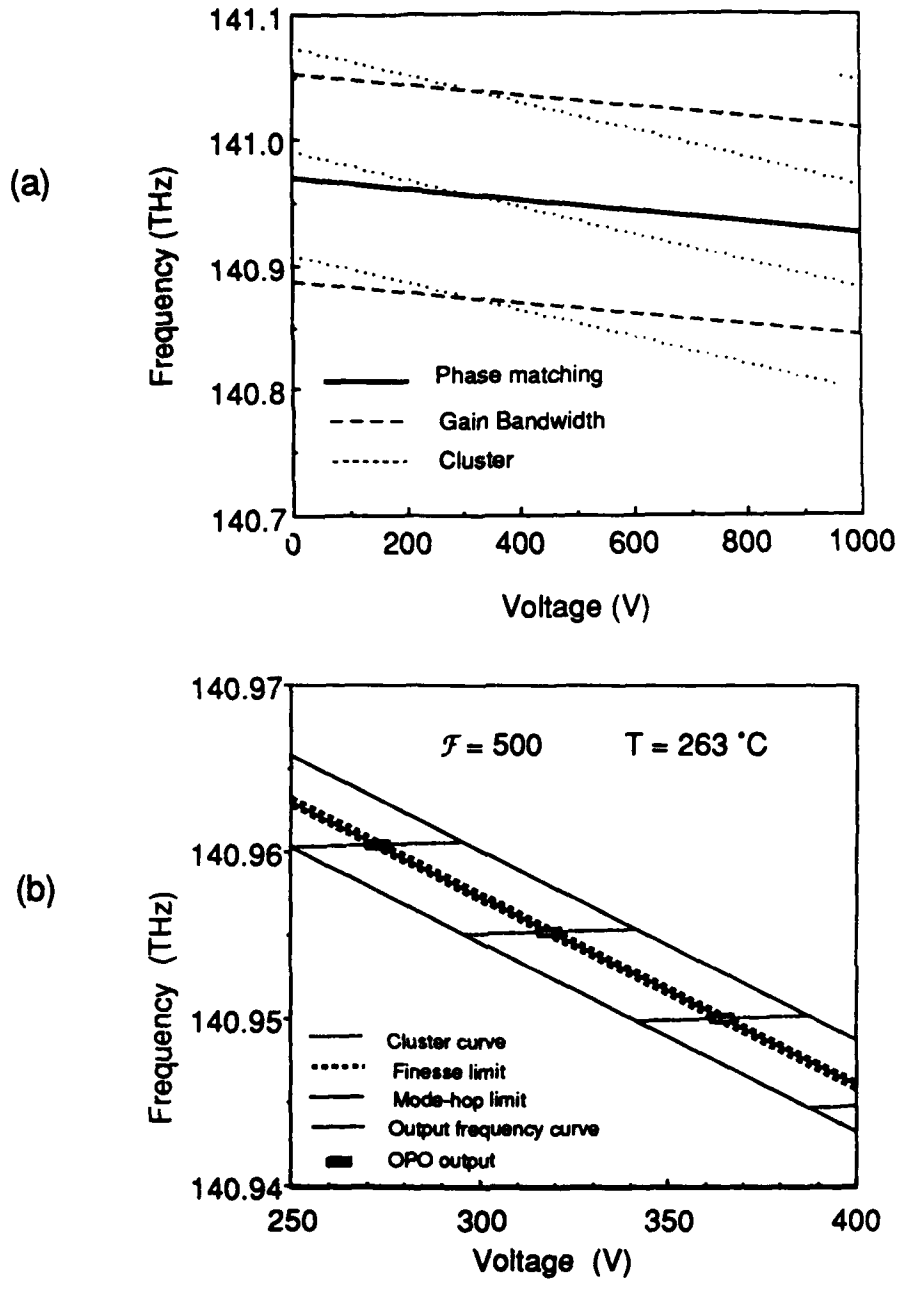

Fig. 2. (a) The cluster curves are also dependent on electric field tuning. An even more detailed examination of tuning along a cluster curve will show the DRO tuning in mode hops (b). The DRO cavity finesse may limit output to only a fraction of the spacing between mode hops.

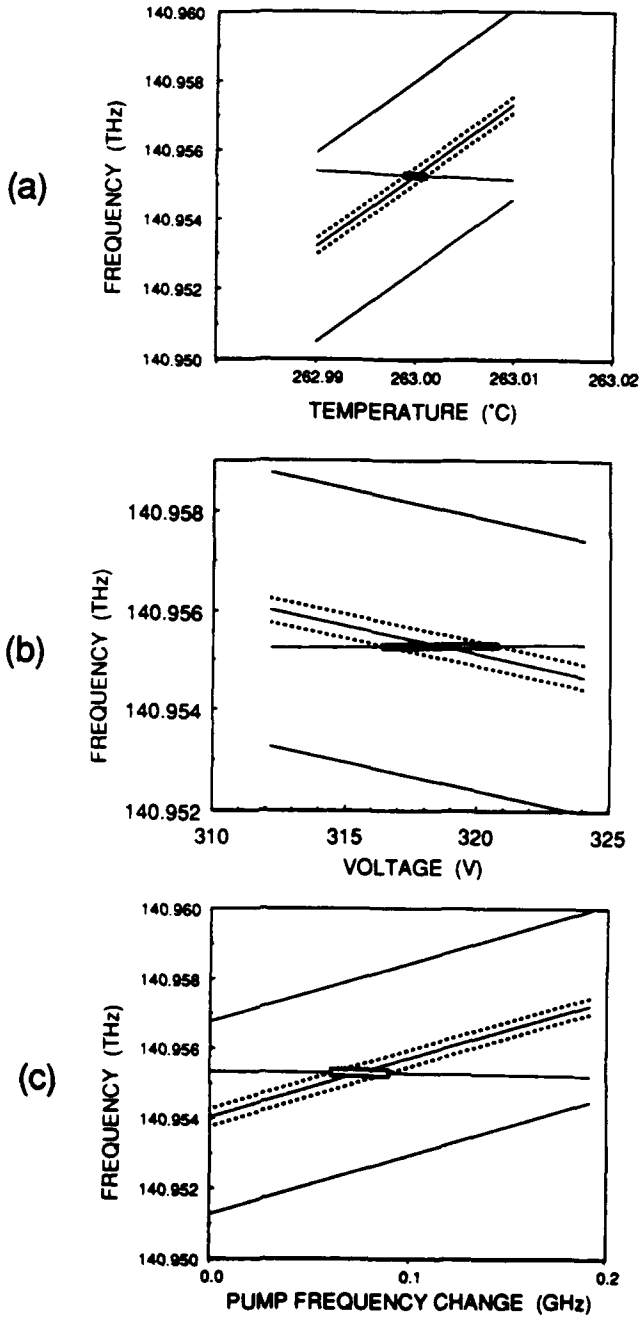

Fig. 3. Tuning calculations displayed on a further expanded scale show the tolerances required of a single tuning parameter when the other parameters are held constant. These calculations are centered on $\lambda p = 532$ nm, $T = 263$ °C, and $V = 318.7$ V. Applied potential is varied while pump frequency and temperature are held constant in (a). Temperature is varied in (b), and pump frequency is varied in (c).

Parameter tolerances are similar to those for the near-degeneracy DRO. Changes in the pump frequency will be nearly equally divided between signal and idler until a mode hop occurs. At any given temperature within the broad phase-matching range, stable operation will require applied potential be held within approximately one volt. Temperature can be adjusted to reach optimum phase matching, provided voltage adjustment can follow to maintain frequency matching of the cavity modes. Voltage dither-and-lock techniques should be well suited for this application. It will be required that the dither frequency be greater than the cutoff frequency for thermal effects in the monolithic resonator. The tuning and control requirements of this 2–μm DRO are within the capabilities of existing technology.

c. Issues to be resolved

We are now to the stage of having components prepared to attempt 2-μm DRO operation in a standing wave cavity. This will provide the first experimental measurement of threshold and will demonstrate that the high-reflection coatings can stand up to the thermal cycle. After this demonstration, the standing wave resonators will be fabricated into ring geometry and electrodes will be applied for electric field tuning.

Several problems became apparent in the course of the pulsed and CW DRO experiments. The MgO:$LiNbO_3$ exhibited a lifetime of approximately 100 hours of use in resonant cavity second harmonic generation and parametric oscillation. Congruent $LiNbO_3$ has performed well at high temperatures with good damage resistant properties. There is reason to expect that this material will also perform well for a 2-μm OPO pumped at 532 nm. We are investigating the use of other nonlinear optical material to achieve stable, high-power second harmonic generation. In preliminary results, 1 watt CW power at 532 nm has been achieved using barium metaborate. Other materials including KTP, $LiIO_3$, LiB_3O_5, and $KNbO_3$ are also being considered for harmonic generation. We are

also continuing to work with $MgO:LiNbO_3$ searching for conditions in which the long term damage can be avoided.

Another problem is related to heating in the nonlinear material. There is some optical absorption in any material. The 0.37% internal loss per round trip transit that we observed in the CW DRO is caused by scattering and absorption in the bulk material and on the surfaces. The portion that is due to absorption will cause heating of the crystal and instability in the operation of a monolithic DRO. The observation that stable operation could be achieved for a minute at a time with no feedback control indicated that this problem is manageable in $MgO:LiNbO_3$. However, the difference in tuning from two directions indicates the presence of an absorption problem. Tuning from one direction seems to be self stabilizing. As the resonance is approached, the oscillation builds up causing heating in the crystal having the effect of preventing the resonance from being approached more closely. Tuning from the other direction, however, the heating quickly draws the oscillation into and through the resonance. We have assembled a laser calorimeter capable of measuring small levels of absorption. We plan to evaluate nonlinear materials for bulk and surface absorption.

III. Summary

The demonstration of a 2-μm OPO with stable, single-frequency, CW output suitable for use in injection seeding pulsed Holmium or Thulium lasers or injection locking CW lasers continues to be an active research project. We have made a number of advances toward this goal, and have shown that this technique remains viable. In the course of this investigation, more general use of optical parametric oscillation as a precise and versatile technique for optical frequency synthesis have become apparent.

It was show that both pulsed and CW DROs routinely produce single axial mode signal and single axial mode idler radiation. The additional constraint of the double resonance condition provides the frequency selectivity that makes this possible, but also results in a complex tuning behavior. We have extended DRO tuning and control theory to more fully describe the tuning behavior. This theory extension was based on the experimental observations made with the monolithic DROs operating near degeneracy. The tuning of the DRO is complicated enough that this theoretical description should be useful in attaining stable, single-frequency, continuously tuned, and incrementally tuned operation of the DRO.

Measurements of the coherence properties of the DRO demonstrate the ability to reproduce the frequency stability of the pump radiation in the output of the DRO. The diode-laser-pumped solid-state lasers used to generate pump radiation are inherently stable source which produce frequency stability in the 10 kHz range over fractional-second periods and a few MHz long term stability. Sub-hertz relative stability has be achieved by locking to reference cavities, and absolute frequency stability of a few hundred hertz by locking to molecular absorptions now appears possible. The doubly resonant optical parametric oscillator has the potential to convert the frequency stability to arbitrary frequencies extending over broad tuning ranges. This optical frequency synthesis capability will be a valuable tool in spectroscopy, remote sensing, metrology, communications, and optical signal processing.

IV. List of Byer Group publications and presentations since July 1, 1988

PUBLICATIONS

1. F. M. Schellenberg, R. L. Byer, J. Zavislan and R. D. Miller, "Nonlinear polysilane thin films," Reserearch Report RJ 6466 (62939), (IBM Almaden Research Center, San Jose, Sept. 30, 1988).

2. M. K. Reed and R. L. Byer, "Performance of a Conduction Cooled Nd:Glass Zig-Zag-Slab Laser," Proc. SPIE **1021**, *High Power Solid-State Lasers*, pp. 128-35 (Sept. 1988).

3. Y. X. Fan, R. C. Eckardt, R. L. Byer, J. Nolting and R. Wallenstein, "Visible BaB_2O_4 optical parametric oscillator pumped at 355 nm by a single-axial-mode pulsed source," *Appl. Phys. Lett.* **53**, pp. 2014-2016 (21 Nov. 1988).

4. William J. Kozlovsky, "Efficient Nonlinear Conversion of Frequency-Stable Lasers," Ph.D. dissertation, Stanford University (Nov. 1988); Ginzton Laboratory Report No. 4445 (Stanford University, Stanford, CA, Nov. 1988).

5. Y. X. Fan, R. C. Eckardt, R. L. Byer, J. Nolting and R. Wallenstein, "A violet to mid-infrared barium borate optical parametric oscillator," *Optics News* **14**, pp. 19-20 (Dec. 1988).

6. W. J. Kozlovsky, C. D. Nabors and R. L. Byer, "High efficiency second harmonic generation of a cw frequency stable laser," *Optics News* **14**, pp. 20-21 (Dec. 1988).

7. W. J. Kozlovsky, E. K. Gustafson, R. C. Eckardt and R. L Byer, "An efficient monolithic MgO:$LiNbO_3$ singly resonant optical parametric oscillator," *Opt. Lett.* **13**, pp. 1102-1104 (December 1988).

8. Gregory W. Faris and Robert L. Byer, "Three-Dimensional Beam-Deflection Optical Tomography of a Supersonic Jet," *App. Opt.* **27**, 5202 (Dec. 15, 1988).

9. G. Huber, P. Mitzscherlich, T. Y. Fan and R. L. Byer, "Energy Transfer and Inversion Saturation in Tm,Ho:YAG," *J. Luminescence* **40, 41**, pp. 509-510, (1988)

10. J. A. Trail, R. L. Byer and J. B. Kortright, "The Stanford Tabletop Scanning X-ray Microscope," in *X-Ray Microscopy II*, ed. by D. Sayre, M. Howells, J. Kinz and H. Rarback (Springer-Verlag, Berlin 1988), pp. 310-315.

11. J. A. Trail and R. L. Byer, "First images from the Stanford tabletop scanning soft X-ray microscope," *OSA Proceedings on Short Wavelength Coherent Radiation: Generation and Applications, Vol. 2*, R. W. Falcone and J. Kirz, eds. (Optical Society of America, Washington, D.C., 1988), pp. 290-294.

12. W. J. Kozlovsky, C. D. Nabors, R. C. Eckardt and R. L Byer, "Monolithic MgO:$LiNbO_3$ doubly resonant optical parametric oscillator pumped by a frequency-doubled diode-laser-pumped Nd:YAG laser," *Opt. Lett.* **14**, pp. 66-68 (Jan. 1, 1989).

13. E. J. Lim, M. M. Fejer, and R. L. Byer, "Second harmonic generation of green light in periodically poled planar lithium niobate waveguide," *Electron. Lett.* **25**, pp. 174-175 (Feb. 2, 1989).

14. M. M. Fejer, S. J. B. Yoo, R. L. Byer, Alex Harwit, and J. S. Harris, Jr., "Observation of Extremely Large Quadratic Susceptibility at 9.6 - 10.8 μm in Electric-Field-Biased AlGaAs Quantum Wells," *Phys. Rev. Lett.* **62**, pp. 1041-1042 (Feb. 27, 1989).

15. R. L. Byer, "Nonlinear Frequency Conversion Enhances Diode Pumped Lasers," *Laser Focus World* **25**, pp. 77-86 (March 1989).

16. A. Nilsson, E. Gustafson, and R. L. Byer, "Eigenpolarization theory of monolithic nonplanar ring oscillators," *IEEE J. Quantum Electron.* **25**, pp. 767-790, (April 1989).

17. E. J. Lim, M. M. Fejer, R. L. Byer, and W. J. Kozlovsky, "Blue light generation by frequency doubling in periodically poled lithium niobate channel waveguide," *Electron. Lett.* **25**, pp. 731-732 (May 25, 1989).

18. R. A. Lacy, A. C. Nilsson, R. L. Byer, W. T. Silfast, O. R. Wood II and S. Svanberg, "Photoionization-pumped gain at 185 nm in a laser-ablated indium plasma," *J. Opt. Soc. Am. B* **6**, pp. 1209-1216 (June 1989).

19. J. A. Trail and R. L. Byer, "Compact scanning soft-x-ray microscope using a laser-produced plasma source and normal-incidence multilayer mirrors," *Opt. Lett.* **14**, pp. 539-541, (June 1, 1989).

20. Y. X. Fan, R. C. Eckardt, R. L. Byer, Chuangtian Chen and A. D. Jiang, "Barium Borate Optical Parametric Oscillator," *IEEE J. Quantum Electron.*, **25**, pp. 1196-1199 (June 1989).

21. A. C. Nilsson,, T. Day, A. D. Farinas, E. K. Gustafson and R. L. Byer, "Narrow linewidth operation of diode-pumped nonplanar ring oscillators," in *Frequency Standards and Metrology*, A. DeMarchi, ed. (Springer Verlag, Berlin, 1989), pp. 225-230.

22. T. Day, A. C. Nilsson, M. M. Fejer, A. D. Farinas, E. K. Gustafson, C. D. Nabors and R. L. Byer, "30-Hz-linewidth, diode-laser-pumped, Nd:GGG nonplanar ring oscillators by active frequency stabilization," *Electron. Lett.* **25**, pp. 810-812 (June 22, 1989).

23. R. L. Byer, "From klystrons to lasers," *Optoelctronics - Devices and Technology* **4**, (Tokyo), pp. 106-108, (June 1989).

24. D. H. Jundt, M. M. Fejer and R. L. Byer, "Growth and optical properties of single-crystal sapphire fibedrs," Proc. SPIE **1048**, pp. 39-43 (Aug. 1989).

25. Alan C. Nilsson, "Eigenpolarization Theory and Experimental Linewidth Study of Monolithic Nonplanar Ring Oscillators" Ph.D. dissertation, Stanford University (Aug. 1989); Ginzton Laboratory Report No. 4552 (Stanford University, Stanford, CA, Aug. 1989).

26. C. D. Nabors, R. C. Eckardt, W. J. Kozlovsky, and R. L. Byer, "Efficient, single-axial-mode operation of a monolithic MgO:$LiNbO_3$ optical parametric oscillator," *Opt. Lett.* **14**, pp. 1134-1136 (Oct. 15, 1989).

27. C. D. Nabors, A. D. Farinas, T. Day, E. K. Gustafson, and R. L. Byer, "Injection locking of a 13-watt cw Nd:YAG ring laser," *Opt. Lett.* **14**, pp. 1189-91 (Nov. 1 1989).

28. D. H. Jundt, M. M. Fejer, and R. L. Byer, "Characterization of single-crystal sapphire fibers for optical power delivery systems," *Appl. Phys. Lett.* **55**, pp. 2170–2172 (Nov. 20, 1989).

29. R.L. Byer, "Ultra narrow linewidth solid state oscillators," in *Laser Spectroscopy IX: Proceedings of the NICOLS Conference*, Michael Feld, John E. Thomas, and Aram Mooradian, eds. (Academic, 1989), pp. 228-231.

30. M. M. Fejer, G. A. Magel, and E. J. Lim, "Quasi-phase-matched interactions in lithium niobate," Proc. SPIE **1148**, pp. 213-224, (1989).

31. G. A. Magel, E. J. Lim, M. M. Fejer, and R. L. Byer, "Second harmonic generation in periodically-poled $LiNbO_3$," Optics News **15**, pp. 20-21, (Dec. 1989).

32 Charles David Nabors, "Coherence and Two-Color Squeezing in Doubly Resonant Optical Paramentic Oscillators" Ph.D. dissertation, Stanford University (Dec. 1989); Ginzton Laboratory Report No. 4619 (Stanford University, Stanford, CA, Dec. 1989).

33. M. M. Fejer, G. A. Magel, and E. J. Lim, "Quasi-phase-matched interactions in lithium niobate," Proc. SPIE **1148** *Nonlinear Optical Properties of Materials*," pp. 213-224 (1989).

34. G., A. Magel, M. M. Fejer, and R. L. Byer, "Quaisi-phase-matched second-harmonic generation of blue light in periodically poled $LiNbO_3$," *Appl. Phys. Lett.* **56**, pp. 108-110 (Jan. 8, 1990).

35. S. Basu and R. L. Byer, "Short pulse injection seeding og Q-switched Nd:glass laser oscillators - theory and experi-ment," IEEE J. Quantum Electron. **26**, pp. 149-157, (Jan, 1990).

36. D. H. Jundt, M. M. Fejer, and R. L. Byer, "Optical properties of lithium-rich lithium niobate fabricated by vapor transport equilibration," *IEEE J. Quantum Electron.* **26**, pp. 135-138, (Jan. 1990).

37. T. Day, E. K. Gustafson and R. L. Byer, "Active frequency stabilization of a 1.062-μm, Nd:GGG, diode-laser-pumped nonplanr ring oscillator to less than 3 Hz of relative linewidth," *Opt. Lett.* **15**, pp. 221-223 (Feb. 15, 1990).

38. F. M. Schellenberg, R. L. Byer, and R. D. Miller, "Fabrication of birefringent gratings using nonlinear polysilane thin films," *Opt. Lett.* **15**, pp. 242-244 (Feb. 15, 1990).

39. M. S. Pronko, R. H. Lehmberg, S. Obenschain, C. J. Pawley, C. K. Manka, and R. Eckardt, "Efficient second harmonic conversion of broadband high-peak-p;ower Nd:Glass laser radiation using large-apertue DKP crystals in quadrature," *IEEE J. Quantum Electron.* **26**, pp. 337-347 (Feb. 1990).

40. T. Day, A. D. Farinas, and R. L. Byer "Demonstration of a low bandwidth 1.06 μm optical phase-locked loop for coherent homodyne communication," IEEE Photonics Tech. Lett. **2**, pp. 294-296, (April 1990).

41. S. Basu, R. L. Byer, and J. R. Unternahrer, "Slab lasers move to increase power," *Laser Focus World* **26**, pp. 131-141 (April 1990).

42. F. M. Schellenberg and R. L. Byer, "Two-photon-induced birefringence in polysilanes," *Chem. Phys. Lett.*, **166**, pp. 331-339, (March 2, 1990).

43. H. M. Hertz and R. L. Byer, "Tomographic imaging of micrometer-sized optical and x-ray beams," *Opt. Lett.* **15**, 396-398, (April 1, 1990).

44. S. Basu and R. L. Byer, "Average power limits of diode-laser-pumped solid state lasers," *Appl. Optics.* **20**, pp. 1765-1771, (April 20, 1990).

45. S. Sudo, I. Yokohama, A. Cordova-Plaza, M. M. Fejer, and R. L. Byer, "Uniform refractive index cladding for $LiNbO_3$ single-crystal fibers," Appl. Phys. Lett. **56**, pp. 1931-1933, (May 14, 1990).

46. C. D. Nabors, S. T. Yang, T. Day, and R.L Byer, "Coherence properties of a doubly-resonant monolithic optical parametric oscillator," J. of Opt. Soc. of Am. B **7**, pp. 815-820, (May 1990).

47. D. H. Jundt, M. M. Fejer, and R. L. Byer, "Growth of optical Quality sapphire single crystal fibers," Mat. Res. Soc. Symp. Proc. **172**, pp. 273-277, (1990).

SUBMITTED FOR PUBLICATION

C. D. Nabors and R. L. Byer, "Monolithic Optical Parametric Oscillators for Quantum Optics," to be published in *Coherence and Quantum Optics 6*, (Plenum, New York).

M. K. Reed and R. L. Byer, "The output beam quality of a Q-switched Nd:glass slab laser," submitted to IEEE J. Quantum Electron.

M. K. Reed and R. L. Byer, "Mode-locked operation of a Nd:YLF laser and amplification in a Q-switched Nd:glass slab laser," submitted to IEEE J. Quantum Electron.

T. Day, E. K. Gustafson, and R. L. Byer, "Active frequency stabilization of monolithic, diode laser pumped, solid state lasers," to be published in Proc. International Conf. Lasers '89, p. 3502, (1990).

C. D. Nabors and R. M. Shelby, "Two-Color Squeezing and Sub-Shot-Noise Signal Recovery in Doubly Resonant Optical Parametric Oscillators," submitted to Phys. Rev. Lett.

T. Day, E. K. Gustafson, and R. L. Byer, "Acitve frequency stabilization of diode laser pumped, non-planar ring oscillators," paper 1223-22, to be published in Proc. SPIE **1223**.

R. C. Eckardt, H. Masuda, Y. X. Fan, and R. L. Byer, "Absolute and relative nonlinear optical coefficients of KDP, KD*P, BaB_2O_4, $LiIO_3$, $MgO:LiNbO_3$, and KTP measured by phase-matched second harmonic generation," to be published, IEEE J. Quantum Electron. **26**, (May 1990).

R. C. Eckardt, C. D. Nabors, W. J. Kozlovsky, and R. L. Byer, "Optical parameteric oscillator frequency tuning and control," submitted to *J. Opt. Soc. Am.* B,

INVITED PRESENTATIONS

1. F. M. Schellenberg R. L. Byer, J. Zavislan, R. D. Miller, "Nonlinear Polysilane Thin Films", presented at Symposium on Nonlinear Optics of Organics and Semiconductors, Univ. of Tokyo, Japan, July 1988;

2. F. M. Schellenberg, R. L. Byer, J. Zavislan, R.D. Miller, and R. Sooriyakumaran, "Two-Photon Induced effects in Nonlinear Polysilane Thin Films", presented at: SONY Corp, Electro-Optics Lab, Shinagawa, Tokyo, Japan, July, 1988; Nishihara Research group, Osaka University, Osaka, Japan, Aug. 1988; Stegeman research group, U. of Arizona, Tucson, AZ, Aug, 1988.

3. R. L. Byer, "Efficient Nonlinear Conversion of Diode Pumped Solid State Lasers," XIII International Conference on Coherent and Nonlinear Optics, Minisk, USSR, Sept., 1988.

4. C. D. Nabors and R. L. Byer, "Diode-pumped Crystal Lasers and Frequency Extension by Nonlinear Optics," presented at the Adriatico Research Conference on: Coherent Sources for Frontier Spectroscopy, Trieste, Italy, August 30, 1988.

5. A. Nilsson E. Gustafson and R. L. Byer, "Frequency Stable Diode Pumped Solid State Lasers," Fourth Symposium on Frequency Standards and Metrology, Ancona, Italy, Sept. 1988.

6. R. L. Byer, "Renaissance of Solid State Lasers and Parametric Oscillators," given at Vilnius University, Lithuania, September, 1988.

7. R. L. Byer, "High Power Solid State Lasers", given at The Technical University of Berlin, September, 1988.

8. R. L. Byer, "Solid-State Lasers," plenary paper, 1988 Annual Meeting, IEEE Lasers and Electro-Optics Society, Santa Clara, CA, Nov. 1988.

9. R.L. Byer, "Tunable Solid State Lasers," presented at ILS-IV, Atlanta, Ga., Oct., 1988.

10. R. L. Byer, "Credible and Incredible Solid State Lasers," presented at the 1989 Annual Conference of the Western Spectroscopy Association, Asilomar, CA, January, 1989.

11. R. L. Byer, "Solid State Lasers for Accelerator Applications," presented at the Conference on Advanced Accelerator Concepts, Lake Arrowhead, California, January 1989.

12. R. L. Byer, "The Fragility of Research," presented to the Office ofo Planning & Management, Stanford University, February, 1989.

13. R. L. Byer, "The Centennial of Coherent Radiation: from Radios to Lasers," presented at Stanford Alumni Association (Stanford Club of Connecticut), April, 1989.

14. R. L. Byer, "Efficient nonlinear conversion of diode pumped solid state lasers," presented at CLEO Conference, Baltimore, MD, April, 1989.

15. R. L. Byer, "Diode pumped solid state lasers," paper ThJJ3, presented at QELS Conference, Baltimore, MD, April, 1989.

16. R. L. Byer, "Solid state lasers: the next ten years," presented at the Sunrise Club, Stanford University, May 1989.

17. R. L. Byer, "Solid State Lasers for Gravitational Wave Interferometry," given at the 12th International Conference on General Relativity and Gravitation, Univ. of Colorado, Boulder, Colorado, July, 1989.

18. R. L. Byer, "Efficient Nonlinear Conversion of Diode Pumped Lasers," given at The Gordon Conference, New Hampshire, July 1989.

19. R. L. Byer, "Solid State Lasers: The Next Ten Years," OLLRC Topical Workshop, Toronto, Canada, September, 1989.

20. R. L. Byer, "Hertz Linewidth Diode Pumped Solid State Lasers," given as invited paper ELT 3.6 at 1989 LEOS Annual Meeting, Orlando, Florida, October 15-20, 1989.

21. R. L. Byer, "Solid State Lasers and Nonlinear Optics," presented at Quantum Electronics Seminar, Applied Physics Dept, Stanford University, October, 1989.

22. R. L. Byer, "Infrared Diode-Pumped Solid State Lasers and Efficient Frequency Conversion Techniques," given at 1989 OSA Annual Meeting, Orlando, Florida, October 16-20, 1989.

23. R. L. Byer, "University Partnerships," given at the dedication of the IBM Advanced Semiconductor Technology Center, East Fishkill Facility, Hopewell Junction, New York, October 25, 1989.

24. M. K. Reed and R. L. Byer, "A Nd:glass Slab Laser for X-ray Lithography," presented at Lasers 89, New Orleans, Louisiana, December 1989.

25. T. Day, E.K. Gustafson, and R.L. Byer, "Active Frequency Stabilization of Monolithic Diode-Laser-Pumped Solid State Lasers," presented at Lasers 89, New Orleans, Louisiana, December 1989.

26. T. Day, E.K. Gustafson, and R.L. Byer, "Active Frequency Stabilization of Diode-Laser-Pumped Non-Planar Ring Oscillator," presented at SPIE OELase '90, January, 1990.

    M.K. Reed and R.L. Byer, "A Nd:glass Slab Laserfor X-ray Lithography," to be presented at ECO, the Hague, the Netherlands, March 1990.

27. M. M. Fejer and E. J. Lim, Quasi-phase-matched second-harmonic generation In $LiNbO_3$ waveguides," invited paper Tul1, OSA-IEE topical meeting on Integrated Photonics Research, Hilton Head, SC, March 26-28, 1990.

28. M. M. Fejer, "Second-order nonlinearities in asymmetric quantum wells," invited paper QWA1 International Quantum Electonics Conference, Anaheim, CA, May, 1990.

CONTRIBUTED PRESENTATIONS

1. F. M. Schellenberg, R. L. Byer, R. D. Miller and R. Sooriyakumaran, "Two-Photon Absorption Induced Effects in Crystalline Polysilane Films," International Quantum Electronic Conf. paper ThI-4, Tokyo, July, 1988.
2. M. K. Reed and R. L. Byer, "The Performance of a Conduction Cooled Nd:Glass Zig-Zag Slab Laser," International Conference on Optical Science and Engineering, Hamburg, West Germany, Sept., 1988.
3. M. K. Reed , "Slab Lasers," (Tutorial Course) The International Conference on Optical Science and Engineerin, Hamburg, West Germany, Sept,. 1988.
4. R. C. Eckardt,C. D. Nabors, W. J. Kozlovsky and R. L. Byer, "Simultaneous Electro-optical and temperature tuning of a doubly resonant optical parametric oscillator," paper TuN4, Annual Meeting of the Optical Society of America, Santa Clara, California, Nov., 1988.
5. F. M. Schellenberg, R. L. Byer and R. D. Miller, "Polarization-Sensitive Optical Elements Using Polysilane Films," paper WK2, Annual Meeting of the Optical Society of America, Santa Clara, California, Nov., 1988.
6. E. J. Lim, M. M. Fejer, and R. L. Byer, "Second harmonic generation of blue and green light in periodically-poled planar lithium niobate waveguides," postdeadline paper PD3, Topical Meeting on Nonlinear Guided Wave Devices: Physics and Applications, 2-4 February 1989, Houston, Texas.
7. C.D. Nabors, R.C. Eckardt, W.J. Kozlovsky and R.L. Byer, "Monolithic MgO:LiNbO3 Optical Parametric Oscillator Pumped by a cw Frequency Doubled Diode-Laser-Pumped Nd:YAG", paper FK2, Conference on Lasers and ElectroOptics (CLEO), 24-28 April 1989, Baltimore, Maryland.
8. M.K. Reed and R.L. Byer, "A Nd:Glass Slab Laser for Soft X-ray Lithography", paper MB4, Conference on Lasers and ElectroOptics (CLEO), 24-28 April 1989, Baltimore, Maryland.
9. E.C. Rea, D. Craven, A.C. Nilsson, R.L. Byer, "Single Frequency, Undirectional, Monolithic Nonplanar Ring Laser in Nd:Glass", paper WH4, Conference on Lasers and ElectroOptics (CLEO), 24-28 April 1989, Baltimore, Maryland.
10. G.A. Magel, M.M. Fejer, R.L. Byer, "Second Harmonic Generation of Blue Light in Periodically-poled Lithium Niobate", paper ThQ3, Conference on Lasers and ElectroOptics (CLEO), 24-28 April 1989, Baltimore, Maryland.
11. E. J. Lim, M. M. Fejer, and R. L. Byer, "Second harmonic generation of green light in a periodically-poled planar lithium niobate waveguide," paper ThQ4, Conference on Lasers and ElectroOptics (CLEO), 24-28 April 1989, Baltimore, Maryland.
12. Dieter H. Jundt, Martin M. Fejer, and Robert L. Byer, "Optical properties of stoichiometric lithium niobate fabricated by vapor transport equilibration", paper WF64, Conference on Lasers and ElectroOptics (CLEO), 24-28 April 1989, Baltimore, Maryland.
13. T. Day, A.C. Nilsson, A.D. Farinas, E.K. Gustafson and R.L. Byer, "Active linewidth narrowing of diode laser pumped non-planar ring oscillators," paper WDD27, Conference on Lasers and ElectroOptics (CLEO), 24-28 April 1989, Baltimore, Maryland.
14. C. D. Nabors and R. L. Byer, "Monolithic Optical Parametric Oscillators for Quantum Optics," paper MAc2, Sixth Rochester Conference on Coherence and Quantum Optics, June 1989.
15. R. L. Byer, "Ultranarrow Linewidth Solid State Oscillators," postdeadline paper, 9th International Conference on Laser Spectroscopy, Bretton Woods, NH, June 1989.
16. C. D. Nabors, A. D. Farinas, T. Day, S. T. Yang, E. K. Gustafson, and R. L. Byer, "Injection locking of a 13-watt Nd:YAG ring laser," poster WL14, OSA Annual Meeting, Orlando, Florida, October 15-20, 1989.

17. T. Day, E.K. Gustafson, and R.L. Byer, "Active Frequency Stabilization of Monolithic Diode-Laser-Pumped Solid State Lasers," presented at Lasers 89, New Orleans, Louisiana, December 1989.

18. C.D. Nabors and R.L. Byer, "High Coherence Operation and Optical Frequency Division in a Monolithic Optical Parametric Oscillator," paper MD2 at OSA topical meeting on Advance Solid-State Lasers, Salt Lake City, March 5-7, 1990.

19. F.M. Schellenberg, R.L. Byer, and R.D. Miller, "Substituted Polysilanes for Integrated Optics," paper MF5, OSA-IEE topical meeting on Integrated Photonics Research, Hilton Head, SC, March 26-28, 1990.

20. R.C. Eckardt, H. Masuda, and Y.X. Fan, and R.L. Byer "Re-measurement of Some Nonlinear Optical Coefficients by Phase-Matched Second Harmonic Generation," paper CWF25, Conference on Lasers and Electro-Optics, Anaheim, CA, May, 1990.

21. F. M. Schellenberg, R. L. Byer, and R. D. Miller," paper QThI5, International Quantum Electonics Conference, Anaheim, CA, May, 1990.

SUBMITTED PRESENTATIONS

R. C. Eckardt, S. T. Yang, E. K. Gustafson, and R. L. Byer, "Frequency tuning and control of doubly resonant optical parametric oscillators," to be presented at the Annual Meeting of the Optical Society of America, Boston, Nov. 1990.

Efficient, single-axial-mode operation of a monolithic $MgO:LiNbO_3$ optical parametric oscillator

C. D. Nabors, R. C. Eckardt, W. J. Kozlovsky,* and R. L. Byer

Edward L. Ginzton Laboratory, Stanford University, Stanford, California 94305

Received March 27, 1989; accepted June 20, 1989

A monolithic doubly resonant optical parametric oscillator (OPO) fabricated from $MgO:LiNbO_3$ was pumped by a cw, frequency-doubled, diode-laser-pumped Nd:YAG laser. The threshold for cw operation was 12 mW, and pump depletions of up to 78% were observed two times above threshold. The total OPO output power was 8.15 mW, with a conversion efficiency for the incident pump of 34% and combined conversion efficiency for the 1064-nm laser light of 14%. The OPO was temperature tuned from 1007 to 1129 nm, operated on a single-axial-mode pair over most of the range, and could be electric field tuned by as much as 38 nm near degeneracy.

Optical parametric oscillators[1] (OPO's) are currently enjoying a revival of interest. New materials and improved pump sources are enabling OPO's to live up to their decades-old promise of providing efficient, narrow-band, widely tunable sources of light. In the cw long-pulse regime OPO's have been demonstrated in lithium niobate ($LiNbO_3$) as narrow-linewidth sources using the singly resonant configuration[2] and in $LiNbO_3$ waveguide devices with low thresholds.[3] A single-mode injection-seeded pump source was used in a demonstration of a pulsed narrow-bandwidth $LiNbO_3$ OPO for high-resolution spectral measurements near 3.4 μm.[4] Barium metaborate (BaB_2O_4) has been used in OPO's with an injection-seeded laser pump source for improved linewidth and stability[5] and to extend pulsed OPO operation to ultraviolet wavelengths.[6] Improved infrared nonlinear materials such as silver gallium selenide ($AgGaSe_2$) have been used for broadly tunable mid-infrared OPO's.[7] OPO's are also widely used in studies on squeezed states of light.[8-10] We report here on the stable cw single-mode operation of a doubly resonant OPO pumped by a frequency-doubled, diode-laser-pumped Nd:YAG laser.

Early efforts at running doubly resonant OPO's were plagued by instabilities. As the doubly resonant OPO is overconstrained by the requirements of energy conservation, phase matching, and simultaneous resonance of signal and idler waves,[11,12] perturbations on the pump frequency or OPO cavity length can cause large power fluctuations and mode hopping of the OPO. However, because OPO's are of great potential importance as spectroscopic sources, as sources for injection seeding or locking, and for quantum optics, we have worked to overcome the problems of doubly resonant OPO's by using frequency-stable, single-mode, diode-laser-pumped solid-state lasers. The high efficiency, compactness, and exceptional frequency stability of these laser pumps have led to excellent stability and efficiency for OPO operation. The monolithic cavity design of the OPO also contributes to the device performance, making possible an OPO with a low threshold that runs in a single-mode pair as discussed below.

Previously we demonstrated a pulsed doubly resonant OPO (DRO) of monolithic design fabricated from 5% magnesium-oxide-doped $LiNbO_3$ ($MgO:LiNbO_3$).[13] $MgO:LiNbO_3$ was chosen because of its low loss at 1064 nm, noncritical phase matching, and reduced photorefractive effect. The 400-nsec pulse lengths of the pump light were too short for the DRO to reach steady-state operation. In spite of excellent pump depletion, energy conversion efficiencies were relatively low owing to the long buildup time that extended across much of the pump pulse. The pulsed DRO appeared to run in a single-mode pair over much of its range but would drift from mode to mode as the pump power and crystal temperature fluctuated.

To achieve cw operation we fabricated a monolithic OPO resonator of $MgO:LiNbO_3$ with reduced output coupling, and thus lowered the threshold. Two spherical surfaces of 10-mm radius of curvature were polished on the ends of the 12.5-mm-long crystal along with a total-internal-reflection face perpendicular to the z axis to provide a ring resonant path. Metal electrodes were deposited on the two surfaces perpendicular to the y axis to allow electric-field tuning. The ring geometry was used to obtain maximum conversion and to avoid feedback problems.[14] Dielectric mirrors were deposited directly onto the ends of the crystal, with the specification that the output coupler be 0.5% transmitting and the other end be highly reflecting at 1064 nm and highly transmitting at 532 nm. The double-resonance condition for the signal and idler was satisfied by operating near degeneracy. The pump light was not resonated in this DRO.

The finesse of the DRO resonator was measured using the 1064-nm Nd:YAG laser. An electric field was applied across the crystal y axis, and the r_{22} electro-optic and d_{21} piezoelectric coefficients were used to scan the optical cavity length. The finesse at 1064 nm was measured to be 960, with a voltage of 1506 V required to scan the 5.1-GHz free spectral range. This finesse implies a cold cavity loss of 0.58%. The crystal

0146-9592/89/201134-03$2.00/0

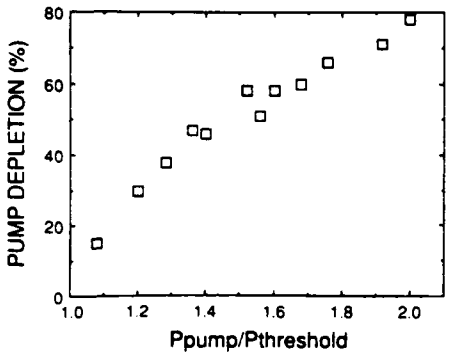

Fig. 1. Pump depletion of the cw DRO versus the number of times above threshold (pump power divided by threshold power).

bulk losses are expected to be of the order of 0.4%.[15] The high-reflector (pump) end of the crystal had a transmittance at 532 nm of 87%.

The DRO was pumped with the resonantly enhanced second harmonic of the cw diode-laser-pumped Nd:YAG laser.[15] The second-harmonic power was approximately 24 mW in a single mode for 57 mW of 1064-nm light incident upon the crystal. Pump light at 532 nm was mode matched into the DRO with a single lens.

For total cavity losses of 0.58%, the calculated threshold[1,16] of the DRO is 3.2 mW of incident pump power at 532 nm, assuming perfect spatial mode coupling of the pump into the OPO resonator. The threshold was measured experimentally to be 12 mW. The discrepancy can be accounted for by noting the extreme sensitivity of the DRO threshold to cavity losses and to mode matching.

Pump depletion of the 532-nm pump radiation versus the number of times above threshold is shown in Fig. 1. These data were taken by scanning the crystal voltage with the DRO oscillating at a signal wavelength of 1035 nm and idler of 1096 nm and observing the point of maximum pump depletion. At two times above threshold the pump depletion was 78%. The DRO resonator is tightly focused (w_0 = 27 μm), thus limiting the applicability of existing theories for pump depletion of Gaussian-intensity pump radiation. However, the pump-depletion data are in good agreement with the plane-wave, transient-regime theory of Bjorkholm.[14]

With no active feedback control, the DRO would run cw and almost always in a single-mode pair at a fixed temperature and voltage. In this context single mode refers to operation with a single signal and a single idler axial mode, or two unique frequencies. A dither-and-lock servo was used on the crystal voltage to lock the OPO to its maximum power point. For the DRO running at a 1043-nm signal and a 1085-nm idler, a total output power of 8.15 mW of signal and idler power was observed for approximately 24 mW of incident 532-nm pump light. The conversion efficiency is 34% for the incident pump and 39% for the transmitted pump. With 57.4 mW of 1064-nm light incident upon the doubling crystal, this represents a 14.2% conversion efficiency of the Nd:YAG laser light to tunable single-axial-mode power after two nonlinear processes, and a 1.6% conversion efficiency of the 500-mW diode laser used to pump the Nd:YAG laser. At an estimated 75% pump depletion, the conversion efficiency implies an output-coupler efficiency of 50%, which is somewhat higher than expected from the loss as deduced from the finesse measurement and the presumed bulk crystal losses. The stability of the OPO output power and servo locking was limited by that of the frequency-doubling system to operation of only a few minutes at a time.

The single-mode condition could be confirmed at a fixed voltage using a scanning confocal interferometer with a 300-MHz free spectral range. Figure 2 shows an interferometer scan of slightly more than one interferometer free spectral range. The stability of the transmission peaks suggested that the DRO frequency was stable to within a few megahertz (the resolution of the instrument) and potentially was much more stable. With the DRO servo locked to a particular axial-mode pair, the DRO signal frequency could track laser frequency tuning as much as 90 MHz without a mode hop. This tuning bandwidth was observed for a signal wavelength of 1043 nm and an idler wavelength of

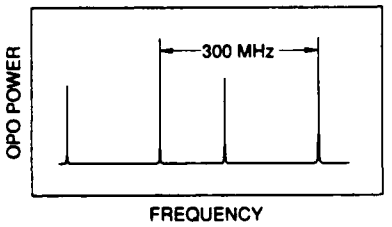

Fig. 2. Scanning interferometer trace of the DRO output light. The higher peaks are signal, the lower peaks are idler. The difference is attributed to the wavelength dependence of detector sensitivity.

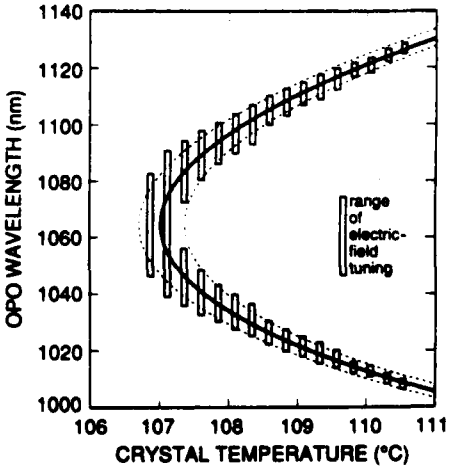

Fig. 3. Temperature tuning of the DRO showing signal and idler wavelengths. The bars represent the extent over which the DRO could be tuned at a fixed temperature by the applied electric field (V_{max} = 1100 V). The solid curve shows the gain center as determined by the temperature-tuned phase-matching condition, and the dashed curves are drawn at plus and minus one cluster spacing away from the gain center.

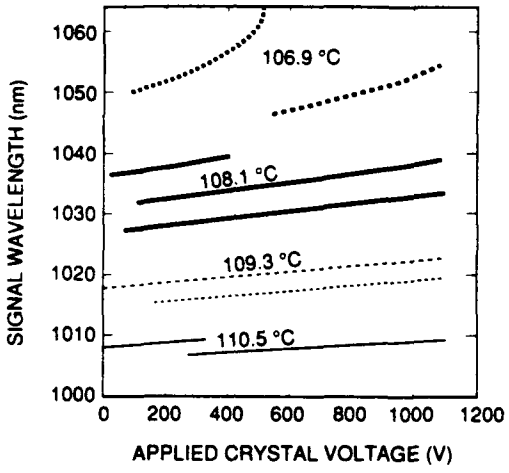

Fig. 4. Voltage tuning of the DRO showing the signal wavelengths only. At a fixed temperature several different clusters are able to oscillate.

1085 nm and is expected to be a strong function of operation relative to degeneracy.

Coarse tuning of the output wavelengths was accomplished by adjusting the crystal temperature, with fine control provided by the applied crystal voltage that controlled the cystal optical path length and birefringence. The DRO could be tuned from degeneracy with both signal and idler at 1064 nm to a signal wavelength of 1007 nm and a corresponding idler of 1129 nm. The temperature tuning range was limited by the bandwidth of the dielectric coatings. Figure 3 shows the wavelength temperature tuning dependence. The bars represent the extent that the voltage scan of 1100 V was able to tune the output at a fixed temperature and are not error bars. As the crystal voltage was scanned, the double-resonance condition would change and the DRO would hop axial modes. The mode hopping occurred along series of adjacent axial-mode pairs known as a clusters.[12,17] The solid curve in Figure 3 shows the gain center as determined by the temperature-tuned phase-matching condition, and the dashed curves are drawn at plus and minus one cluster spacing away from the gain center, which is also equal to the gain bandwidth.

At a fixed temperature two or even three clusters were able to oscillate in a small voltage range. Figure 4 shows the cluster tuning as a function of applied voltage with the curves parameterized by crystal temperature for four different temperatures. The clusters may have their signal wavelengths separated by as much as 17 nm near degeneracy and are separated by ≈3 nm for operation near the tuning limit. Near degeneracy a single cluster's signal wavelength could be scanned as much as 18.6 nm (or 5.0 THz) with the application of 924 V to the crystal. This gives a total wavelength scan for the cluster of 38 nm (or 10.0 THz) when the idler wavelength is included.

In conclusion, we have demonstrated stable, efficient, cw single-mode operation of a DRO pumped by a frequency-doubled, diode-laser-pumped Nd:YAG laser. The device was tuned from 1007 to 1129 nm and exhibited a 34% conversion efficiency from 532-nm pump light to signal and idler power. Pump depletions of 78% were observed. Detailed studies and modeling of the microscopic tuning behavior and OPO linewidths are being carried out. The possibility of DRO's with a signal-to-idler frequency ratio of 3:1 and cw singly resonant OPO's and the use of this class of OPO for production of sub-shot-noise correlation light beams are being explored.

This research was supported by the U.S. Office of Naval Research under contracts N00014-88-0576 and N00014-88-K-0701. The $MgO:LiNbO_3$ was provided by Crystal Technology, Inc., of Palo Alto, California. C. D. Nabors and W. J. Kozlovsky thank the Fannie and John Hertz Foundation for its continuing and past support.

* Permanent address, IBM Almaden Research Center, MS K69/803, 650 Harry Road, San Jose, California 95120.

References

1. For reviews of OPO's see R. L. Byer, in *Treatise in Quantum Electronics*, H. Rabin and C. L. Tang, eds. (Academic, New York, 1973), pp. 587–702, and R. G. Smith, in *Advances in Lasers*, A. K. Levine and A. J. DeMaria, eds. (Dekker, New York, 1976), Vol. 4, pp. 189–307.
2. W. J. Kozlovsky, E. K. Gustafson, R. C. Eckardt, and R. L. Byer, Opt. Lett. **13**, 1102 (1988).
3. H. Suche, B. Hampel-Vogedes, R. Ricken, W. Sohler, and H. Teichmann, in *Digest of Conference on Nonlinear Guided-Wave Phenomena: Physics and Applications* (Optical Society of America, Washington, D.C., 1989), paper THA1.
4. T. K. Minton, S. A. Reid, H. L. Kim, and J. K. McDonald, Opt. Commun. **69**, 289 (1989).
5. Y. X. Fan, R. C. Eckardt, R. L. Byer, J. Nolting, and R. Wallenstein, Appl. Phys. Lett. **53**, 2014 (1988).
6. W. R. Bosenberg, L. K. Cheng, and C. L. Tang, Appl. Phys Lett. **54**, 13 (1989).
7. R. C. Eckardt, Y. X. Fan, R. L. Byer, C. L. Marquardt, M. E. Storm, and L. Esterowitz, Appl. Phys. Lett. **49**, 608 (1986).
8. L.-A. Wu, M. Xiao, and H. J. Kimble, J. Opt. Soc. Am. B **4**, 1465 (1987).
9. A. Heidmann, R. J. Horowicz, S. Reynaud, E. Giacobino, C. Fabre, and G. Camy, Phys. Rev. Lett. **59**, 2555 (1987).
10. P. Grangier, R. E. Slusher, B. Yurke, and A. LaPorta, Phys. Rev. Lett. **59**, 2153 (1987).
11. J. Falk, IEEE J. Quantum Electron. **QE-7**, 230 (1971).
12. R. G. Smith, IEEE J. Quantum Electron. **QE-9**, 530 (1973).
13. W. J. Kozlovsky, C. D. Nabors, R. C. Eckardt, and R. L. Byer, Opt. Lett. **14**, 66 (1989).
14. J. E. Bjorkholm, IEEE J. Quantum Electron. **QE-7**, 109 (1971).
15. W. J. Kozlovsky, C. D. Nabors, and R. L. Byer, IEEE J. Quantum Electron. **24**, 913 (1988).
16. G. D. Boyd and D. A. Kleinman, J. Appl. Phys. **39**, 3597 (1968).
17. J. A. Giordmaine and R. C. Miller, Appl. Phys. Lett. **9**, 298 (1966).

Coherence properties of a doubly resonant monolithic optical parametric oscillator

C. D. Nabors,* S. T. Yang, T. Day, and R. L. Byer

Edward L. Ginzton Laboratory, Stanford University, Stanford, California 94305

Received September 27, 1989; accepted January 9, 1990

We describe a doubly resonant optical parametric oscillator (DRO) pumped with the second harmonic of a narrow-linewidth Nd:YAG laser. The linewidth of the DRO signal was less than 13 kHz, the DRO was shown to generate a phase-locked subharmonic of the pump at degeneracy, and the signal and the idler were shown to be mutually coherent with the pump and to be phase anticorrelated with each other away from degeneracy. The signal–idler heterodyne linewidth was 500 Hz, and pump phase modulation was shown to transfer to the DRO phase at degeneracy.

1. INTRODUCTION AND REVIEW

Doubly resonant optical parametric oscillators[1] (DRO's) are the only type of optical parametric oscillator to be routinely operated above threshold cw and thus have the greatest potential for narrow-linewidth coherent operation. Coherence studies of DRO's have been limited historically by the DRO's extreme sensitivity to cavity stability and pump fluctuations since they are overconstrained by the requirements of energy conservation, phase matching, and simultaneous resonance of signal and idler waves.[2] In pioneering research, Smith[3] reviewed DRO operation and tuning theory and pumped a Ba_2NaNbO_5 DRO with a frequency-stabilized argon-ion laser to achieve single-mode operation for a few seconds at a time. More recently workers studying squeezed states have operated DRO's[4] and triply resonant optical parametric oscillators[5–7] (OPO's) above threshold but have not reported on the linewidths or other coherence properties. Triply resonant OPO's are even more highly constrained above threshold than are DRO's. Advances have also been made in the field of singly resonant OPO's,[8,9] but here linewidths have been limited to greater than 30 MHz (Ref. 10) by the need for pulsed laser pump sources.

The basic operations of our monolithic doubly resonant OPO has been described in Refs. 11 and 12. To summarize, we reported on a DRO fabricated from $MgO:LiNbO_3$ pumped by a cw, frequency-doubled, diode-laser-pumped Nd:YAG laser.[11] $MgO:LiNbO_3$ was chosen for its low loss, high nonlinearity, and noncritical phase matching. The monolithic crystal resonator design is shown in Fig. 1. Dielectric mirrors were deposited directly upon the spherically curved surfaces of the resonator, and a traveling-wave ring path was formed for the ordinary polarized signal and idler waves by the use of the total-internal-reflection surface. Pump light, which was polarized extraordinarily, was not resonant for the ring path because of bireflection at the crystal surfaces. The length of the crystal was 12.5 mm, and the radii of the mirrors were 10 mm, providing a 27-μm focus inside the crystal at 1064 nm and a resonator free spectral range of 5.088 GHz. The crystal was heated in an oven to 107°C or greater to phase match the parametric interaction noncritically.

Threshold for cw operation was 12 mW, and pump depletions of as much as 78% were observed at 2 times above threshold. The total DRO output power was 8.15 mW, with a conversion efficiency for the incident pump of 34% and a combined conversion efficiency for the 1064-nm laser light of 14%. The DRO was temperature tuned from 1007 to 1129 nm, operated on a single-axial-mode pair over most of the range, and could be electric-field tuned by as much as 38 nm near degeneracy.

In this paper we describe the coherence properties of the DRO, including its narrow linewidth and exceptional stability. The high performance of the device permitted the demonstration of pump–DRO phase locking at degeneracy, pump–DRO phase correlations, signal–idler heterodyne measurements, and pump–DRO phase transmodulation, which have not to our knowledge previously been observed.

2. PUMP SYSTEMS

The DRO was previously pumped with the resonantly doubled output of a diode-laser-pumped, single-frequency, cw Nd:YAG laser. Because of problems with residual photorefractive damage in the $MgO:LiNbO_3$ doubler and the need for greater power at the second-harmonic (532-nm) wavelength, we developed a multiwatt injection-locked Nd:YAG laser system capable of producing as much as 13 W of cw power at 1064 nm with an estimated linewidth of 5–10 kHz.[14] Single-pass frequency doubling in a 2-cm piece of $MgO:LiNbO_3$ produced more than 120 mW of power at 532 nm for 10-W input at 1064 nm. As will be seen below, it is highly advantageous to use the second harmonic of a master laser as an OPO pump. The second-harmonic pump source is derived from the 1064-nm fundamental, which provides a local-oscillator frequency and phase reference that can be used in coherence measurements of degenerate and near-degenerate operation of the DRO.

3. DRO SIGNAL LINEWIDTH

Earlier[12] we estimated an upper bound of the DRO linewidth to be a few megahertz, based on scanning Fabry–Perot interferometer measurements. To determine the linewidth rigorously we performed a heterodyne beat-note measurement,

0740-3224/90/050815-06$02.00

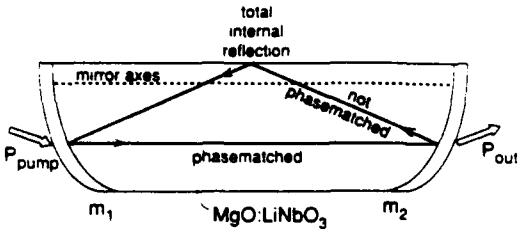

Fig. 1. Monolithic DRO crystal cavity design. Dielectric mirrors that are highly reflective for the signal and the idler and transmit the pump are deposited directly upon the curved ends of the MgO:LiNbO$_3$ resonator. m_1, highly reflecting at 1064 nm, $T = 85\%$ at 532 nm. m_2, $T = 0.5\%$ at 1064 nm.

using an independent Nd:GGG single-frequency nonplanar ring laser.[15] The Nd:GGG laser oscillator has a wavelength of 1062.2 nm instead of the Nd:YAG wavelength of 1064.2 nm, and this enabled us to perform the beat-note measurement well away from degeneracy (by ~ 531 GHz, or 104 DRO free spectral ranges). The free-running linewidth of this type of monolithic ring laser has been measured by a number of workers[16-18] to be of the order of 5–10 kHz for short-term jitter.

The experimental layout is shown in Fig. 2. The injection-locked Nd:YAG pump laser was frequency doubled, and the fundamental and the second harmonic were separated with a Pellin–Broca prism. The second-harmonic power was mode matched into the monolithic DRO cavity, and the output power (signal and idler) was combined with the Nd:GGG oscillator output on a beam splitter. One beam was then detected with a fast photodiode and analyzed with a Hewlett-Packard 8566B 22-GHz rf spectrum analyzer. The other beam was sent through an $f = 1$ m spectrometer with a charge-coupled-device camera focused on its image plane to monitor the coincidence of the DRO signal wavelength with the Nd:GGG laser line. The DRO was tuned with temperature to near degeneracy, and then the voltage was adjusted to fine-tune the signal frequency until a beat note was observed. The idler frequency was too far away (1 THz) to play a role in the heterodyne measurement. The DRO was free running and was not servo locked for this measurement.

A typical rf beat-note spectrum is shown in Fig. 3. The 3-dB full linewidth of the beat note was 13 kHz, limited by beat-note carrier jitter. The sidebands at 230 and 530 kHz are due to relaxation oscillation (amplitude) noise on the Nd:GGG and Nd:YAG laser systems, respectively. As both the doubled Nd:YAG laser pumping the DRO and the Nd:GGG laser have linewidths of the order of 5–10 kHz, we see that the operation of the DRO reproduces the linewidth of the pump laser system. This assertion is supported by the OPO self-beat-note experiment described in Section 5. We emphasize that this measurement, using two independent oscillators, yields the true linewidth, i.e., the convolution of both oscillators' linewidths, and has no implicit common-mode rejection as is present in many measurements of laser oscillator relative linewidths.

4. DEGENERATE OPERATION: PUMP-DRO PHASE LOCKING

It was previously predicted[19-21] that the phase of an OPO operating with degenerate signal and idler waves would be phase locked to the pump with either 0 or π relative phase.[22] This has been elegantly demonstrated in degenerate squeezed-state experiments below threshold.[5] To test the theory above threshold we ran the DRO at degeneracy and combined the DRO output beam with a 1064-nm reference beam from the Nd:YAG laser. This reference beam is phase correlated with the second harmonic used to pump the DRO. One of the combined beams was imaged onto a screen and observed with the charge-coupled-device camera. The other beam was sent through a scanning Fabry–Perot interferometer to monitor the axial mode structure of the DRO at degeneracy. The beam incident upon the Fabry–Perot interferometer was blocked during data taking to prevent potential feedback effects. Great care was taken to ensure that there was no injection locking of the degenerate OPO by stray light from the Nd:YAG laser by using a prism to separate the 1064-nm laser light from the green 532-nm pump beam. The pump light was passed through a highly reflecting mirror for the infrared ($T = 0.05\%$ at 1064 nm) and then through an aperture.

Figure 4 shows the stable fringes obtained by interfering the degenerate DRO with the Nd:YAG laser. The DRO

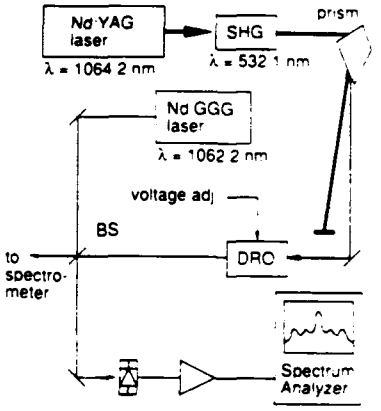

Fig. 2. Experimental layout showing the DRO pumped by the frequency-doubled injection-locked Nd:YAG laser for heterodyning with the Nd:GGG laser. SHG, second-harmonic generator; BS, beam splitter.

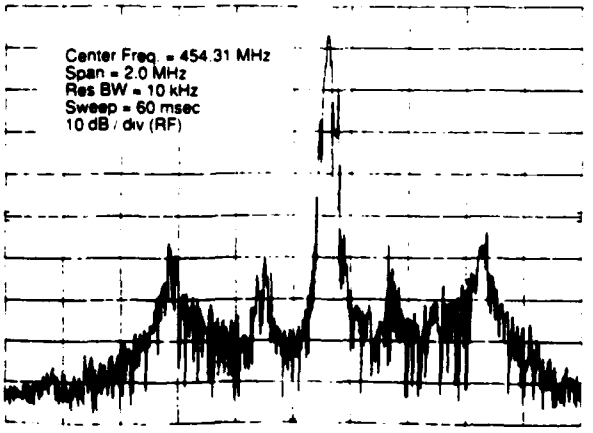

Fig. 3. Heterodyne rf beat-note spectrum of the independent DRO signal and Nd:GGG laser oscillators. The 3-dB full width of the central peak is 13 kHz.

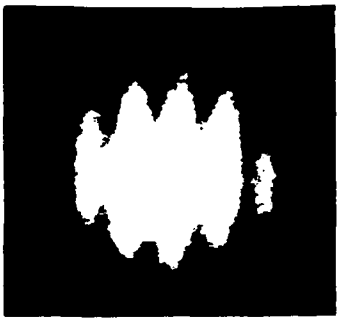

Fig. 4. Stable fringe pattern produced by interfering the degenerate DRO beam with a reference beam from the Nd:YAG laser.

would run at degeneracy for as long as 20 min at a time with no servo control and no applied tuning voltage.

When the pump was interrupted, the overall phase of the fringe pattern was observed to jump phase randomly by 0 or π. This is a good indication that no injection locking of the DRO from the laser was taking place. An attempt was made to observe the tunneling of the OPO phase between the 0 and π states,[23] which was unsuccessful owing to excess DRO relative amplitude noise during near-threshold operation. Both standing-wave and ring path DRO configurations were tested. Operation with the standing-wave geometry was less stable in frequency and amplitude than for the ring path, and the DRO was more susceptible to feedback effects.

The stable fringes show that the degenerate DRO is a true phase-locked subharmonic of the pump. We investigated the high-frequency phase fidelity by performing a heterodyne rf beat-note experiment with the reference laser beam frequency shifted by 45 MHz, using an acousto-optic modulator driven by a rf synthesizer. Figure 5 shows the rf beat-note spectrum. The asymmetry of the phase noise is due to amplitude noise on the DRO signal. Most of the noise in the subkilohertz band can be attributed to mechanical vibration of the mirrors in the interferometer, which limits the low-frequency sensitivity of the measurement.[14] For reference, the phase-noise spectral density $S_\phi(f)$ at 5 kHz was determined from the plot to be 2×10^{-9} rad^2/Hz.

5. NONDEGENERATE OPERATION: PUMP-DRO PHASE CORRELATIONS AND SIGNAL-IDLER HETERODYNE LINEWIDTH

Away from degeneracy the DRO signal and idler phases are no longer locked to the pump but diffuse randomly in such a way that the sum of their phases is either 0 or π.[24] (For simplicity we will assume that the overall phase is 0, with no loss of generality.) Diffusion of the relative phase is analogous to the phase diffusion seen in lasers that is responsible for the Schawlow–Townes linewidth. The phase sum was recently analyzed, using a quantum-mechanical Hamiltonian, and is a candidate squeezed-state observable.[25] We can write the relevant DRO electric fields as

$$\mathbf{E}_{\text{pump}} = E_{\text{pump}} \exp(2i\omega_L t), \tag{1}$$

$$\mathbf{E}_{\text{DRO}} = E_{\text{DRO}}(\exp[i[(\omega_L + \Delta)t + \phi(t)]] + \exp[i[(\omega_L - \Delta)t - \phi(t)]]), \tag{2}$$

where the first and second terms in Eq. (2) are the signal and the idler fields, respectively, ω_L is the Nd:YAG laser frequency (equal to the degenerate DRO frequency), Δ is the DRO frequency displacement from degeneracy, and $\phi(t)$ is the relative DRO phase. We have assumed that the DRO is operating near enough to degeneracy that the output couplings (and thus the powers) of the signal and the idler are equal. We also introduce a local oscillator derived from the laser:

$$\mathbf{E}_L = E_L \exp[i(\omega_L t + \theta)], \tag{3}$$

where the phase θ can be adjusted experimentally. If we heterodyne the signal and the idler waves with the laser local oscillator, the voltage seen on the photodetector will be

$$V \sim E_{\text{DRO}}^2 \cos[2\Delta t + 2\phi(t)] + 2E_L E_{\text{DRO}} \cos(\theta)\cos[\Delta t + \phi(t)]. \tag{4}$$

The first term at frequency 2Δ represents the mixing of the signal and the idler, and the second term at frequency Δ the mixing of the signal and the idler each with the laser local oscillator. Relation (4) predicts that the beat-note amplitude of the signal at frequency Δ will depend on the phase of the local oscillator and vanish for $\theta = \pi/2, 3\pi/2$, etc. If the phases of the signal and the idler were not exactly anticorrelated with respect to the pump, the Δ beat note would not vanish. Additionally, relation (4) predicts that the linewidth of the beat note at 2Δ is four times as broad as that at Δ, assuming white frequency noise,[26] and twice as broad assuming a $1/f$ frequency noise spectral density, as is typical in most free-running laser systems.

In our experiments the DRO was operated one axial mode away from degeneracy so that $\Delta = 5.088$ GHz. The output of the DRO was mixed at a beam splitter with a local oscillator from the laser and then sent down a single-mode fiber to a Hewlett-Packard Model 71400A Lightwave Optical spectrum analyzer. Figure 6 shows the signal–idler beat-note spectrum at $2\Delta = 10.17$ GHz, taken with the local oscillator blocked. The vertical scale is 5 dB/division for optical power, which is the equivalent of 10 dB/division of rf power. The full width at half-maximum (3-dB rf) of the central peak is ≈500 Hz, with a resolution bandwidth of 300 Hz and

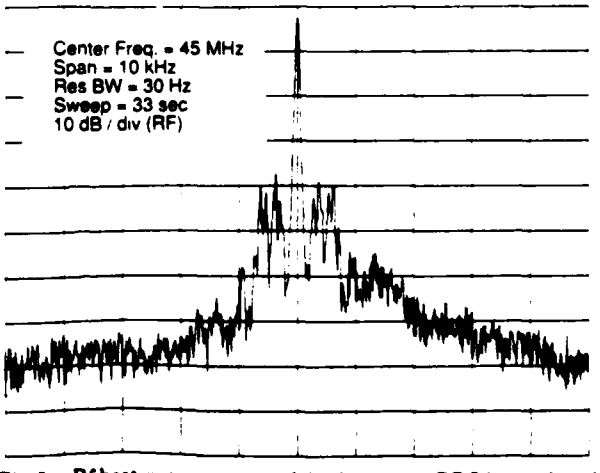

Fig. 5. Rf beat-note spectrum of the degenerate DRO heterodyned with a reference beam from the laser, which has been shifted 45 MHz with an acousto-optic modulator.

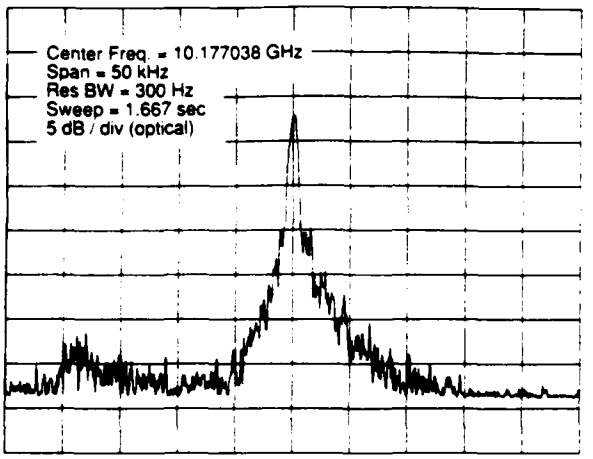

Fig. 6. Beat-note spectrum of the DRO signal with idler frequencies displaced one axial mode from degeneracy. The central peak has a width of 500 Hz, and there is a 1-Hz trace-to-trace jitter in its position.

a trace-to-trace jitter of ≈1 kHz for 1.67-sec sweeps. The jitter is approximately 1 part in 10^7 of the beat note and corresponds to fluctuations in the optical path length of $\delta(nL) \approx 6$ nm.

This observation substantiates the claim made in Section 3 that the off-degeneracy DRO does not add significant excess linewidth when pumped by a 5–10-kHz-linewidth laser. The asymmetry in the spectrum is again caused by amplitude noise, and the artifact at the left is possibly due to a small transverse mode effect. The beat-note linewidth of the signal at 5.088 GHz (not shown) is also ≈500 Hz, with a jitter similar to the 10.17-GHz note, and since this width is so close to the resolution bandwidth of the spectrum analyzer the relative linewidth prediction is problematic.

To confirm that the DRO signal and the idler were phase anticorrelated we varied the phase of the laser local oscillator, using a $LiNbO_3$ electro-optic phase modulator with $V_{2\pi}$ = 624 V. A 1-kV/50-msec ramp voltage was applied to the phase modulator, and the spectrum analyzer was triggered at the start of the ramp and also swept at 50 msec. The spectrum analyzer center frequency was 5.088 GHz, and the span was 0 Hz, with a large enough resolution bandwidth (100 kHz) to pass most of the rf power. The horizontal axis of the spectrum analyzer trace is thus proportional to the local-oscillator phase, and with the vertical axis on a linear scale displaying rms volts we expect to see a wave proportional to $|\cos(\theta)|$, the rectification due to the spectrum analyzer's power detector law. Figure 7 shows the experimental trace with the independently determined calibration of the phase axis. The waveform is precisely as predicted, which verifies that the DRO signal and the idler phase are collectively coherent with the pump phases and anticorrelated with each other away from degeneracy.

6. PUMP-DRO PHASE TRANSMODULATION

There are a number of predictions of how an OPO should tune with a chirped or frequency-modulated pump.[27,28] The OPO is interesting in this respect, as the tuning rate near degeneracy can be much larger than the pump tuning rate. We were unable to tune our pump rapidly but instead phase modulated the pump and measured the effects on the DRO output frequency spectrum.

We assume that, like that of the pump, the DRO output is purely phase modulated and write the electric fields as

$$\mathbf{E}_{\text{pump}} = E_{\text{pump}} \exp\{i[2\omega_L t + \beta \sin(\omega_{\text{mod}} t)]\} \tag{5}$$

and

$$\mathbf{E}_{\text{DRO}} = E_{\text{DRO}} \exp\{i[\omega_L t + \delta \sin(\omega_{\text{mod}} t + \xi)]\}. \tag{6}$$

For small modulation depth, zero cavity detuning, and pump decay rate much greater than the DRO cavity decay rate we can use the degenerate OPO equations of motion[21] to solve for δ and ξ to get

$$\delta = \frac{\beta}{2}\left[1 + \frac{1}{r}(\omega_{\text{mod}}/\omega_c)^2\right]^{-1/2}, \tag{7}$$

$$\tan(\xi) = -\frac{\omega_{\text{mod}}}{\omega_c} r^{-1/2}, \tag{8}$$

where ω_c is the DRO cavity power bandwidth and r is the number of times above threshold for the DRO.

We detect the phase modulation by mixing the DRO with a frequency-shifted laser local oscillator

$$\mathbf{E}_{\text{LO}} = E_{\text{LO}} \exp[i(\omega_L + \omega_{\text{rf}})t] \tag{9}$$

to generate the rf voltage measured on a photodiode given by

$$V \sim \cos[\omega_{\text{rf}} t + \delta \sin(\omega_{\text{mod}} t + \xi)]. \tag{10}$$

We used a $MgO:LiNbO_3$ electro-optic phase modulator (heated to 130°C to avoid photorefraction) with $V_{2\pi}$ = 609 V to modulate the 532-nm DRO pump at frequencies from 1 kHz to 20 MHz. The driving voltage on the electro-optic modulator was 20 V peak to peak, which corresponds to a modulation index on the pump of β = 0.103 rad.

For small modulation index and low modulation frequency the detected rf power in the sidebands at $\omega_{\text{rf}} \pm \omega_{\text{mod}}$ will decrease by $J_1(\delta)^2 \approx \beta^2/16$ relative to the carrier at ω_{rf}, or 4 times less (−6 dBc) than the modulation on the pump. For β = 0.103 rad the level is calculated to be −31.8 dBc, which is

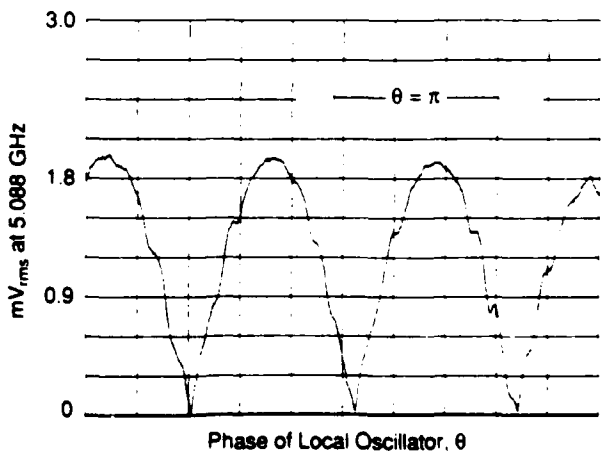

Fig. 7. Amplitude of local oscillator–DRO beat note at 5.088 GHz versus local-oscillator phase. The rectified cosine waveform is as expected from relation (4).

in excellent agreement with the experimental result of −31.1 dBc for low modulation frequencies. At higher frequencies the transmodulation is limited by the bandwidth of the DRO cavity and has the frequency response

$$\text{rel. sideband power} = \frac{\beta^2}{16}\left[1 + \frac{1}{r}(\omega_{\text{mod}}/\omega_c)^2\right]^{-1}, \quad (11)$$

with a −3-dB rolloff observed at frequency $\omega_{\text{mod}}/2\pi \approx 8$ MHz. We estimate that $r \approx 1.5$ for this experiment and obtain a measure of the total DRO cavity losses of 0.8%, in rough agreement with our earlier results.[12]

The MgO:$LiNbO_3$ phase modulator had residual amplitude and polarization modulation, which caused amplitude modulation on the DRO with modulation index 0.012 and contributed to the 1-3-dB imbalance seen on the DRO phase sidebands. The DRO amplitude modulation alone is not enough to account for the imbalance, and the remainder may be due to cavity-detuning effects or to drift in the number of times above threshold of the DRO.

Away from degeneracy the signal and idler phases are anticorrelated with respect to the pump, and no transmodulation of the signal–idler is predicted. Rf sidebands are observed on the 10.17-GHz signal–idler beat note at −40 dBc, but they can be accounted for by the DRO amplitude modulation alone and are not the result of phase modulation.

The good agreement between theory and experiment for the transfer of phase modulation from the pump to the DRO signal suggests that the theoretical model should also be valid for the more interesting case of a frequency-modulated or chirped pump.

7. DISCUSSION AND CONCLUSIONS

We have demonstrated a cw monolithic doubly resonant optical parametric oscillator with exceptionally high coherence. The linewidth was shown to be limited to that of the laser pumping it and was less than 13 kHz. The DRO operated reliably at degeneracy without any form of injection locking and was a phase locked subharmonic of the pump. Away from degeneracy, the signal and the idler were heterodyned, and a linewidth of 500 Hz was measured for short-time stability. The signal and the idler were also shown to be phase anticorrelated with respect to the pump away from degeneracy. Pump phase modulation was shown to transfer to the DRO at degeneracy with good agreement with theory, which may have applications for FM spectroscopy.

Future improvements to and applications of the DRO system will include pumping with frequency-stabilized sources such as locking the Nd:YAG pump and Nd:GGG lasers to the same reference cavity for relative stabilities of less than 3 Hz,[29] spectroscopy with the DRO as a tunable source, demonstration of a DRO with signal-to-idler frequency ratio of 3:1, and further DRO tuning and modulation studies. The DRO output can be line-narrowed by locking to a high-finesse reference interferometer, or the self-beat-note between signal and idler at 10.17 GHz could be phase locked to a rf synthesizer to stabilize the DRO directly. We are currently investigating the cw DRO as a source with sub-shot-noise correlations of signal and idler amplitudes. When the quantum phase correlations are also considered, the DRO is a direct example of the Einstein–Podolsky–Rosen paradox.[25,30]

The phase locking of the DRO at degeneracy is a demonstration of a coherent 2:1 optical frequency divider. This result is significant for metrology and spectroscopy, for which frequency chains are needed across a variety of spectral bands.[31] The proposed 3:1 DRO can also act as a 1.33:1 and 4:1 frequency divider for the pump frequency. The difficulty lies in detecting the point of exact 3:1 signal:idler operation, which is not a problem at degeneracy. We propose several possible solutions. If the DRO pump is the second harmonic of some master laser, the laser (possibly offset by some rf) and the idler could be summed to yield a color near the signal. The sum frequency output will be coherent with the DRO signal wave only when the signal and idler frequencies are exactly in the ratio 3:1. The sum of the laser and the idler could also be optically fed back to injection lock the signal phase, or the laser could be deeply phase modulated (modulation index $\approx \pi$) and mixed with both the signal and the idler. This would alternately sum the laser with the idler frequency to get signal and subtract the laser from the signal frequency to get idler as the laser phase is varied, and it would produce an AM output only when the exact 3:1 condition were met. The phases of the signal and sum waves will not in general be coherent, as the OPO phase $\phi(t)$ is not canceled out, and some type of active phase-lock-loop servo will be required to implement these schemes.

If no master laser at half the pump frequency were available, the idler could be frequency tripled and compared with the signal, which is the technique required to lock an OPO to the 2:1 operating point, where the idler can be frequency doubled and compared with the signal. The 2:1 OPO will act as a 1.5:1 and 3:1 frequency divider for the pump frequency but would, however, be difficult to fabricate as a doubly resonant OPO by using conventional quarter-wave-stack dielectric mirrors. Higher-order phase-locked frequency dividers (5:1, 6:1, . . .) will be progressively harder to realize in practice as the summing or doubling steps become more numerous, and conventional frequency multiplying from below becomes more practical than parametrically dividing down from above.

What we have again learned experimentally is that monolithic resonator designs and excellent pump mode quality (spatial, temporal, and linewidth) are highly desirable for high-performance laser and nonlinear-optical devices. We fully expect that with improved frequency- and amplitude-stabilized pump sources the DRO performance will continue to improve.

ACKNOWLEDGMENTS

This research has been supported by NASA contract NAGW-1760 and U.S. Office of Naval Research contract N00014-88-K-0701. The authors thank Coherent Laser Products, Inc., for the use of the Antares laser head used in the high-power Nd:YAG laser and Crystal Technology, Inc., for providing the MgO:$LiNbO_3$. The authors also thank R. M. Shelby of the IBM Almaden Research Center for many helpful discussions and suggestions. C. D. Nabors and S. T. Yang are grateful for the support of the Fannie and John Hertz Foundation.

* Present address, MIT Lincoln Laboratory, 244 Wood Street, Lexington, Massachusetts 02173.

REFERENCES

1. For reviews of OPO's see R. L. Byer, in *Treatise in Quantum Electronics*, H. Rabin and C. L. Tang, eds. (Academic, New York, 1973) pp. 587–702; R. G. Smith, in *Advances in Lasers*, A. K. Levine and A. J. DeMaria, eds. (Dekker, New York, 1976), Vol. 4.; Yuan Xuan Fan and R. L. Byer, "Progress in optical parametric oscillators," in *New Lasers for Analytical and Industrial Chemistry*, A. Bernhardt, ed., Proc. Soc. Photo-Opt. Instrum. Eng. **461**, 27–32 (1984).
2. J. Falk, "Instabilities in the doubly resonant parametric oscillator: a theoretical analysis," IEEE J. Quantum Electron. **QE-7**, 230–235 (1971).
3. R. G. Smith, "A study of factors affecting the performance of a continuously pumped doubly resonant optical parameteric oscillator," IEEE J. Quantum Electron. **QE-9**, 530–541 (1973).
4. A. Heidmann, R. J. Horowicz, S. Reynaud, E. Giacobino, C. Fabre, and G. Camy, "Observation of quantum noise reduction on twin laser beams," Phys. Rev. Lett. **59**, 2555–2557 (1987).
5. Ling-Ann Wu, Min Xiao, and H. J. Kimble, "Squeezed states of light from an optical parametric oscillator," J. Opt. Soc. Am. B **4**, 1465–1475 (1987).
6. P. Grangier, R. E. Slusher, B. Yurke, and A. LaPorta, "Squeezed-light-enhanced polarization interferometer," Phys. Rev. Lett. **59**, 2153–2156 (1987).
7. S. F. Pereira, K.-C. Peng, and H. J. Kimble, "Squeezed state generation and QND detection by nondegenerate parametric down conversion," presented at the Sixth Rochester Conference on Coherence and Quantum Optics, Rochester, New York, June 26–28, 1989.
8. W. J. Kozlovsky, E. K. Gustafson, R. C. Eckardt, and R. L. Byer, "Efficient monolithic MgO:$LiNbO_3$ singly resonant optical parametric oscillator," Opt. Lett. **13**, 1102–1104 (1988).
9. T. K. Minton, S. A. Reid, H. L. Kim, and J. K. McDonald, "A scanning, single mode, $LiNbO_3$, optical parametric oscillator," Opt. Commun. **69**, 289–293 (1989).
10. J. Pinard and J. F. Young, "Interferometric stabilization of an optical parametric oscillator," Opt. Commun. **4**, 425–427 (1972).
11. W. J. Kozlovsky, C. D. Nabors, R. C. Eckardt, and R. L. Byer, "Monolithic MgO:$LiNbO_3$ doubly resonant optical parametric oscillator pumped by a frequency-doubled diode-laser pumped Nd:YAG laser," Opt. Lett. **14**, 66–68 (1989).
12. C. D. Nabors, R. C. Eckardt, W. J. Kozlovsky, and R. L. Byer, "Efficient, single-axial-mode operation of a monolithic MgO:$LiNbO_3$ optical parametric oscillator," Opt. Lett. **14**, 1134–1136 (1989).
13. W. J. Kozlovsky, C. D. Nabors, and R. L. Byer, "Efficient second harmonic generation of a diode-laser-pumped cw Nd:YAG laser using monolithic MgO:$LiNbO_3$ external resonant cavities," IEEE J. Quantum Electron. **24**, 913–919 (1988).
14. C. D. Nabors, A. D. Farinas, T. Day, S. T. Yang, E. K. Gustafson, and R. L. Byer, "Injection locking of a 13-W cw Nd:YAG ring laser," Opt. Lett. **14**, 1189–1191 (1989).
15. T. Day, A. C. Nilsson, M. M. Fejer, A. D. Farinas, E. K. Gustafson, C. D. Nabors, and R. L. Byer, "30-Hz linewidth diode-laser-pumped, Nd:GGG nonplanar ring oscillators by active frequency stabilisation," Electron. Lett. **25**, 810–812 (1989).
16. T. J. Kane, A. C. Nilsson, and R. L. Byer, "Frequency stability and offset locking of a laser-diode-pumped Nd:YAG monolithic nonplanar ring oscillator," Opt. Lett. **12**, 175–177 (1987).
17. S. P. Bush, A. Gungor, and C. C. Davis, "Studies of the coherence properties of a diode-pumped Nd:YAG ring laser," Appl. Phys. Lett. **53**, 646–647 (1988).
18. K. J. Williams, A. Dandridge, A. D. Kersey, J. F. Weller, A. M. Yurek, and A. B. Tveten, "Interferometric measurement of low-frequency phase noise characteristics of diode laser-pumped Nd:YAG ring laser," Electron. Lett. **25**, 774–775 (1989).
19. W. H. Louisell, *Coupled Mode and Parametric Electronics* (Wiley, New York, 1960).
20. W. H. Louisell, A. Yariv, and A. E. Siegman, "Quantum fluctuations in parametric processes. I," Phys. Rev. **124**, 1646–1654 (1961).
21. P. D. Drummond, K. J. McNeil, and D. F. Walls, "Non-equilibrium transitions in sub/second harmonic generation 1. Semiclassical theory," Opt. Acta **27**, 321–335 (1980).
22. Ling-An Wu and H. J. Kimble, "Interference effects in second-harmonic generation within an optical cavity," J. Opt. Soc. Am B **2**, 697–703 (1985).
23. P. D. Drummond and P. Kinsler, "Quantum tunneling and thermal activation in the parametric oscillator," Phys. Rev. A **40**, 4813–4816 (1989).
24. R. Graham and H. Haken, "The quantum fluctuations of the optical parametric oscillator," Z. Phys. **210**, 276–302 (1968).
25. M. D. Reid and P. D. Drummond, "Quantum correlations of phase in nondegenerate parametric oscillation," Phys. Rev Lett. **60**, 2731–2733 (1988).
26. D. S. Elliot, R. Roy, and S. J. Smith, "Extracavity laser band-shape and bandwidth modification," Phys. Rev. A **26**, 12–18 (1982).
27. A. I. Kovrigin and R. L. Byer, "Stability factor for optical parametric oscillators," IEEE J. Quantum Electron. **QE-5**, 384–385 (1969).
28. A. Piskarskas, A. Stabinis, and A. Yankauskas, "Parametric frequency modulation of picosecond light pulses in quadratically nonlinear crystals," Sov. J. Quantum Electron. **15**, 1179–1180 (1985).
29. T. Day, E. K. Gustafson, and R. L. Byer, "Active frequency stabilization of a 1.062-μm, Nd:GGG, diode-laser-pumped nonplanar ring oscillator to less than 3 Hz of relative linewidth," Opt. Lett. **15**, 221–223 (1990).
30. A. Einstein, B. Podolsky, and N. Rosen, "Can quantum-mechanical description of physical reality be considered complete?" Phys. Rev. **47**, 777–780 (1935).
31. D. H. McIntrye and T. W. Hansch, "Novel optical frequency divider and synthesizer," in *Digest of 1988 OSA Annual Meeting* (Optical Society of America, Washington, D.C., 1988), p 131.

Submitted to J. Opt. Soc. Am. B, May 15, 1990

Optical parametric oscillator frequency tuning and control

Robert C. Eckardt, C. D. Nabors*, William J. Kozlovsky† and Robert L. Byer
Edward L. Ginzton Laboratory, Stanford University, Stanford, CA 94305-4085

abstract

The frequency tuning and control properties of monolithic doubly resonant optical parametric oscillators are analyzed for stable single-mode pump radiation. Single-axial-mode operation is observed on idler and signal for both pulsed and continuous pumping. Projections are made for tuning parameter tolerances required to maintain stable single frequency oscillation. Continuous frequency tuning is possible by the simultaneous adjustment of two or three parameters thus allowing synthesis of specific frequencies within the broad tuning range of the doubly resonant optical parametric oscillator.

I. Introduction

An analysis of the frequency tuning properties of doubly resonant optical parametric oscillators (DROs) based on both experimental observations and theoretical modeling is presented. Specific details in this presentation of frequency control and synthesis apply to monolithic DROs constructed from $LiNbO_3$. Where possible, however, results are given with more general applicability. The purpose is to gain a quantitative understanding of the conditions required for stable single-axial-mode parametric oscillation and the resulting frequency stability of the DRO output. Approaches to frequency synthesis and continuous frequency tuning based upon the simultaneous adjustment of two or three tuning variables are described.

The potential of optical parametric oscillators (OPOs) for the generation of tunable coherent radiation was recognized more than twenty-five years ago.[1] The complex tuning properties of the DRO were also realized in early demonstrations and analyses.[2,3,4] Optical parametric oscillation has been discussed in detail in a number of reviews,[5,6,7] and it is a subject treated in more general terms in a number of books that discuss nonlinear optics.[8] Improvements in the quality of nonlinear optical materials and the coherence of pump sources have lead to a number of advances in the performance of OPOs. Using recent experimental results obtained with stable single-mode pump sources and monolithic DROs constructed from high-quality $LiNbO_3$ nonlinear optical material, we are able to apply and extend the earlier analyses.

Resonating both the signal and idler frequencies, double resonance, offers an advantage of lower threshold for parametric oscillation than single resonance. Double resonance also provides additional frequency selectivity in OPO operation. These desirable properties of double resonance, however, come with a considerable increase in the complexity of tuning and more restrictive tolerances on pump stability and cavity stability. Diode pumped solid-state lasers provide the required pump frequency stability, and monolithic cavities provide the required mechanical stability in the OPO. Continuous tuning is difficult in DROs, which typically tune in axial mode hops and cluster jumps over hundreds of axial modes. Nevertheless, with improved pump sources and nonlinear optical materials coupled with multiple parameter control, DROs can in principle be operated stably and tuned continuously thus widening their range of applications.

DROs have the capability to provide highly coherent output reproducing the statistical properties of the pump with very little additional noise. This has been shown theoretically by Graham and Haken [9] in a quantum mechanical analysis of the DRO, and it has been demonstrated in experimental measurements of the coherence properties of the DRO. The quantum mechanical analysis showed that the diffusion of the sum of the signal and idler wave phases follow the phase diffusion of the pump wave adiabatically. Although the phase difference of the signal and idler may diffuse in an undamped manner, the statistical properties of a DRO are basically the same as those of an ideal laser. A result of these properties is the addition of only a small amount of phase noise in the output of the DRO above that present in the pump. This has been confirmed in coherence measurements of the output of a cw DRO.[10] For periods of approximately one minute, the free-running DRO which was not servo-locked would oscillate on a single mode pair without a mode hop. That the DRO did not add significant excess linewidth over that present on the pump was demonstrated with the measurement of beating between the DRO output and an independent diode-laser-pumped solid-state laser during the periods between mode hops. The beatnote linewidth was 13 kHz, which was the expected value for the typically 10-kHz linewidths of the pump laser and independent reference laser. Additional coherence measurements showed that the signal and idler were phase-anticorrelated when referenced to the pump laser. Also, the width of the signal-idler beatnote with the DRO near but not at degeneracy was less than 1 kHz. The signal-idler beatnote indicates the frequency fluctuations added to the DRO output in addition to those present on the pump.

The results of the classical stationary analysis presented here are consistent with the earlier analyses and measurements. The main point of this presentation is to explain the complex tuning properties of the DRO to more fully utilize its remarkable coherence and spectral properties. The theoretical presentation of section II begins in part A with a qualitative overview of DRO tuning. This overview is used to establish the extensive terminology required for this discussion. In part B of section II, the threshold condition for parametric oscillation is reviewed and recast in terms more easily adopted to tuning calculations. The theoretical

basis of frequency selection is discussed in part C of section II. Experimental tuning data is presented in section III. The degree to which our theoretical model describes the observed tuning allows some confidence in using it for predictive calculations treated in section IV. Results are summarized and discussed in section V. Finally, the properties of MgO:LiNbO3 required to model the experimental data are reviewed in an appendix.

II. Theory

A. DRO tuning overview

A nonlinear optical material pumped by intense optical radiation at frequency ω_p can provide gain at two lower frequencies called signal and idler and related by the conservation of energy condition

$$\omega_p = \omega_s + \omega_i . \qquad (1)$$

The parametric interaction is phase dependent, and proper phasing is required for energy to flow from the from the pump field to the signal and idler fields. Phase velocity matching assures that the relative phases of the three waves do not change with propagation through the nonlinear material. Phase matching is described by the wavevector mismatch, which for the case of collinear propagation can be expressed by the scalar relationship

$$\Delta k = k_p - k_s - k_i = (n_p\omega_p - n_s\omega_s - n_i\omega_i)/c , \qquad (2)$$

where k_p, k_s, and k_i are the respective wavevectors magnitudes of the pump, signal and idler waves, with corresponding indices of refraction given by n_p, n_s, and n_i, and where c is the velocity of light. Useful parametric gain exists in the range of signal and idler frequencies for which $|\Delta k| \lesssim \pi/l$ where l is the length of the nonlinear material. The parametric gain is maximum near $\Delta k = 0$. Phase matching is often achieved by controlling the birefringence of a nonlinear crystal through temperature or angle of propagation.

An OPO requires feedback at either or both signal or idler frequencies. If there is feedback at only one frequency, the device is called a singly resonant oscillator (SRO). Doubly resonant oscillators (DROs) have feedback at both signal and idler frequencies. Feedback can be provided by placing the nonlinear material in a cavity formed by two external mirrors, or in the case of monolithic OPOs, highly reflecting coatings can be applied directly to the nonlinear material. Ring cavity configurations offer advantages of reduced feedback to the pump source and improved OPO conversion efficiency.[11] Figure 1 illustrates schematically several configurations for parametric oscillators. Both standing wave and ring cavity monolithic DROs were used for the experimental observations described in this paper. The tuning properties were quite similar, and the same model of tuning properties could be used for both because the return path length differed little from the gain path in the ring resonators.

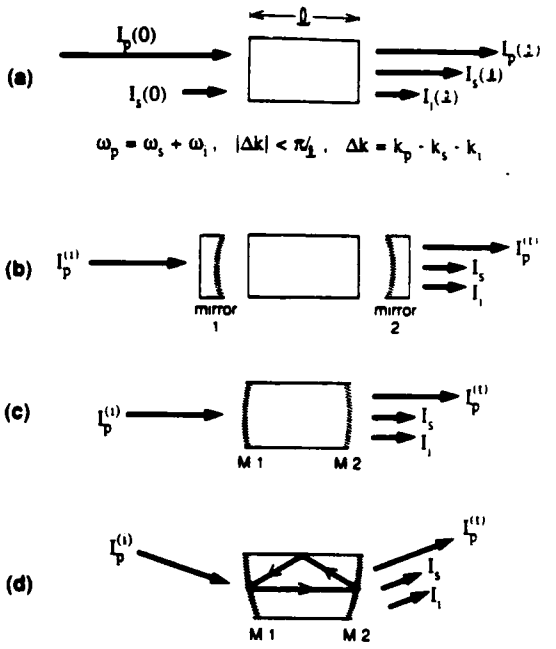

Fig. 1. (a) Schematic representation of optical parametric amplification. Optical parametric oscillators can be formed by the addition of mirrors separate from the nonlinear material as shown in (b). Monolithic oscillators (c),(d) with highly reflecting coatings applied directly to the nonlinear material have advantages of low loss and stability important in stable, single-frequency DRO operation. Ring oscillators (d) offer the advantages reduced feedback and improved conversion efficiency over standing wave oscillators.

Phase matching is the major factor in determining broad tuning properties of an OPO although cavity resonances have the major effect on details of frequency tuning. The conditions $\omega_p = \omega_s + \omega_i$ and $\Delta k = 0$ define phase-matching curves. The most commonly shown OPO phase-matching curve is the parabola-like shape for type-I phase matching in a birefringent crystal, for which the signal and idler waves have the same polarization and the pump wave has the orthogonal polarization. Figure 2a shows a near degeneracy ($\omega_s \sim \omega_i$) section of the temperature tuning curve for a $LiNbO_3$ noncritically-phase-matched OPO. Propagation is along a crystal principal axis in noncritical phase matching which reduces dependence on propagation direction and eliminates birefringent walkoff.

The spectral width of the parametric gain is also determined by phase matching. A typical spectral distribution for single pass gain at a fixed temperature is shown in Fig. 2b. A DRO has the additional requirement of simultaneous signal and idler resonance. Dispersion results in different cavity axial mode frequency spacings for the two waves, and the simultaneous resonance condition thus occurs only at intervals in frequency. The regions of simultaneous resonance, called cluster frequencies, are indicated in Fig. 2c. Early DROs were observed to oscillate on a group or cluster of adjacent cavity axial modes. The

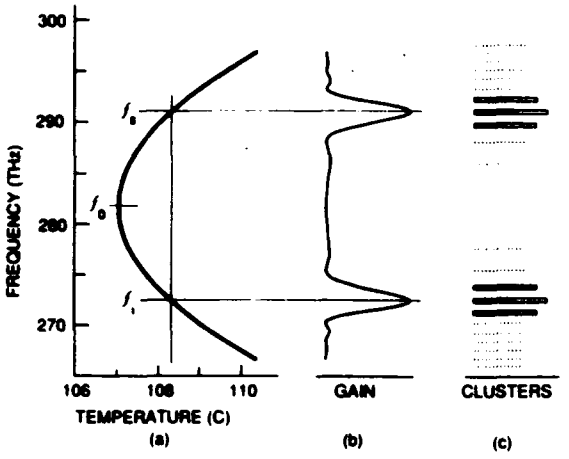

Fig. 2. (a) A typical OPO tuning curve near the degeneracy frequency $f_0 = f_p/2$ where f_p is the pump frequency. The signal and idler frequencies are shown for a $LiNbO_3$ OPO as a function of tuning parameter, in this case temperature. For a fixed value of tuning parameter, single-pass parametric gain exists in bands centered on the phase-matching wavelengths as shown in (b). DROs have an added constraint that the signal and idler cavity resonances must coincide in satisfying the condition $f_p = f_s + f_i$, which results in output at cluster frequencies (c). Only two or three clusters, represented by open lines, are located within the gain bandwidth. Usually one cluster, represented by the longest line, dominates.

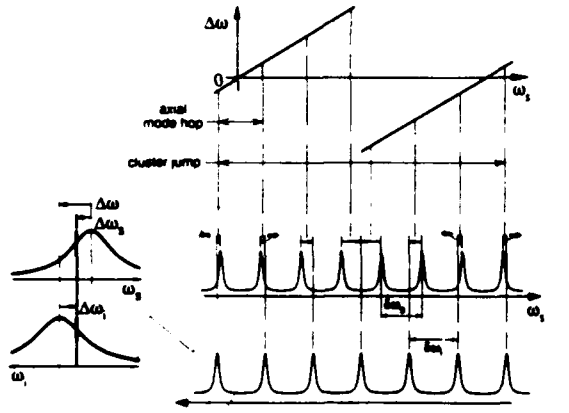

Fig. 3. A diagram [ref. 2] that shows the relationship between the DRO signal and idler resonance frequencies and the conservation of energy condition. Signal resonances are plotted as a function of signal frequency ω_s on an ordinary linear scale with frequency increasing from left to right. The idler frequency scale is determined by that of the signal and the relationship $\omega_p = \omega_s + \omega_i$. In the display of idler resonances, therefore, frequency increases from right to left. A signal-idler pair that has both resonances centered on a vertical line are in coincidence for satisfying $\omega_p = \omega_s + \omega_i$. In general there will be some frequency mismatch $\Delta\omega$ for each mode pair. The frequency mismatch is the frequency shift required of either signal or idler resonance to produce coincidence. The detail on the left shows shows the frequency mismatch $\Delta\omega$ for a mode pair and its components $\Delta\omega_s$ and $\Delta\omega_i$ which are the respective frequency displacements from the centers of the signal and idler cavity resonances to the frequencies most favorable for parametric oscillation. Dispersion is exaggerated in this schematic representation. There are typically hundreds of cavity axial modes between the cluster frequencies where $\Delta\omega = 0$.

wavelength of the cluster would at first shift continuously with tuning followed by a discontinuous jump to another cluster of modes. The curves of Fig. 2 are intended to illustrate some general properties of frequency tuning of DROs. They were calculated for the 12.5-mm-long monolithic $MgO:LiNbO_3$ oscillators pumped at 564 THz (532 nm) that are discussed in this paper.

A useful device for understanding the requirement of simultaneous cavity resonances is a diagram used by Giordmaine and Miller [2] in which the cavity resonances near the oscillating signal and idler frequencies are plotted as a function of the respective frequencies as shown schematically in Fig. 3. The difference between signal and idler axial mode spacings, $\delta\omega_s$ and $\delta\omega_i$, respectively, is exaggerated in this figure for the purpose of illustration. One frequency, here the signal, increases going from left to right. The other frequency scale, the idler, is determined by the first scale and the conservation of energy condition in such a way that a vertical line drawn through the diagram will give signal and idler frequencies that satisfy Eq. (1). If a signal-idler resonance pair lie on a vertical line, they satisfy the simultaneous resonance condition. If temperature or dc electric field applied to the crystal is changed, the position of the resonances will advance along the scales, one to the left and the other to the right, at slightly different rates due to dispersion, but the scales will not change. If pump frequency is changed, the frequencies of the cavity resonances will not change, but one of the frequency scales will be displaced with respect to the other, and the respective resonances will move with that scale.

Two types of discontinuous frequency shifts are indicated in Fig. 3. One is an axial mode hop, and the other is a cluster jump. As a tuning variable is changed, better coincidence in satisfying the conservation of energy condition is attained on adjacent signal and idler axial modes. It then becomes advantageous for the oscillation frequencies to hop to the adjacent modes, one higher in

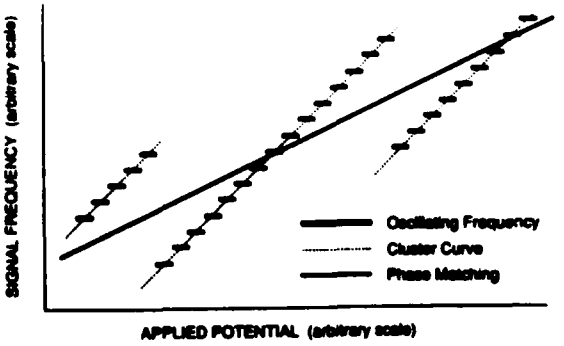

Fig. 4. A schematic representation of a detailed portion of an idealized tuning curve for a DRO. Oscillation progresses along cluster curves in discontinuous frequency changes called axial mode hops as a tuning variable is changed. A larger discontinuous frequency change of a cluster jump occurs when better phase matching exists on an adjacent cluster curve.

frequency and the other lower. This type of discontinuous frequency change is referred to as a mode hop. Other factors such as phase matching also effect the selection of the oscillation frequencies. As the tuning variable changes, phase matching also changes, and at some point the oscillator finds it advantageous to jump to the next cluster. This is illustrated in the schematic tuning curve of Fig. 4. The signal or idler oscillation frequency progresses along a cluster curve in a series of mode hops until another cluster curve more closely approaches phase matching. At that point the larger discontinuous frequency change of a cluster jump takes the oscillation to the next cluster curve. Figures 3 and 4 are only schematic with dispersion greatly exaggerated. Typically there several hundred axial modes between adjacent cluster frequencies.

Simultaneous resonance of signal-idler mode pairs occurs as a tuning parameter is continuously adjusted. In general, however, coincidence is not perfect, and oscillation of a particular mode pair depends on the degree of frequency matching and phase matching. The frequency mismatch $\Delta\omega$ of a signal-idler mode pair can be defined as the shift in frequency required of either signal or idler to bring the two resonances into coincidence to satisfy Eq. (1). It is convenient to express the frequency mismatch as the sum of two components

$$\Delta\omega = \Delta\omega_s + \Delta\omega_i \,. \tag{3}$$

Here $\Delta\omega_s$ is the frequency shift from the peak of the signal resonance to the signal frequency most favorable for oscillation for that mode pair. Correspondingly $\Delta\omega_i$ is the frequency shift from the peak of the idler resonance to the idler frequency most favorable for oscillation as illustrated in Fig. 3. The signal component is measured on the signal frequency scale, and the idler component is measured on the idler frequency scale. The directions of these scales are opposite. One increases from left to right and the other is reversed increasing from right to left. Therefore, $\Delta\omega_s$ and $\Delta\omega_i$ appear in opposite directions in this illustration, even though they have the same sign. The frequency displacements of the signal and idler from their respective resonance peaks are discussed in detail in part C of this section. It is useful to first consider the dependence OPO threshold on frequency mismatch and phase mismatch.

B. DRO threshold with imperfect signal-idler frequency coincidence

Even a very small frequency mismatch can have significant effects on frequency selection and threshold of the DRO, particularly when cavity finesse is high. The threshold relationship obtained here is the same as that derived in the quantum mechanical analysis of Graham and Haken [10] and similar to but more detailed than the threshold equation given by Giordmaine and Miller.[2] The result given here is in terms of classical electromagnetic theory and more easily applied to the tuning analysis that follows. This threshold relationship is limited to cavities with moderate to infinitesimal losses. The effect of phase and frequency mismatch on the thresholds of DROs with arbitrary cavity losses was addressed by Falk.[12] That result is used to estimate the conditions over which the threshold equation used here is appropriate.

The threshold for oscillation is obtained by setting the parametric gain equal to the cavity losses. The electric field of the pump, signal and idler waves are expressed in terms of complex amplitude and exponentials

$$E_j(z,t) = \frac{1}{2}\left\{E_j(z)\exp i\,(k_j z - \omega_j t) + \text{c.c.}\right\},$$

where the subscript j indicates signal, idler or pump, k is the wavevector, ω is the angular frequency, z is the coordinate in the direction of propagation, and t is time. The coupled equations describing parametric amplification of monochromatic plane waves traveling in the z-direction are [7]

$$\frac{dE_s}{dz} = i\,\kappa_s E_p E_i^{*}\exp(i\,\Delta k\, z)\,, \tag{4a}$$

$$\frac{dE_i}{dz} = i\,\kappa_i E_p E_s^{*}\exp(i\,\Delta k\, z)\,, \tag{4b}$$

$$\text{and}\quad \frac{dE_p}{dz} = i\,\kappa_p E_s E_i\exp(-i\,\Delta k\, z)\,, \tag{4c}$$

where MKS units are used and

$$\kappa_s = \frac{\omega_s d_{\text{eff}}}{n_s c}\,,\quad \kappa_i = \frac{\omega_i d_{\text{eff}}}{n_i c}\,,\quad \text{and}\quad \kappa_p = \frac{\omega_p d_{\text{eff}}}{n_p c}$$

with n_s, n_i, and n_p the respective refractive indices for signal, idler, and pump, c the velocity of light, and d_{eff} the effective nonlinear optical coefficient. The solution used here assumes that, at threshold, pump depletion is insignificant, and the respective changes in signal and pump amplitudes, ΔE_s and ΔE_i, are small compared to the amplitudes. Hence, E_s and E_i are treated as constant in calculating the changes, that is,

$$\Delta E_s = i\,\kappa_s E_p E_i^{*} l\ \text{sinc}(\Delta k\, l/2) \tag{5a}$$

$$\text{and}\quad \Delta E_i = i\,\kappa_i E_p E_s^{*} l\ \text{sinc}(\Delta k\, l/2)\,. \tag{5b}$$

The length of the nonlinear crystal is again given by l, and the sinc function is defined by $\text{sinc}(x) = \sin(x)/x$.

For the low loss doubly resonant oscillators considered here, Eqs. (5) are adequate to model the parametric gain. Other solutions to Eqs. (4) included general monochromatic-plane-wave solutions that allow both pump depletion and arbitrary changes in E_s and E_i [13] and somewhat more restrictive solutions which assume no pump depletion but with arbitrarily large changes in E_s and E_i .[5,7] The latter was used in [12] for threshold analysis of DROs with arbitrary strength of resonance.

The parametric gain must compensate for both a decrease in amplitude and for the phase change due to propagation in the cavity. The phasor diagram shown in Fig. 5 helps illustrate this discussion. After a round trip cavity transit, the signal electric field amplitude is reduced by a factor $(1-a_s)$, and the phase is shifted by an angle ψ_s. Similarly, the idler amplitude is reduced by $(1-a_i)$, and the phase is shifted by ψ_i. At threshold this change is balanced

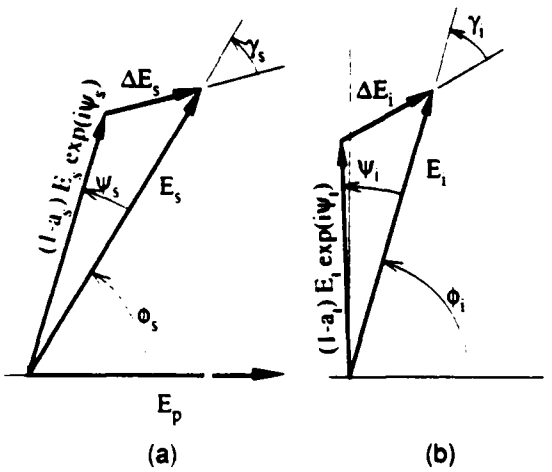

Fig. 5. Phasor diagrams schematically show amplitude losses, a_s and a_i, and phase shifts, ψ_s and ψ_i, after one round-trip cavity transit for signal an idler respectively. At threshold the increments of electric field amplitude added by optical parametric amplification, ΔE_s and ΔE_i, must restore the original fields.

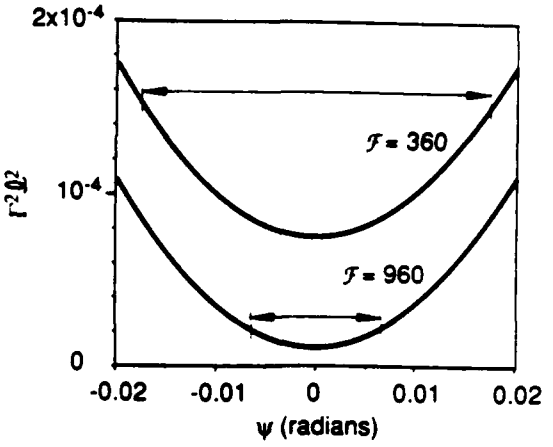

Fig. 6. A comparison of the thresholds for DROs with different cavity finesse. Thresholds are calculated as a function of the sum of the cavity-round-trip phase shifts ψ using Eq. (12) for two DROs with cavity finesse $\mathcal{F}_s = \mathcal{F}_i = 360$ and $\mathcal{F}_s = \mathcal{F}_i = 960$. The shape of the curve does not change, but the width defined as the region over which threshold is less than twice its minimum value decreases for higher finesse.

by the increments of electric field ΔE_s and ΔE_i added by the parametric interaction:

$$(1 - a_s)\exp(i\,\psi_s)\,E_s + \Delta E_s = E_s \quad , \tag{6a}$$

and $$(1 - a_i)\exp(i\,\psi_i)\,E_i + \Delta E_i = E_i \quad . \tag{6b}$$

Choosing time so that the pump amplitude is real $E_p = |E_p|$, expressing the signal and idler amplitudes as $E_s = |E_s|\exp(i\,\phi_s)$ and $E_i = |E_i|\exp(i\,\phi_i)$, and applying the conditions that a_s, a_i, ψ_s, and ψ_i all are small, Eqs. (6) can be written as

$$\Delta E_s = |E_s|\sqrt{a_s^2+\psi_s^2}\;\exp(i\,\phi_s - i\,\gamma_s) \tag{7a}$$

and $$\Delta E_i = |E_i|\sqrt{a_i^2+\psi_i^2}\;\exp(i\,\phi_i - i\,\gamma_i) \quad , \tag{7b}$$

where $\gamma_s = \tan^{-1}(\psi_s / a_s)$ and $\gamma_i = \tan^{-1}(\psi_i / a_i)$.

Substituting Eqs. (7) into Eqs. (4) results in two equations for the complex arguments and two equations for the magnitudes. The relationships for the complex arguments,

$$\phi_s + \phi_i = \gamma_s + \pi/2 \tag{8a}$$

and $$\phi_s + \phi_i = \gamma_i + \pi/2 \quad , \tag{8b}$$

immediately yield $\gamma_s = \gamma_i$ for the stationary solution or

$$\frac{\psi_s}{a_s} = \frac{\psi_i}{a_i} \quad . \tag{9}$$

Note that this is consistent with the result that the sum of the signal and idler phases are constant when referenced to the phase of the pump for stable single-mode-pair operation.[10]

The sum of the unpumped-cavity-round-trip phase shifts,

$$\psi = \psi_s + \psi_i \quad , \tag{10a}$$

is useful for the purpose of comparison with the results of ref. [12] and for conversion to frequency mismatch. Combining Eqs. (9) and (10a), the individual phase shifts can be expressed in terms of the sum by

$$\psi_s = \frac{a_s}{a_s + a_i}\,\psi \tag{10b}$$

and $$\psi_i = \frac{a_i}{a_s + a_i}\,\psi \quad . \tag{10c}$$

The threshold equation is obtained by taking the product of the two equations for the magnitudes that are obtained when Eqs. (7) are substituted into Eqs. (4) with the result

$$\sqrt{(a_s^2+\psi_s^2)(a_i^2+\psi_i^2)} = \kappa_s\kappa_i E_p^{\,2} l^2 \mathrm{sinc}^2(\Delta k\, l/2)$$

$$= \Gamma^2 l^2 \mathrm{sinc}^2(\Delta k\, l/2) \quad . \tag{11}$$

The quantity Γ^2 is the parametric gain for perfect phase matching, and it is proportional to the pump intensity.[7] Using Eqs. (10b) and (10c), the threshold relationship given by Eq. (11) can be written in the form

$$\Gamma^2 l^2 = \frac{a_s a_i}{\mathrm{sinc}^2(\Delta k\, l/2)}\left\{1 + \frac{\psi^2}{(a_s+a_i)^2}\right\} \quad . \tag{12}$$

Figure 6 shows the DRO threshold parameter $\Gamma^2 l^2$ as a function of the phase shift sum ψ as given by Eq. (12) for

two sets of cavity losses $a_s = a_i = 0.0087$ and $a_s = a_i = 0.0033$ corresponding to finesse values $\mathcal{F} = 360$ and $\mathcal{F} = 960$ of the DROs used in the experimental measurements. The shape of the threshold curve does not change significantly, but the minimum value is translated toward zero as the losses decrease. The width of the threshold curves defined as the region over which threshold is less than twice the minimum value, therefore, decreases as cavity losses decrease.

In the application of Eq. (12), thresholds are expressed in terms of cavity finesse because it is easier to measure the ratio of resonance width to spacing than it is to directly measure losses. A comparison of the above analysis with that of a parallel plate interferometer [14] or optical cavities in general [15] shows that the amplitude loss coefficients, a_s and a_i, are related to the cavity finesse at signal and idler frequencies, $\mathcal{F}_s$ and $\mathcal{F}_i$ respectively, by

$$\mathcal{F}_s \approx \pi / a_s \quad \text{and} \quad \mathcal{F}_i \approx \pi / a_i \ . \tag{13a,b}$$

It is also more convenient to use frequency mismatch than phase shift. The components of the frequency mismatch are related to the phase shifts by

$$\Delta\omega_s = \frac{\delta\omega_s \psi_s}{2\pi} \quad \text{and} \quad \Delta\omega_i = \frac{\delta\omega_i \psi_i}{2\pi} \ . \tag{14a,b}$$

Combining Eqs. (12), (13), (14), and (3) the threshold equation becomes

$$\Gamma^2 l^2 = \frac{\pi^2}{\mathcal{F}_i \mathcal{F}_s \operatorname{sinc}^2(\Delta k\, l/2)} \left\{ 1 + \left(\frac{2\Delta\omega \mathcal{F}_i \mathcal{F}_s}{\mathcal{F}_i \delta\omega_s + \mathcal{F}_s \delta\omega_i} \right)^2 \right\} \ . \tag{15}$$

The threshold relationship given by Eqs. (12) or (15) agrees with other threshold expressions under appropriate conditions. This result was obtained using a first-order-plane-wave approximation for parametric gain. In the case of perfect phase matching $\Delta k = 0$ and no frequency mismatch $\Delta\omega = 0$, these equations reduce to $\Gamma^2 l^2 = a_s a_i$, which is the result obtained directly for this case.[7] Focusing and coupling to cavity modes [16] must be considered for quantitative threshold calculations. The plane-wave derivation of threshold is adequate for the analysis of tuning where it is required only to know the relative dependence of threshold on Δk and $\Delta\omega$.

There is also agreement with the central result of Falk's analysis [12] in the limit of high cavity finesse, that is, $a_s \ll 1$ and $a_i \ll 1$. Rewritten in the notation used here, Falk's Eq. (9) becomes

$$\frac{\Gamma^2 l^2}{2} = \frac{B \sin\left\{ 2\tan^{-1}\left(\frac{\sin\psi}{C + \cos\psi} \right) - \psi \right\}}{\sin\left\{ \tan^{-1}\left(\frac{\sin\psi}{C + \cos\psi} \right) \right\} \operatorname{sinc}^2\left(\frac{\Delta k\, l}{2} \right)} - \frac{1}{\operatorname{sinc}^2\left(\frac{\Delta k\, l}{2} \right)} \tag{16}$$

where, defining $R_s = 1 - a_s$ and $R_i = 1 - a_i$,

$$B = \frac{R_i (1 - R_s^2)}{R_i^2 - R_s^2} \quad \text{and} \quad C = \frac{R_s}{R_i} \frac{1 - R_i^2}{1 - R_s^2} \ .$$

Equation (16) is a more accurate approximation of DRO threshold applicable for arbitrary cavity loss. However, it is unwieldy and must be evaluated as a limit when $\psi = 0$ or when $a_s = a_i$. Evaluation of Eq. (12) yields threshold values that differ from those obtained from Eq. (16) by approximately the fraction $\sqrt{a_s a_i}$. There is a fortuitous partial compensation for this disparity in the approximation for finesse given in Eqs. (13). For $\mathcal{F}_s = \mathcal{F}_i = 5$, the difference between Eqs. (15) and (16) is less than 13% at the frequency mismatch for which threshold is twice its minimum value, and the difference decreases with decreasing frequency mismatch. For $\mathcal{F}_s = \mathcal{F}_i = 10$, the difference is 4% at twice minimum threshold, and the agreement again improves as minimum threshold is approached.

Equations (12) or (15) could be used directly to determine the mode pair with lowest threshold for oscillation. It is more convenient, however, to restrict the possible mode pairs on which oscillation may take place to a small number based on frequency mismatch and wavevector mismatch considerations. This is done in the next section where it is shown that there are three mode pairs in the phase-matching bandwidth for which the frequency mismatch is a minimum. Which of these three mode pairs has the lowest threshold depends on the respective values of Δk and $\Delta\omega$ and the cavity finesse.

C. Frequency selection in the DRO

The selection of signal and idler frequencies in a cw DRO operating on a single mode pair is determined by two conditions: the conservation of energy stated in Eq. (1), and minimum threshold for oscillation. An approximation for the threshold condition was given in Eq. (15). The conservation of energy condition becomes implicit in the analysis of the condition of minimum threshold. In this analysis it is convenient to follow the approach used by Boyd and Ashkin [3] and define the signal and idler axial mode numbers

$$m_s = 2l n_s / \lambda_s = l\, n_s \omega_s / (\pi c) \tag{17a}$$

and $$m_i = 2l n_i / \lambda_i = l\, n_i \omega_i / (\pi c) \ , \tag{17b}$$

which are continuous variables taking on integer values at cavity resonances. The free space wavelengths of the signal and idler are given by λ_s and λ_i respectively, and $2ln_s$ and $2ln_i$ are the respective optical lengths for a round-trip cavity transit. The free spectral ranges or mode spacings of the signal idler resonances, $\delta\omega_s$ and $\delta\omega_i$ respectively, are the frequency changes which change the mode numbers m_s and m_i by one, that is, [4]

$$\frac{\partial m_s}{\partial \omega_s} = \frac{l}{\pi c} \left(n_s + \omega_s \frac{\partial n_s}{\partial \omega_s} \right) = \delta\omega_s^{-1} \tag{18a}$$

and $$\frac{\partial m_i}{\partial \omega_i} = \frac{l}{\pi c}\left(n_i + \omega_i \frac{\partial n_i}{\partial \omega_i}\right) = \delta \omega_i^{-1} \ . \qquad (18b)$$

The sum of the mode numbers

$$m = m_s + m_i \ , \qquad (19)$$

which is also a continuous variable, is useful for the description of cluster effects. A pair of signal and idler frequencies which satisfy Eq. (1) and for which m is an integer are called cluster frequencies. In general, cavity resonances are not located precisely at the cluster frequencies. Only the sum $m_s + m_i$ must be an integer at the cluster frequencies; the individual mode numbers in general differ from integers by amounts equal in magnitude but opposite in sign. The cavity resonance pairs most closely satisfying the conservation of energy condition, and therefore most favorable for oscillation, are also the resonances for which m is most nearly an integer. Equivalently, oscillation frequencies of a DRO are displaced from a frequency pair at which m is integer by no more than one-half of the respective axial mode spacings, whereas there are typically hundreds of modes between between adjacent signal or idler cluster frequencies at which m is integer.

Two further quantities useful for the description of the mode hops and cluster jumps of DRO tuning, Δm and Δm_s, are obtained by subtracting the integer nearest the mode number from the mode number:

$$\Delta m = m - \text{ROUND}(m) \qquad (20a)$$

and $$\Delta m_s = m_s - \text{ROUND}(m_s) \ . \qquad (20b)$$

These parameters are used in the calculation of oscillation frequencies and tuning variable tolerances.

At optimum operating conditions, the parameters Δk, Δm, *and* Δm_s will all be zero indicating perfect phase matching and simultaneous cavity resonances at the desired signal and idler frequencies. Adjustment of three independent parameters is required to reach this condition. The discussion presented here is given in general terms using parameters Δk, m, *and* m_s and in specific terms of the tuning or control parameters used in the experimental observations. The experimental observations use temperature T and applied potential V as adjustable parameters to control the variable parameter signal frequency ω_s. Pump frequency ω_p is used as the required third adjustable parameter for the calculations. Simple Taylor's expansions for Δk, m, *and* m_s were found adequate to model the observed frequency tuning:

$$\Delta k = \left(\frac{\partial \Delta k}{\partial \omega_s}\right)_{\omega_p} (\omega_s - \omega_{s,0}) + \frac{1}{2}\left(\frac{\partial^2 \Delta k}{\partial \omega_s^2}\right)_{\omega_p} (\omega_s - \omega_{s,0})^2$$

$$+ \left(\frac{\partial \Delta k}{\partial \omega_p}\right)_{\omega_s} (\omega_p - \omega_{p,0}) + \frac{\partial \Delta k}{\partial T}(T - T_0) + \frac{\partial \Delta k}{\partial V} V + \Delta k_0 \ , \qquad (21)$$

$$m = \left(\frac{\partial m}{\partial \omega_s}\right)_{\omega_p} (\omega_s - \omega_{s,0}) + \frac{1}{2}\left(\frac{\partial^2 m}{\partial \omega_s^2}\right)_{\omega_p} (\omega_s - \omega_{s,0})^2$$

$$+ \left(\frac{\partial m}{\partial \omega_p}\right)_{\omega_s} (\omega_p - \omega_{p,0}) + \frac{\partial m}{\partial T}(T - T_0) + \frac{\partial m}{\partial V} V + m_0 \ , \qquad (22)$$

and

$$m_s = \frac{\partial m_s}{\partial \omega_s}(\omega_s - \omega_{s,0}) + \frac{1}{2}\frac{\partial^2 m_s}{\partial \omega_s^2}(\omega_s - \omega_{s,0})^2$$

$$+ \frac{\partial m_s}{\partial T}(T - T_0) + \frac{\partial m_s}{\partial V} V + m_{s,0} \ . \qquad (23)$$

Second order is used for signal frequency because the first order derivatives $(\partial \Delta k/\partial \omega_s)_{\omega_p}$ and $(\partial \Delta m/\partial \omega_s)_{\omega_p}$ become zero at degeneracy, and dispersion of $\partial m_s/\partial \omega_s$ is essential to the analysis.

The notation of a partial derivative in parentheses with a parameter subscript to the right parenthesis indicates that the parameter of the subscript is held constant for the differentiation. The conservation of energy condition is introduced through this device. Consider a function which is dependent on the signal, idler and pump frequencies $f = f(\omega_s, \omega_i, \omega_p)$ and require that the conservation of energy condition $\omega_s + \omega_i = \omega_p$ holds. Differentiation with respect to ω_s with ω_p held constant requires that as ω_s is increased ω_i must decrease, or

$$\left(\frac{\partial f}{\partial \omega_s}\right)_{\omega_p} = \frac{\partial f}{\partial \omega_s} - \frac{\partial f}{\partial \omega_i} \ ,$$

and similarly, $$\left(\frac{\partial f}{\partial \omega_p}\right)_{\omega_s} = \frac{\partial f}{\partial \omega_p} + \frac{\partial f}{\partial \omega_i} \ .$$

The derivatives used in Eqs. (21), (22) and (23) are expanded in Table I. The differentiation is straight forward and can be verified by inspection of Eqs. (2), (17) and (19).

1. The phase-match curve and the cluster curves

A number of equations considered below are identical except for exchange of the tuning variable. An economy of notation is possible using a general tuning parameter ζ, which is T, V or ω_p in the specific example or more generally any single parameter used to tune a DRO. A phase-matching curve as used here gives the signal frequency for which $\Delta k = 0$ as a function of tuning parameter ζ, and is denoted by $\omega_{s,PM}(\zeta)$. This curve is obtained from Eq. (21) or a similar equation by setting the other adjustable parameters to fixed values and setting $\Delta k = 0$. The cluster curves $\omega_{s,Cl}(\zeta)$ give the signal cluster frequencies as a function of the tuning parameter ζ. The cluster curves can be obtained from Eq. (22) or a similar equation by setting m to integer values and again setting the other adjustable parameters to fixed values. For type-I phase matching, the phase-matching curve is a parabola-like curve as shown in

TABLE I. Derivatives used to calculate tuning of a monolithic DRO.

$$\frac{\partial^2 m_s}{\partial \omega_s^2} = \frac{l}{\pi c}\left(2\frac{\partial n_s}{\partial \omega_s} + \omega_s \frac{\partial n_s^2}{\partial \omega_s^2}\right)$$

$$\frac{\partial m_s}{\partial T} = \frac{l\,\omega_s}{\pi c}\frac{\partial n_s}{\partial T} + \frac{\omega_s n_s}{\pi c}\frac{\partial l}{\partial T}$$

$$\frac{\partial m_s}{\partial V} = \frac{\omega_s}{\pi c}\left(n_s \frac{\partial l}{\partial V} + l\frac{\partial n_s}{\partial V}\right)$$

$$\left(\frac{\partial m}{\partial \omega_s}\right)_{\omega_p} = \frac{l}{\pi c}\left(n_s - n_i + \omega_s \frac{\partial n_s}{\partial \omega_s} - \omega_i \frac{\partial n_i}{\partial \omega_i}\right)$$

$$\left(\frac{\partial^2 m}{\partial \omega_s^2}\right)_{\omega_p} = \frac{l}{\pi c}\left\{2\left(\frac{\partial n_s}{\partial \omega_s} + \frac{\partial n_i}{\partial \omega_i}\right) + \omega_s \frac{\partial^2 n_s}{\partial \omega_s^2} + \omega_i \frac{\partial^2 n_i}{\partial \omega_i^2}\right\}$$

$$\left(\frac{\partial m}{\partial \omega_p}\right)_{\omega_s} = \frac{l}{\pi c}\left(n_i + \omega_i \frac{\partial n_i}{\partial \omega_i}\right)$$

$$\frac{\partial m}{\partial T} = \frac{l}{\pi c}\left(\omega_s \frac{\partial n_s}{\partial T} + \omega_i \frac{\partial n_i}{\partial T}\right) + \frac{1}{\pi c}\left(\omega_s n_s + \omega_i n_i\right)\frac{\partial l}{\partial T}$$

$$\frac{\partial m}{\partial V} = \frac{n_s \omega_s + n_i \omega_i}{pc}\frac{\partial l}{\partial V} + \frac{l}{\pi c}\left(\omega_s \frac{\partial n_s}{\partial V} + \omega_i \frac{\partial n_i}{\partial V}\right)$$

$$\left(\frac{\partial \Delta k}{\partial \omega_s}\right)_{\omega_p} = \left(n_i - n_s + \omega_i \frac{\partial n_i}{\partial \omega_i} - \omega_s \frac{\partial n_s}{\partial \omega_s}\right)/c = -\frac{\pi}{l}\left(\frac{\partial m}{\partial \omega_s}\right)_{\omega_p}$$

$$\left(\frac{\partial^2 \Delta k}{\partial \omega_s^2}\right)_{\omega_p} = -\frac{\pi}{l}\left(\frac{\partial^2 m}{\partial \omega_s^2}\right)_{\omega_p}$$

$$\left(\frac{\partial \Delta k}{\partial \omega_p}\right)_{\omega_s} = \left(n_p - n_i + \omega_p \frac{\partial n_p}{\partial \omega_p} - \omega_i \frac{\partial \omega_i}{\partial \omega_i}\right)$$

$$\frac{\partial \Delta k}{\partial T} = \frac{\omega_p}{c}\frac{\partial n_p}{\partial T} - \frac{\omega_s}{c}\frac{\partial n_s}{\partial T} - \frac{\omega_i}{c}\frac{\partial n_i}{\partial T}$$

$$\frac{\partial \Delta k}{\partial V} = \frac{\omega_p}{c}\frac{\partial n_p}{\partial V} - \frac{\omega_s}{c}\frac{\partial n_s}{\partial V} - \frac{\omega_i}{c}\frac{\partial n_i}{\partial V}$$

Fig. 1, and the cluster curves are a family of parabola-like curves. The oscillating frequencies are closest to the cluster curves near the points where the cluster curves intersect the phase-matching curve.

The signal frequency separation of adjacent clusters Ω_s can be obtained from the second-order approximation

$$\Delta m \text{ (cluster)} = \pm 1 = \left(\frac{\partial m}{\partial \omega_s}\right)_{\omega_p} \Omega_{S\pm} + \frac{1}{2}\left(\frac{\partial^2 m}{\partial \omega_s^2}\right)_{\omega_p} \Omega_{S\pm}^2 . \tag{24}$$

Away from degeneracy the first order term dominates, and Eq. (24) is approximated by

$$\Omega_{S\pm} \approx \pm\left(\frac{\partial m}{\partial \omega_s}\right)^{-1}_{\omega_p} = \pm\frac{\delta\omega_i \delta\omega_s}{\delta\omega_i - \delta\omega_s} , \tag{25}$$

in agreement with ref. [4]. Phase-matching limitations result in a gain bandwidth with half maximum values at the frequencies where $\Delta k = \pm 0.886\pi / l \approx \pm \pi / l$ and a corresponding signal frequency full width at half maximum of

$$\Delta\omega_s(\text{Gain-FWHM}) = \left|\frac{2\pi}{l}\left(\frac{\partial \Delta k}{\partial \omega_s}\right)^{-1}_{\omega_p}\right| . \tag{26}$$

In the specific case of the monolithic DRO, for which derivatives are given in Table I, $\pi/l\,(\partial m/\partial\omega_s)_{\omega_p} = -(\partial\Delta k/\partial\omega_s)_{\omega_p}$, and $\Delta\omega_s$(Gain-FWHM) $= 2\,\Omega_S$. Since the frequency separation of the clusters is approximately one-half of the parametric gain bandwidth, there are two or three clusters within the gain bandwidth. This is true for any DRO in which the nonlinear crystal is the only dispersive component and the crystal is traversed twice in each round-trip cavity transit but has parametric gain in only one direction.

2. Oscillation frequencies

The oscillation frequencies are determined by phase matching, the center frequencies of the signal and idler cavity resonances, the frequency mismatch of the resonances, the finesse values of the resonances, and the axial mode spacings. To model experimental observations, the frequencies of the parametric oscillation are calculated with the following procedure. First, the signal frequency for phase matching $\omega_{s,PM}$ is found for specified tuning parameters using the condition $\Delta k = 0$. Next the signal cluster frequency $\omega_{s,Cl}$ closest to $\omega_{s,PM}$ is found using the condition $\Delta m = 0$. If the DRO cavity has only moderate or low finesse, and the precise oscillating frequency and mode hops are not of concern, these two steps are all that is required. The extra resolution of frequency tuning can be obtained from the value of Δm_s at the cluster frequency $\omega_{s,Cl}$. This value is called $\Delta m_{s,Cl}$ to indicate that it is calculated at the cluster frequency $\omega_{s,Cl}$ for the specified tuning conditions. Knowledge of the cavity finesse and mode spacing in addition to the value of $\Delta m_{s,Cl}$ permits the detailed calculation of oscillation frequencies.

The procedure for determining the fine details of tuning is illustrated in Fig. 7. The signal cluster frequency $\omega_{s,Cl}$ obtained by the steps described above is a reference point from which to start. The center of the nearest signal resonance is displaced from $\omega_{s,Cl}$ by frequency $-\Delta m_{s,Cl}\delta\omega_s$ where $\delta\omega_s$ is the signal axial-mode frequency separation. The center of the nearest idler resonance is displaced by $-\Delta m_{i,Cl}\delta\omega_i$ from the complementary idler cluster frequency $\omega_{i,Cl} = \omega_p - \omega_{s,Cl}$ where $\delta\omega_i$ is the idler mode frequency separation and ω_p is the pump frequency. Since $\omega_{s,Cl}$ is a cluster frequency where $\Delta m = 0$, $\Delta m_{i,Cl} = -\Delta m_{s,Cl}$ allowing the frequency mismatch of the signal-idler mode pair to be expressed as

$$\Delta\omega = \Delta m_{s,Cl}\,(\delta\omega_s - \delta\omega_i)\ . \qquad (27)$$

Recall that the frequency mismatch is the shift in frequency of either signal or idler resonance required to bring the resonance pair into coincidence for satisfying the conservation of energy condition.

The displacement of the signal oscillation frequency $\omega_{s,Osc}$ from the center of the signal cavity resonance is $\Delta\omega_s$, and the displacement of the idler oscillation frequency $\omega_{i,Osc}$ from the center of the idler cavity resonance is $\Delta\omega_i$. Using the earlier definitions and conditions imposed on round-trip cavity phase shifts for a stationary solution given in Eqs. (3), (10), (13), and (14), it follows that

$$\Delta\omega_s = \Delta\omega\,\delta\omega_s\mathcal{F}_i\,/\,(\delta\omega_s\mathcal{F}_i + \delta\omega_i\mathcal{F}_s) \qquad (28a)$$

and

$$\Delta\omega_i = \Delta\omega\,\delta\omega_i\mathcal{F}_s\,/\,(\delta\omega_s\mathcal{F}_i + \delta\omega_i\mathcal{F}_s)\ . \qquad (28b)$$

Finally, the signal oscillation frequency is given by the sum of the cluster frequency plus the frequency separation of the signal cavity resonance from the cluster frequency plus the frequency shift from the center of the signal cavity resonance, that is,

$$\omega_{s,Osc} = \omega_{s,Cl} - \Delta m_{s,Cl}\,\delta\omega_s + \Delta\omega_s$$

$$= \omega_{s,Cl} - \Delta m_{s,Cl}\,\frac{\delta\omega_s\delta\omega_i\,(\mathcal{F}_s + \mathcal{F}_i)}{\delta\omega_s\mathcal{F}_i + \delta\omega_i\mathcal{F}_s}\ . \qquad (29)$$

Equations (27) and (28a) are substituted to obtain the second step of Eq. (29).

The tuning rate for a general tuning parameter ζ could be obtained by direct differentiation of Eq. (29), or more simply by considering the tuning rates of the cavity resonances. The tuning rate for the frequency of the signal mode is $-\delta\omega_s\times\partial m_s/\partial\zeta$, and that for the frequency of the idler is $-\delta\omega_i\times\partial m_i/\partial\zeta$. The tuning rates of the cavity resonances are combined to yield the rate of change of the frequency mismatch,

$$\frac{\partial\Delta\omega}{\partial\zeta} = \delta\omega_s\frac{\partial m_s}{\partial\zeta} + \delta\omega_i\frac{\partial m_i}{\partial\zeta} = (\delta\omega_s - \delta\omega_i)\frac{\partial m_s}{\partial\zeta} + \delta\omega_i\frac{\partial m}{\partial\zeta}\ .$$

The tuning rate of the signal oscillation frequency is the sum of tuning rate of the signal resonance plus the fraction $\delta\omega_s\mathcal{F}_i/(\delta\omega_s\mathcal{F}_i + \delta\omega_i\mathcal{F}_s)$ of $\partial\Delta\omega/\partial\zeta$, that is,

$$\frac{\partial\omega_{s,Osc}}{\partial\zeta} = \frac{\delta\omega_s\delta\omega_i}{\delta\omega_s\mathcal{F}_i + \delta\omega_i\mathcal{F}_s}\left(\mathcal{F}_i\frac{\partial m}{\partial\zeta} - (\mathcal{F}_s + \mathcal{F}_i)\frac{\partial m_s}{\partial\zeta}\right)\ . \qquad (30)$$

This tuning is limited to a small range by mode hops or increased cavity losses as the oscillation is pulled off the peaks of the cavity resonances. On a broader scale, tuning progresses along a cluster curve in a series of mode hops. If finesse is high it is possible that the oscillation jumps back and forth between adjacent cluster curves as well as hops from one mode-pair to the next along each of the cluster curves. The analysis of cluster jumps requires the mode-hop structure on two or three cluster curves closest to phase matching be compared to determine which cluster curve provides conditions most favorable for oscillation.

The dependance of the continuous tuning on cavity finesse is apparent in Eq. (30).
The higher finesse resonance more strong pulls the frequency of oscillation than complementary resonance with lower finesse and greater width. Some caution, however, is required in the use of this equation. For example the calculation of $\partial\omega_{s,Osc}/\partial V$ and $\partial\omega_{s,Osc}/\partial T$ for DROs with nearly equal signal and idler finesse involves the small difference of two quantities. In such situations it is important that the terms on the right hand side of Eq. (30) be evaluated accurately for the specified operating conditions.

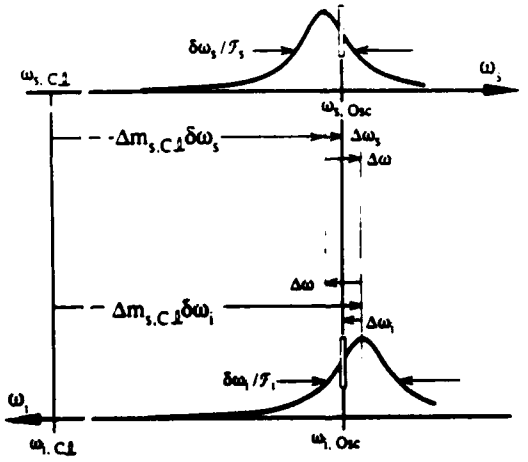

Fig. 7. A signal-idler resonance diagram similar to Fig. 3 expanded in detail to show relationships between parameters. The signal and idler cavity resonances on which oscillation occurs are displaced from the respective cluster frequencies $\omega_{s,Cl}$ and $\omega_{i,Cl}$ for the general case of nonzero frequency mismatch. The DRO oscillating frequencies $\omega_{s,Osc}$ and $\omega_{i,Osc}$ divide the frequency mismatch $\Delta\omega$ into the components $\Delta\omega_s$ and $\Delta\omega_i$.

3. Tuning limits and mode hops

Mode hops are periodic along the cluster curves occurring every time $m_{s,Cl}$ changes by one. Recall that $m_{s,Cl}$ is the value of m_s on the cluster curve where $\Delta m = 0$. The change of tuning parameter $\Delta\zeta_{Hop\text{-}spacing}$ that corresponds to a mode hop is a quantity that is easily measured experimentally. Since a mode hop corresponds to

a change of one in $m_{s,Cl}$, it follows that the tuning parameter change corresponding to the mode-hop spacing is

$$\Delta\zeta_{\text{Hop-spacing}} = \left| \left(\frac{\partial m_{s,Cl}}{\partial \zeta} \right)^{-1} \right| . \quad (31)$$

In the evaluation of $\partial m_{s,Cl} / \partial \zeta$ it is helpful to use the derivative

$$\frac{\partial \omega_{s,Cl}}{\partial \zeta} = -\frac{\partial m}{\partial \zeta} \left(\frac{\partial m}{\partial \omega_s} \right)^{-1}_{\omega_p}$$

$$= -\frac{\delta\omega_s \delta\omega_i}{\delta\omega_i - \delta\omega_s} \frac{\partial m}{\partial \zeta} . \quad (32)$$

The first step simply states that the cluster frequency $\omega_{s,Cl}$ must change with the tuning parameter ζ in such a way that m does not change, and the second step is obtained using Eqs. (18) and (19). It is possible to expand the derivative $\partial m_{s,Cl} / \partial \zeta$ first using the chain rule of differentiation and then using Eqs. (18) and (32) to obtain

$$\frac{\partial m_{s,Cl}}{\partial \zeta} = \frac{\partial m_s}{\partial \zeta} + \frac{\partial m_s}{\partial \omega_s} \frac{\partial \omega_{s,Cl}}{\partial \zeta} = \frac{\partial m_s}{\partial \zeta} - \frac{\delta\omega_i}{\delta\omega_i - \delta\omega_s} \frac{\partial m}{\partial \zeta} . \quad (33)$$

Another useful parameter is the maximum frequency shift from the cluster curve that can be achieved without a mode hop $(\omega_{s,Hop} - \omega_{s,Cl})$. This is obtained directly when the extreme values of $\Delta m_{s,Cl} = \pm 1/2$ are inserted into Eq. (29) to yield

$$\omega_{s,Hop} - \omega_{s,Cl} = \pm \frac{1}{2} \frac{\delta\omega_i \delta\omega_s (\mathcal{F}_i + \mathcal{F}_s)}{\delta\omega_i \mathcal{F}_s + \delta\omega_s \mathcal{F}_i} . \quad (34)$$

Cavity finesse can also limit the single parameter tuning range. It follows from Eq. (15) that threshold is double its minimum value when the frequency mismatch $\Delta\omega$ reaches the value

$$\Delta\omega = \pm \frac{\mathcal{F}_i \delta\omega_s + \mathcal{F}_s \delta\omega_i}{2 \mathcal{F}_i \mathcal{F}_s} .$$

The corresponding value of $\Delta m_{s,Cl}$ is obtained from Eq. (27). Upon substitution into Eq. (29) the maximum displacement of signal oscillation frequency from the cluster frequency allowed by cavity finesse is found to be

$$\omega_{s,Fin} - \omega_{s,Cl} = \pm \frac{\mathcal{F}_s + \mathcal{F}_i}{2 \mathcal{F}_s \mathcal{F}_i} \frac{\delta\omega_s \delta\omega_i}{\delta\omega_i - \delta\omega_s} . \quad (35)$$

If finesse is large the frequency displacement allowed by Eq. (35) becomes significantly smaller than the frequency displacement required for a mode hop described by Eq. (34). In this case parametric oscillation on the cluster curve closest to phase matching ceases in a region around the mode hop. It is then possible for the parametric oscillation frequencies to jump to an adjacent cluster curve that is still within the phase-matching gain bandwidth if a favorable coincidence of signal and idler resonance exists on that cluster curve.

Plotting the mode hop frequency limits $\omega_{s,Hop}$ and the finesse frequency limits $\omega_{s,Fin}$ in addition to the cluster curve provides additional information concerning the fine detail of tuning. On a broader scale, it is informative to display curves defining the phase-matching gain bandwidth along with the phase-matching curve. It may also be useful to display more than one cluster curve near the phase-matching curve.

An attempt has been made to keep the results of this section general. For application to the specific case of a monolithic DRO tuned by temperature, applied potential, and pump frequency, the appropriate variables and derivatives from Table I are directly substituted for the terms involving the general tuning parameter ζ. Evaluation of the derivatives for the case of monolithic DROs made from MgO:$LiNbO_3$ with propagation in the x-direction with electric field applied in the y-direction is discussed in Appendix A. Temperature dependent dispersion, thermal expansion, the electro-optic effect and the piezoelectric effect of the nonlinear optical material are used in the evaluation. Results of this evaluation for experimental conditions described in the next section are given in Table II.

III. Experimental observations and modeling

A. Experimental conditions

Two monolithic DROs which have been described earlier [17,18] were used in the experimental observations. One DRO had lower finesse and had to be pulse-pumped to achieve the higher threshold power needed for parametric oscillation. The higher finesse DRO operated above threshold with the available continuous pumping. The pump source was a diode-laser-pumped nonplanar ring oscillator [19,20] constructed of neodymium doped yttrium aluminum garnet (Nd:YAG) with the 1064-nm laser output converted to 532 nm by externally resonant second harmonic generation.[21] Approximately 30 mW of cw pump radiation was generated. The laser operated in a single longitudinal and single transverse mode. For cw operation of the laser, fundamental frequency stability was typically 10 kHz over short periods of time.[22,23] This value is doubled at the second harmonic. Higher peak power at similar average power was obtained by driving the laser into relaxation oscillations by 10% amplitude modulation of the diode laser output at 320 kHz. Good frequency stability and high optical quality of the pump radiation, such as that achieved with the diode-laser-pumped solid-state laser, are important for obtaining stable DRO performance.

Both monolithic DROs were operated with a ring resonator configuration. They were constructed from 5% magnesium oxide doped lithium niobate (MgO:$LiNbO_3$).[24,25] Each of these monolithic resonators was 12.5-mm long with the crystal x-axis in the long direction. The ring paths were formed by reflections from two multilayer dielectric coated surfaces with 10-mm radius

TABLE II. Values of parameters and derivatives used to model tuning of $MgO:LiNbO_3$ Monolithic DROs.

$l = 0.0125$ m, $\omega_{p0} = 3.54070 \times 10^{15}$ rad/s, $\omega_{s0} = 1.77035 \times 10^{15}$ rad/s, $T_0 = 107.04$ C, $V_0 = 0$

$\frac{\partial m_s}{\partial \omega_s} = 3.05 \times 10^{-11}\ (\text{rad/s})^{-1}$	$\left(\frac{\partial m}{\partial \omega_s}\right)_{\omega_p} = 0$	$\left(\frac{\partial \Delta k}{\partial \omega_s}\right)_{\omega_p} = 0$
$\frac{\partial^2 m_s}{\partial \omega_s^2} = 1.10 \times 10^{-27}\ (\text{rad/s})^{-1}$	$\left(\frac{\partial^2 m}{\partial \omega_s^2}\right)_{\omega_p} = 2.20 \times 10^{-27}\ (\text{rad/s})^{-1}$	$\left(\frac{\partial^2 \Delta k}{\partial \omega_s^2}\right)_{\omega_p} = -5.53 \times 10^{-25}\ \frac{\text{rad/m}}{(\text{rad/s})^2}$
$\frac{\partial m_s}{\partial \omega_p} \equiv 0$	$\left(\frac{\partial m}{\partial \omega_p}\right)_{\omega_s} = 3.05 \times 10^{-11}\ (\text{rad/s})^{-1}$	$\left(\frac{\partial \Delta k}{\partial \omega_p}\right)_{\omega_s} = 5.44 \times 10^{-4}\ \frac{\text{rad/m}}{\text{rad/s}}$
$\frac{\partial m_s}{\partial T} = 1.02\ ^\circ\text{C}^{-1}$	$\frac{\partial m}{\partial T} = 2.03\ ^\circ\text{C}^{-1}$	$\frac{\partial \Delta k}{\partial T} = 749\ \frac{\text{rad/m}}{^\circ\text{C}}$
$\frac{\partial m_s}{\partial V} = \frac{-1.81 \times 10^{-6}\ \text{m/V}}{t}$	$\frac{\partial m}{\partial V} = \frac{-3.63 \times 10^{-6}\ \text{m/V}}{t}$	$\frac{\partial \Delta k}{\partial V} = \frac{3.61 \times 10^{4}}{t}\ \frac{\text{rad/m}}{\text{V/m}}$ (a)

(a) The parameter t is the effective thickness of the crystal in meters.

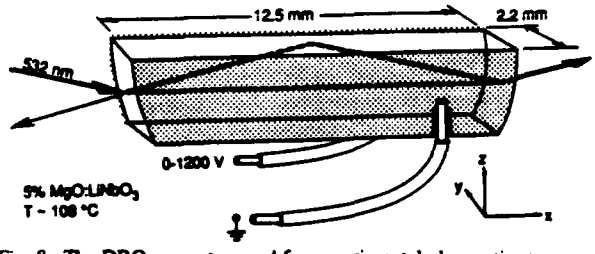

Fig. 8. The DRO geometry used for experimental observations.

of curvature and a totally internally reflecting (TIR) surface. The centers of curvature of the spherical surfaces were on a line parallel to and 180 μm inside the flat TIR surface. A drawing of the monolithic DROs is shown in Fig. 8. The 532-nm pump beam was mode matched for collinear propagation on the segment of the ring path parallel to the crystal x-axis. The pump beam with extraordinary polarization did not follow the closed path of the signal and idler waves with ordinary polarization because of bi-reflection.

Metal coatings for electric field tuning were applied to the crystal surfaces perpendicular to the y-axis. The thickness of the crystals between the electrodes was 2.2 mm. The finesse of both DROs at 1.064 μm was measured using the Nd:YAG laser output directly without second harmonic generation. Electric-field tuning was used to scan the resonators through a free spectral range and transmission through the resonators gave a measure of resonance width relative to the mode spacing. One DRO has a finesse of 360 and the other had finesse of 960. The lower finesse device had an experimentally observed threshold for cw parametric oscillation oscillation of 35 mW, and the higher finesse DRO had a threshold of 12 mW. The pump source could produce approximately 30 mW of cw radiation at 532 nm. The

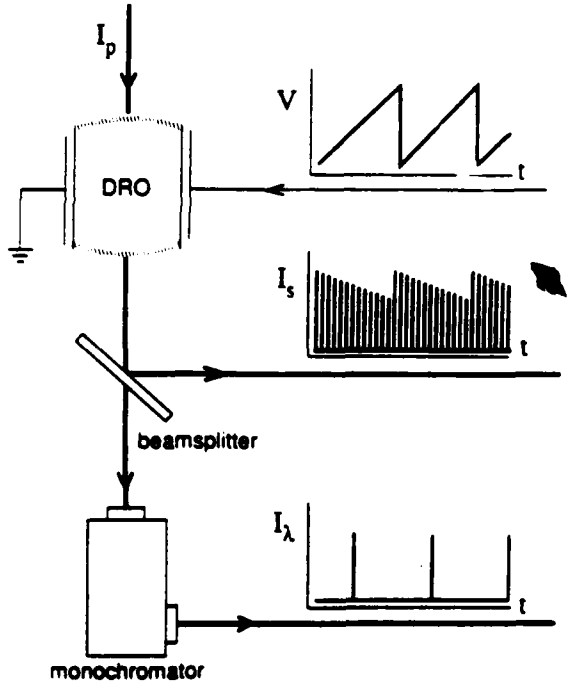

Fig. 9. Schematic representation of the setup used for DRO tuning measurements.

higher threshold OPO was pumped by 532-nm second harmonic which consisted of 400-ns pulses with 230-mW peak power at 320-kHz repetition rate.

The output of the DROs was tuned by temperature and electric field. Noncritical phasematching in $MgO:LiNbO_3$ was achieved for degeneracy at 107 °C, and as temperature

was increased the signal and idler wavelengths separated from the 1.064-μm degeneracy point. For the tuning studies the potential applied to the crystal was repetitively ramped at fixed temperature. Output wavelength measurements were repeated at incrementally changed temperatures. A $f/10$, one-meter grating monochromator with a 600-line/mm grating was used for wavelength measurement. The DRO output directed into the monochromator consisted of a series of pulses; these pulses resulted either from the pulse pumping or from the mode hops produced by the ramped voltage with continuous pumping. The radiation transmitted by the monochromator usually consisted of a few pulses in a narrow spectral band which could be correlated with the potential applied to the DRO electrodes. A schematic representation of the experimental setup is show in Fig. 9.

B. Cluster tuning

The tuning of the high finesse DRO involved spectral jumps back and forth between cluster curves as well as mode hops along the cluster curves. This behavior is illustrated in Fig. 10, where DRO output is displayed for a small voltage range at a constant temperature. In this figure output is resolved on three separate cluster curves. The

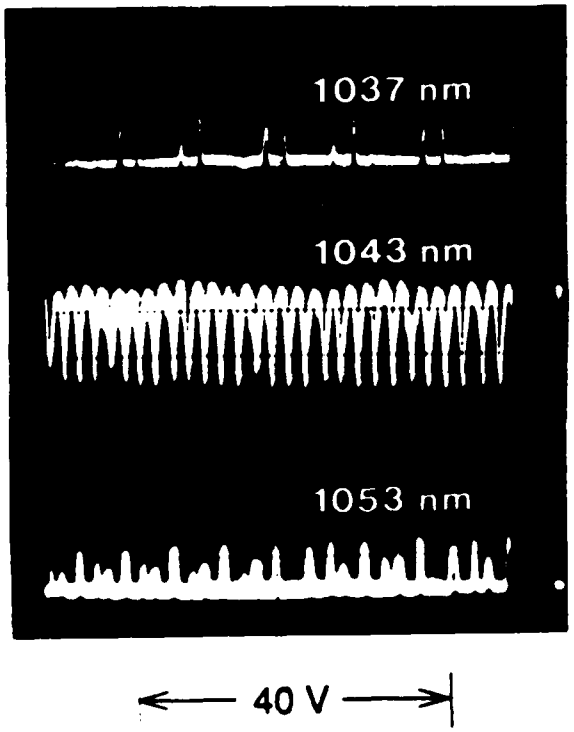

Fig. 10. Oscillograms of cw-pumped DRO output showing simultaneous output on three cluster curves. The signal displayed is that produced by a photodiode placed after a monochromator with slits adjusted for 5-nm bandpass. Each of the oscillograms corresponds to the same portion of the ramped voltage applied to the DRO. The change in applied potential is indicated. The oscillograms differ only in the wavelength setting of the monochromator indicated for the individual traces. The output on the central cluster dominates and is so strong that the oscilloscope trace does not return to the baseline.

monochromator slits were opened to provide 5-nm transmission width, sufficient to resolve the individual clusters while transmitting a number of mode hops. The central cluster curve with signal wavelength near 1043 nm dominated. Two other cluster curves fit within the phase-matching gain bandwidth, and output on these curves was observed near 1053 and 1037 nm. Competition with the central cluster curve, which depletes the pump wave, is evident in the two cluster curves to either side.

Three adjustable parameters were used to fit Eq. (21) and (22) to the observations. A temperature offset correction is used to fit the calculated phase-matching curve. There are inaccuracies in both the absolute measurement of temperature and in the temperature dependance of the dispersion relationships that make this necessary. The temperature adjustment was accomplished by shifting the data a fraction of 1 °C but could have equally well been done by changing the parameter Δk_0 in Eq. (21). Another fitting parameter is required because the optical lengths of the DROs are not precisely known. This is accomplished by changing the value of m_0 in Eq. (22) and has the effect of adjusting the placement of the cluster curves. The thickness of the DRO crystals is also used as a fitting parameter. The electrodes do not completely cover the surfaces, and fringing effects are not considered. Instead, it is assumed that there is a uniform electric field in the y-direction given by $E_y = V/t$ where V is the applied potential and t is an effective thickness. Adjusting the thickness has the effect of changing the slopes of the cluster curves and voltage tuned phase-matching curve. It is interesting to note that the piezoelectric effect in addition to the electro-optic effect is needed to model the observed tuning. When only the electro-optic effect is used, the calculated voltage-tuned cluster curves are parallel to the voltage-tuned phase-matching curve. A fourth fitting parameter not used here is the constant $m_{s,0}$ in Eq. (23). Adjustment of $m_{s,0}$ would allow for different phase shifts at the mirror surfaces for signal and idler and the possibility of different cavity lengths.[3] Adjustment of $m_{s,0}$ will change the calculated position of the mode hops.

The observed and fitted tuning curves for the DROs are shown in Figs. 11 and 12. The theory is most easily expressed in terms of frequency. Frequency, therefore, is used as the primary ordinate scale in these graphs, and wavelength is included as a secondary scale for reference. The temperature-tuned phase-matching curves are shown in the (a) portions of both figures. At each temperature setting, a range of output wavelengths is obtained by voltage tuning. In most cases, the observed tuning ranges cover the space between and extend slightly beyond the calculated temperature-dependent tuning curves for the extreme voltages. Voltage was ramped from 0 to 1150 V, and when the crystal was reversed from 0 to −1150 V. Parts (b) through (d) of Figs. 11 and 12 show the voltage tuning at selected fixed temperatures. The data are the voltages at which output was observed at selected frequencies. Calculated phase-matching curves, gain-bandwidth curves, and cluster curves are shown for comparison. In some instances the data are located in lines parallel to the calculated cluster curves but not on the cluster curves. This most likely is caused by inaccuracy in temperature measurement, and

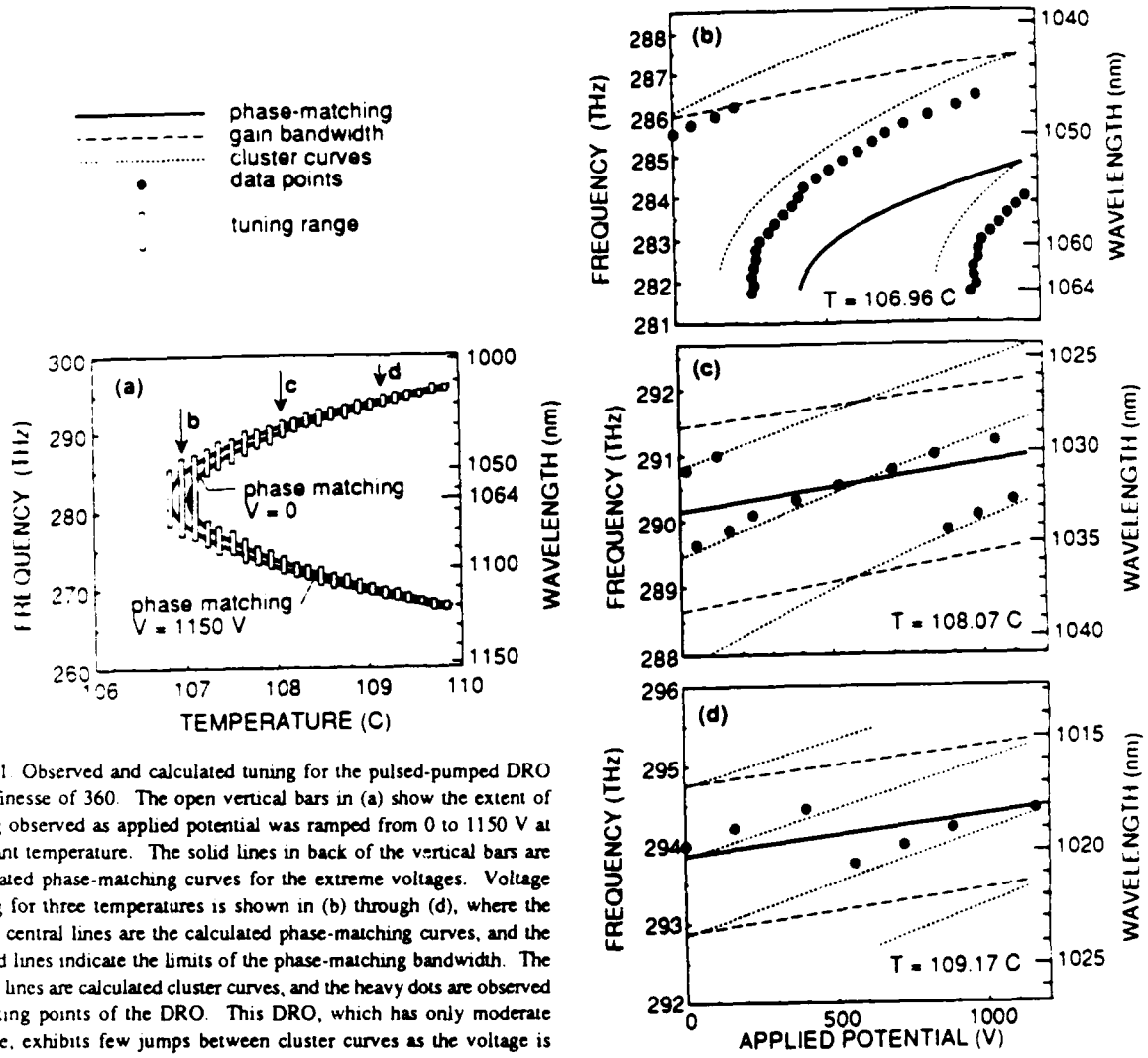

Fig. 11. Observed and calculated tuning for the pulsed-pumped DRO with finesse of 360. The open vertical bars in (a) show the extent of tuning observed as applied potential was ramped from 0 to 1150 V at constant temperature. The solid lines in back of the vertical bars are calculated phase-matching curves for the extreme voltages. Voltage tuning for three temperatures is shown in (b) through (d), where the heavy central lines are the calculated phase-matching curves, and the dashed lines indicate the limits of the phase-matching bandwidth. The dotted lines are calculated cluster curves, and the heavy dots are observed operating points of the DRO. This DRO, which has only moderate finesse, exhibits few jumps between cluster curves as the voltage is ramped. The data are measurements of applied potential for a limited sampling of output frequencies, and do not represent individual mode hops.

coincidence could be obtained by choosing a different temperature calibration for each setting. In practice DRO tuning may provide an accurate measurement of its temperature. The DRO sensitivity to temperature will become more apparent later when the details of tuning are discussed.

Figures 11 and 12 appear similar in a cursory examination; however, one aspect of tuning dependance on finesse is illustrated. The lower finesse DRO, with tuning shown in Fig. 12, usually oscillates on the single cluster curve nearest the phase-matching curve. Sometimes the oscillation jumps back and forth between two cluster curves when they are nearly equal distant from phase matching. The output of the higher finesse DRO with tuning shown in Fig. 12 jumps between two or three cluster curves. This is in agreement with theoretical predictions that show the tuning limit imposed on the $\mathcal{F} = 960$ DRO by the resonance widths, that is, finesse limit of tuning is reached before the mode-hop limit of tuning for most conditions encountered.

The cluster curves also are dependent on temperature. The data displayed in Fig. 12 is interpreted to show temperature tuning at constant voltage in Fig. 13. Here the data points are either interpolated from measurements of cluster tuning with voltage both higher and lower than the selected voltage, or extrapolated from measurements of cluster curve that nearly reached the selected voltage. The calculated phase-matching, gain-bandwidth, and cluster curves are again in reasonable agreement with observation.

C. Axial-mode-hop tuning

There is good agreement between observation and the calculated voltage change required to produce a mode hop. Observations similar to those illustrated in Fig. 10 were

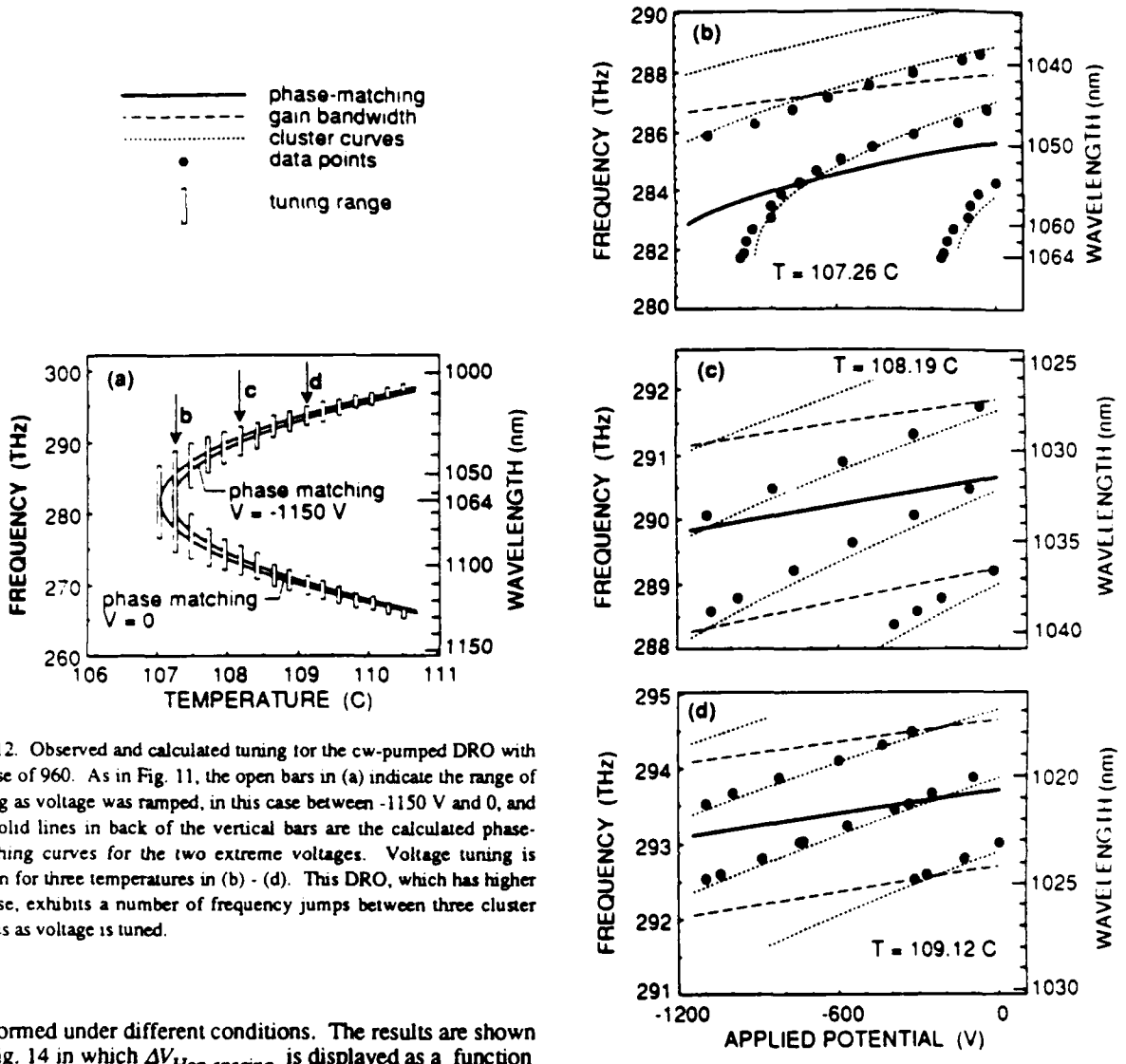

Fig. 12. Observed and calculated tuning for the cw-pumped DRO with finesse of 960. As in Fig. 11, the open bars in (a) indicate the range of tuning as voltage was ramped, in this case between -1150 V and 0, and the solid lines in back of the vertical bars are the calculated phase-matching curves for the two extreme voltages. Voltage tuning is shown for three temperatures in (b) - (d). This DRO, which has higher finesse, exhibits a number of frequency jumps between three cluster curves as voltage is tuned.

performed under different conditions. The results are shown in Fig. 14 in which $\Delta V_{\text{Hop-spacing}}$ is displayed as a function of detuning from degeneracy. The calculated line is obtained from Eqs. (31) and (33). The tuning parameter is voltage and it is necessary to substitute V for ζ in the equations and further substitute the appropriate values from Table II, and evaluate the derivative $(\partial m/\partial \omega_s)_{\omega_p}$ as a function of signal frequency. The approximations given in the next section by Eqs. (37) and (38) also work well in the evaluation of Eq. (31).

Calculations of axial-mode-hop tuning along cluster curves were performed for conditions that would approximate those used to produce Fig. 10. The same fitting parameters were used as in Figs. 12 and 13. An operating temperature and center voltage were chosen to give three cluster curves centered on phase matching at the observed operating frequencies. This was done by manipulation and solution of Eqs. (21) and (22). Calculated phase-matching, gain-bandwidth, and cluster curves in this region are shown in Fig. 15a. Calculated tuning along the three cluster curves with the detail of mode hops is shown in Figs. 15b, c, and d. These tuning curves were obtained using Eq. (22) to calculate the cluster signal frequency $\omega_{s,Cl}$, Eq. (23) to calculate the signal mode number $m_{s,Cl}$ at the cluster frequency, and Eq. (29) to calculated the signal frequency of the oscillation. The mode-hop frequency limits given by Eq. (34) and the finesse frequency limits given by Eq. (36) are also shown.

When the oscillating signal frequency differs from the cluster signal frequency by more than the mode-hop limit, it is advantageous for the oscillation to shift to another signal-idler resonance pair. When the oscillating frequency excursion from the cluster frequency reaches the finesse limit, threshold for parametric oscillation is double the value it had when the oscillation frequencies coincided with the cluster frequencies, and threshold increases for greater excursions of the oscillation frequency from the cluster

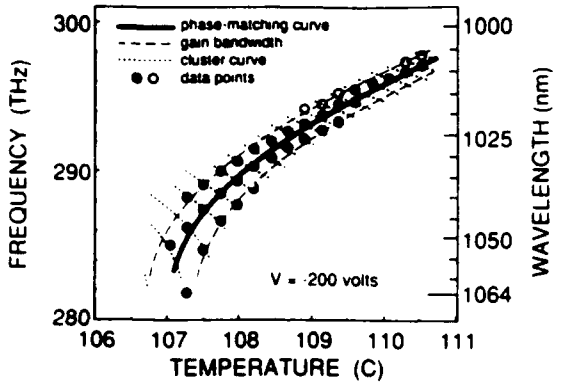

Fig. 13. Observed and calculated tuning for the cw-pumped DRO as a function of temperature. The same tuning data that was used in Fig. 12 is used here. A fixed voltage of -200 V was chosen. For the cases where oscillation on a cluster curve was observed at voltages both higher and lower than this voltage, frequencies were obtained by interpolation and are represented by a solid data points. For the cases in which cluster tuning came close but did not reach this voltage, frequencies were obtained by extrapolation and are represented by open data points. The dotted lines are portions of the calculated temperature dependent cluster curves. The calculated phase-matching curve is the central heavy line, and the dashed lines show the approximate gain bandwidth limits.

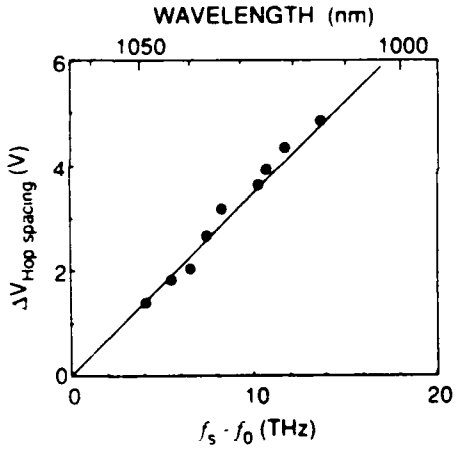

Fig. 14. Mode hop spacing in applied potential as a function of detuning from degeneracy. The dots are data points and the solid line is calculated from theory.

frequency. Figure 15 illustrates how cluster jumps can be interspersed with the mode hops of a single cluster curve. For the calculation presented in the figure, the finesse limit of tuning is reached before the mode-hop limit on the central cluster curve shown in Fig. 15c. Parametric oscillation on the central cluster curve usually dominates because phase matching is best there. When the finesse limit of frequencyexcursion from the cluster curve is reached, however, the parametric oscillation on the central cluster curve decays, and it is possible to have oscillation build up on an adjacent cluster curve before oscillation can build up on the next mode pair of the central cluster curve. Notice that the mode-hop spacing measured by change in tuning variable is different for the three adjacent cluster curves of Fig. 15b, c, and d. Also, the relative positions of the finesse and mode-hop limits change with detuning from degeneracy.

These comparisons show quantitative agreement between observations and the tuning theory of section II. The tuning theory describes the cluster tuning of the DRO, as well as the effects of cavity finesse on the cluster structure in the occurrence of cluster jumps. Also, the theory is able to predict the observed spacing in tuning variable of axial mode hops on a microscopic scale of tuning. This is done using temperature dependent dispersion, thermal expansion, electro-optical and piezoelectric effects. Only three fitting parameters are used: a temperature calibration which entailed the translation of a temperature scale by a fraction of a degree C, an adjustment of cavity length l less than one wavelength, and the use of a effective crystal thickness that compensated for the nonuniformity of electric field inside the crystal. With this agreement, it is reasonable to consider applying the theory to analysis of the DRO for optical frequency synthesis. Specifically, the analysis addresses conditions required to reproduce the coherence of a frequency stable pump having a small degree of tunability at any frequency in the tuning range of the DRO.

IV. Frequency synthesis and tuning variable tolerances

Parameter tolerances and continuous frequency tuning are topics which can be addressed with the theory presented in earlier sections. Knowledge of tolerances is important for stable DRO operation and tuning to oscillation at specific frequencies. *Continuous frequency tuning is of interest in* many applications. Fixed frequency operation with resolution finer than a mode hop may be required, or perhaps truly continuous frequency coverage may be necessary. The DRO output frequencies lie within the widths of cavity resonances. The extent of continuous tuning depends on several factors including frequency shifts of the cavity modes, the spectral range over which the conservation of energy condition can be satisfied while maintaining oscillation within a selected mode pair, and the spectral range over which higher net parametric gain is not available on another mode pair. Multiple parameter tuning in which two or more parameters are synchronously changed is required for continuous tuning over the full free spectral range of the oscillator. Single parameter tuning will provide frequency coverage over small regions separated by the discrete mode hops.

It is easiest to think of tolerances for situations in which only a single parameter is allowed to change. In practice there are advantages in dealing with parameter tolerances in pairs. For example voltage and temperature adjustments could be used to maintain stable oscillation at a fixed frequency. It may not be possible to control temperature to the precision required with fixed voltage, but the lack of required temperature control could be compensated with voltage control. Feedback techniques could be used to adjust voltage to maintain stable oscillation on a signal-idler mode pair even in the presence of temperature fluctuations that would alone cause mode hops. The change in voltage

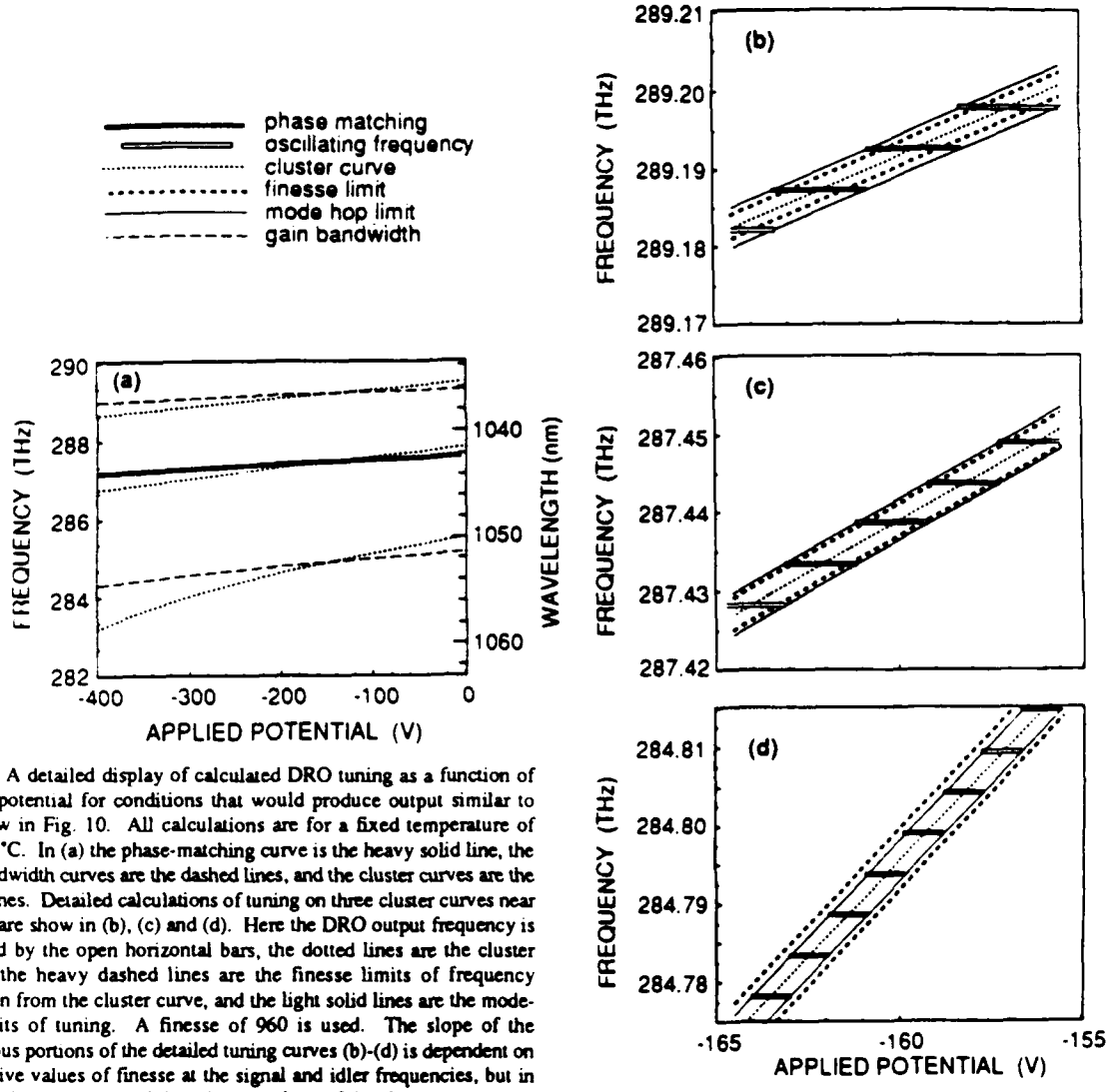

Fig. 15. A detailed display of calculated DRO tuning as a function of applied potential for conditions that would produce output similar to that show in Fig. 10. All calculations are for a fixed temperature of 107.540 °C. In (a) the phase-matching curve is the heavy solid line, the gain bandwidth curves are the dashed lines, and the cluster curves are the dotted lines. Detailed calculations of tuning on three cluster curves near −160 V are show in (b), (c) and (d). Here the DRO output frequency is indicated by the open horizontal bars, the dotted lines are the cluster curves, the heavy dashed lines are the finesse limits of frequency excursion from the cluster curve, and the light solid lines are the mode-hop limits of tuning. A finesse of 960 is used. The slope of the continuous portions of the detailed tuning curves (b)-(d) is dependent on the relative values of finesse at the signal and idler frequencies, but in all cases this slope is much less than the slope of the cluster curves.

required for stable operation could be used as an error signal that would in turn be used to return temperature to the desired value.

Simultaneous adjustment of three parameters could also be used to tune the output frequency of the DRO. As an example, consider the pump frequency ramped in some specified way. The conditions required for stable operation on a single signal-idler mode pair could be provided by feedback control of the potential applied for electro-optic and piezoelectric tuning. The tolerance required for phase matching is much less stringent than that required for stable operation on a single signal-idler mode pair; adequate phase matching could be maintained by temperature control based on a functional relationship dependent on the pump frequency and voltage required for stable operation. With two parameter tuning, frequency matching could be maintained, but it would not be possible to maintain optimum phase matching.

A. Tuning variable tolerances

The parameter tolerances for stable operation are determined by the more restrictive of two conditions. Mode hops are avoided by maintaining operation within a range of adjustment over which higher gain does not develop on another signal-idler mode pair. The range of adjustment over which oscillation can be maintained on a mode-pair may be limited to a smaller value by the resonance width or equivalently the DRO finesse. These tolerances are closely related to the mode-hop spacing and spectral limits of tuning which were discussed earlier, and they can be obtained from detailed tuning curves such as were shown in Fig. 15b, c, and d for voltage tuning. Detailed tuning curves for

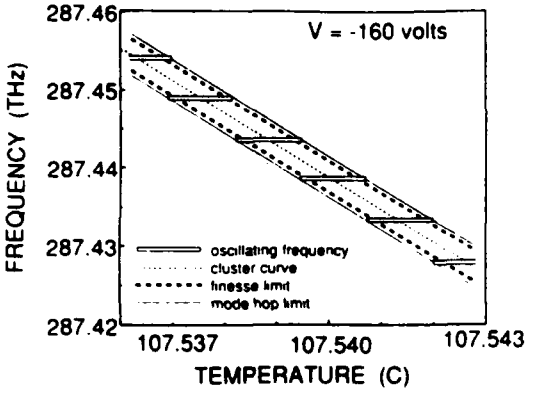

Fig. 16. Calculated detailed tuning as a function of temperature. For this calculation temperature is adjusted while other parameters are held constant at values corresponding to a point near the center of Fig. 15c. The various lines have the same significance as in that figure. Here, also, the slope of the continuous portions of the tuning curve are dependent on the relative values of signal and idler finesse, and this slope is small compared to the slope of the cluster curve.

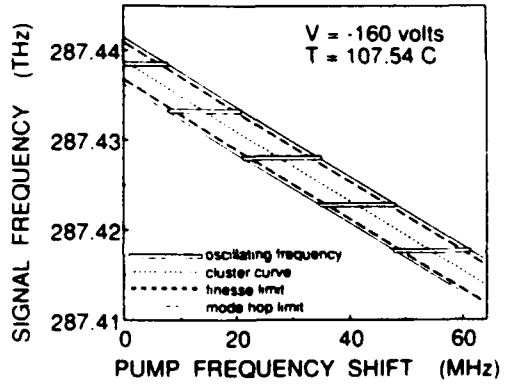

Fig. 17. Calculated detailed tuning as a function of pump frequency. For this calculation, pump frequency is adjusted while other parameters are held constant at values corresponding to a point near the center of Fig. 15c. The various lines have the same significance as in that figure. For pump frequency tuning with equal signal and idler cavity finesse, the slope of the continuous portions of the tuning curve is approximately 0.5. Due to the scale required to display the much greater slope of the cluster curve, the continuous portions of the tuning curve appear to be horizontal.

TABLE III. Calculated single-parameter continuous tuning rates and parameter tolerances for stable operation of the finesse = 960 DRO pumped at 563.6 THz with signal frequency of 287.44 THz.

Tuning parameter ζ	$\frac{\partial \gamma_{s,Cl}}{\partial \zeta}$	$\Delta\zeta_{Hop\text{-}tolerance}$	$\Delta\zeta_{Finesse\text{-}tolerance}$
V (Voltage)	72 kHz/V	± 0.98 V	± 0.80 V
T (Temperature)	−124 MHz/ °C	± 0.00064 °C	± 0.00051 °C
f_p (pump frequency)	0.499 Hz/Hz	± 6.7 MHz	± 5.4 MHz

temperature tuning and pump-frequency tuning are shown in Figs. 16 and 17 respectively.

The conditions for the calculations displayed in Figs. 16 and 17 are the same as those used to produce Fig. 15c. These conditions are $\mathcal{F}_s = \mathcal{F}_i = 960$ for a $MgO:LiNbO_3$ DRO of length $l = 1.25$ cm pumped at 564 THz (532 nm) with signal frequency near 287 THz (1043 nm). Fitting parameters used in these calculations, such as effective thickness $t = 0.277$ cm and a length adjustment corresponding to a change in m of 0.42, are the same as required to fit to the experimental data in Figs. 12 and 13. These characteristics are carried forward to other calculations for the purpose of providing a specific example for comparison.

The detailed tuning curves of Figs. 15, 16, and 17 are similar in many respects. The mode-hop and finesse limits of frequency displacement from the cluster curve are independent of tuning parameter. In each of the figures, the slope of the continuous portion of tuning between mode hops is much smaller than the slope of the cluster curve. The slopes of the continuous portions of tuning are dependent on the relative finesse of signal and idler resonances. The case of equal finesse is shown in the calculated tuning curves. The illustrated curves show that voltage needs to be held within a tolerance of approximately 1 V, temperature within 0.0005 °C, and pump frequency within 3 MHz for stable operation for this example.

Analytic approximations for the parameter tolerances for stable operation are not limited to a specific example. The range over which a parameter can be changed without causing a mode hop is obtained from the condition $\Delta m_{s,Cl} = \pm 1/2$. Recall that $m_{s,Cl}$ is the value m_s for a point on the associated cluster curve, and the cluster curve is a line which gives the values of signal frequency ω_s and a tuning parameter ζ for which $\Delta m = 0$ with the other parameters held at fixed values. It follows that the tuning parameter tolerance is

$$\Delta\zeta_{\text{Hop-tolerance}} = \pm\frac{1}{2}\left(\frac{\partial m_{s,Cl}}{\partial \zeta}\right)^{-1} . \tag{36}$$

The derivative in the above equation can be evaluated with Eq. (33). An approximation of that equation for the case of Type-I phase matching is given by

$$\frac{\partial m_{s,Cl}}{\partial \zeta} \approx -\frac{\delta\omega_0}{\delta\omega_i - \delta\omega_s}\frac{\partial m}{\partial \zeta} \tag{37}$$

where $\delta\omega_0$ is the mode spacing at degeneracy where $\omega_s = \omega_i = \omega_0 = \omega_p/2$. The difference between the idler and signal mode spacing can also be expanded about degeneracy using Eqs. (17) to obtain

$$\delta\omega_i - \delta\omega_s \approx 2\delta\omega_0^2\frac{\partial^2 m_s}{\partial \omega_s^2}(\omega_s - \omega_0) . \tag{38}$$

The last three equations can be combined to give the desired approximation for the mode-hop parameter tolerance, namely,

$$\Delta\zeta_{\text{Hop-tolerance}} \approx \pm\, \delta\omega_0 \frac{\partial^2 m_s}{\partial \omega^2}(\omega_s - \omega_0)\Big/\frac{\partial m}{\partial \zeta} . \quad (39)$$

The adjustable parameter tolerance related to cavity finesse can be obtained from the cavity-round-trip-phase-shift sum for which the pumping threshold is twice its minimum value. From Eqs. (12) and (13) this phase-shift sum is

$$\psi_{\text{Fin}} = \pm\, \pi \left\{ \frac{1}{\mathcal{F}_i} + \frac{1}{\mathcal{F}_s} \right\} . \quad (40)$$

Since $\psi = 2\pi\, \Delta m$, the parameter tolerance determined by cavity finesse is

$$\Delta\zeta_{\text{Fin-tolerance}} \approx \pm \frac{1}{2} \left\{ \frac{1}{\mathcal{F}_i} + \frac{1}{\mathcal{F}_s} \right\} \Big/ \frac{\partial m}{\partial \zeta} . \quad (41)$$

The parameter tolerance related to mode hops given by Eq. (39) is zero at degeneracy and increases linearly with detuning from degeneracy. In practice, however, operation precisely at degeneracy was stable for tens of minutes with no adjustments to the DRO.[10] The parameter tolerance related to cavity finesse given by Eq. (41) remains approximately constant independent of detuning from degeneracy as long as finesse remains constant. Calculated tuning variable tolerances are given in Table III for the $MgO:LiNbO_3$ DRO for the conditions used to generate Fig. 15c, 16, and 17.

B. Single parameter tuning

It has been noted by Smith [4] that the continuous tuning of a DRO is relatively insensitive to tuning parameter changes that change the optical length of the DRO resonator but displays approximately one-half of the change in pump frequency. The reason for this is changes in temperature or applied potential shift signal and idler resonances approximately an equal amount. Until a mode hop occurs, the oscillating frequency remains a compromise between the center frequencies of the resonances. If finesse is nearly the same for signal and idler, the oscillating frequency changes little, but if one of the resonances has higher finesse, it tends to pull the oscillating frequency more. Since the conservation of energy condition Eq. (1) must be satisfied, any change in pump frequency also appears in the sum of changes in signal and idler frequencies.

Single parameter continuous tuning is described by Eq. (30), which can be rewritten using $m = m_s + m_i$ as

$$\frac{\partial \omega_{s,\text{Osc}}}{\partial \zeta} = \frac{\delta\omega_s \delta\omega_i}{\delta\omega_i \mathcal{F}_s + \delta\omega_s \mathcal{F}_i} \left(\mathcal{F}_i \frac{\partial m_s}{\partial \zeta} - \mathcal{F}_s \frac{\partial m_i}{\partial \zeta} \right) .$$

In the mathematical development used here, ω_s and ω_p have been used as independent variables with ω_i determined by Eq. (1). Choosing pump frequency ω_p as the variable parameter ζ requires the substitutions

$$\frac{\partial m_i}{\partial \zeta} \rightarrow \left(\frac{\partial m_i}{\partial \omega_p}\right)_{\omega_s} = \frac{\partial m_i}{\partial \omega_i}$$

and $$\frac{\partial m_s}{\partial \zeta} \rightarrow \left(\frac{\partial m_s}{\partial \omega_p}\right)_{\omega_s} = 0 .$$

The signal and idler mode spacings, $\delta\omega_s$ and $\delta\omega_i$, will differ only a small amount, and if $\mathcal{F}_s$ and $\mathcal{F}_i$ are nearly equal, the tuning rate is $\partial\omega_{s,\text{Osc}}/\partial\omega_p \approx 1/2$. More generally, for differing values of finesse, the tuning rate is in the range $0 < \partial\omega_{s,\text{Osc}}/\partial\omega_p < 1$. Even though approximately half the pump frequency tuning will be reflected in signal tuning, only a relatively small spectral range will be covered before a mode hop is encountered. Calculated single parameter tuning rates for the special case of $\mathcal{F}_s = \mathcal{F}_i$ corresponding the DROs described in section III are given in Table III. The partial derivatives needed in this calculation were evaluated for $\omega_{s,\text{Osc}}$ = 287.44 THz (1043 nm) and T_0 = 107.51 °C instead of taken from Table II. As explained earlier, this is required for the evaluation of $\partial f_{s,\text{Osc}}/\partial V$ and $\partial f_{s,\text{Osc}}/\partial T$, which involve the small differences of two quantities, but has little effect on the other values in the table.

C. Multiple parameter tuning

It is possible to extend the continuous tuning range by synchronously adjusting two or three parameters. Adjusting two parameters simultaneously allows the conditions $\Delta m = 0$ and $\Delta m_s = 0$ to be maintained, but Δk will change. Adjusting three parameters simultaneously permits tuned parametric oscillation while maintaining Δm, Δm_s, and Δk all equal to zero for a specified mode pair, and tuning is limited only by the extent the parameters can be changed.

Generalized tuning parameters with ζ_1 and ζ_2 adjustable and ζ_3 fixed are used for the discussion of two-parameter tuning. For the specific case used here, any permutation of voltage, temperature, and pump frequency can be used for these three parameters. The conditions $\Delta m = 0$ and $\Delta m_s = 0$ determine a relationship between ζ_1 and ζ_2, and use of this relationship allows ω_s and Δk to be expressed as functions of ζ_1. These relationships can be obtained by first differentiating Eqs. (21), (22) and (23) with respect to ζ_1 yielding

$$\frac{dm}{d\zeta_1} = 0 = \left(\frac{\partial m}{\partial \omega_s}\right)_{\omega_p} \frac{d\omega_s}{d\zeta_1} + \frac{\partial m}{\partial \zeta_1} + \frac{\partial m}{\partial \zeta_2}\frac{d\zeta_2}{d\zeta_1} , \quad (42a)$$

$$\frac{dm_s}{d\zeta_1} = 0 = \frac{\partial m_s}{\partial \omega_s}\frac{d\omega_s}{d\zeta_1} + \frac{\partial m_s}{\partial \zeta_1} + \frac{\partial m_s}{\partial \zeta_2}\frac{d\zeta_2}{d\zeta_1} , \quad (42b)$$

and $$\frac{d\Delta k}{d\zeta_1} = \left(\frac{\partial \Delta k}{\partial \omega_s}\right)_{\omega_p} \frac{d\omega_s}{d\zeta_1} + \frac{\partial \Delta k}{\partial \zeta_1} + \frac{\partial \Delta k}{\partial \zeta_2}\frac{d\zeta_2}{d\zeta_1} . \quad (42c)$$

Only a small spectral region is being considered, and it is unnecessary to consider second partial derivatives with

respect to signal frequency. The first partial derivatives, however, must be evaluated for the operating conditions that are being considered. A specific case where this is important is frequency tuning for voltage and temperature adjustment, which again involves a small difference of terms. Equations (42a) and (42b) are solved for $d\omega_s/d\zeta_1$ *and* $d\zeta_2/d\zeta_1$. These values are substituted in Eq. (42c) to obtain a value for $d\Delta k/d\zeta_1$. Results are calculated for three sets of tuning parameters and listed in Table IV. The conditions used for these calculations are the same as those used for Figs. 15 -17 and Table III. The partial derivatives in Eqs. (42) again were evaluated for evaluated for $\omega_{s,Osc}$ = 287.44 THz (1043 nm) and T_0 = 107.51 °C for the generation of Table IV.

TABLE IV. Calculated values for two-parameter tuning of a monolithic $MgO:LiNbO_3$ DRO at f_s = 287.44 THz or λ_s = 1043 nm.

Adjustable parameters	fixed parameter	$\frac{df_s}{d\zeta_1}$	$\frac{d\zeta_2}{d\zeta_1}$	$\frac{d\Delta k}{d\zeta_1}$
$\zeta_1 = f_p$, $\zeta_2 = V$	T = 107.54 °C	0.510	$1.47\times10^{-7}\ \frac{V}{Hz}$	$2.26\times10^{-8}\ \frac{rad/m}{Hz}$
$\zeta_1 = f_p$, $\zeta_2 = T$	V = −160 V	0.511	$-9.4\times10^{-11}\ \frac{°C}{Hz}$	$-6.7\times10^{-8}\ \frac{rad/m}{Hz}$
$\zeta_1 = V$, $\zeta_2 = T$	f_p = 563.6 THz	−7.9 $\frac{kHz}{V}$	$6.4\times10^{-4}\ \frac{°C}{V}$	0.613 $\frac{rad/m}{V}$

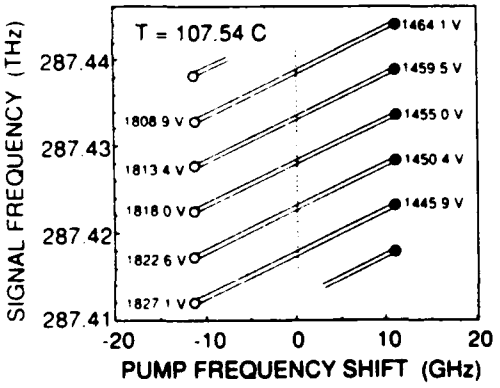

Fig. 18. Calculated tuning for varying voltage and pump frequency simultaneously in a way to maintain $\Delta m = 0$ and $\Delta m_s = 0$. The dashed line is the cluster curve of Fig. 17. Tuning limits are taken are the points at which $\Delta k = \pi / l$ in the 1.25-cm-long crystal.

Two of the examples given in Table IV are briefly noted. Voltage-temperature tuning mentioned earlier is of interest for operation at a fixed frequency. The rate of change of output frequency with applied potential when voltage and temperature are changed simultaneously to maintain $\Delta m = 0$ and $\Delta m_s = 0$ is calculated to be −7.9 kHz/V. The magnitude of this tuning rate is about 10 times smaller than the single parameter voltage tuning rate given in Table III, and significantly smaller than the 3.5 MHz/V tuning rate of the cavity resonance. The reduced sensitivity is important in stable frequency operation of the DRO. The case of simultaneous pump frequency and voltage tuning is useful for continuous coverage of the spectral region between the mode hops of single parameter tuning. Calculated tuning curves for this case are shown in Fig. 18. The same conditions used in Figs. 15-17 again apply to Fig. 18. Tuning is taken to the limits of $\Delta k = \pm\pi / l$ in the figure.

Three parameter tuning is presented in two ways. First a method is described to achieve oscillation at a specified frequency while satisfying the conditions $\Delta k = 0$, $\Delta m = 0$, and $\Delta m_s = 0$. The description is in mathematical terms, but has analogy to what could be done experimentally. The first step is to adjust temperature to achieve phase matching for the specified frequency. This is just a matter of changing temperature to the value determined by Eq. (20). Next the pump frequency and temperature are adjusted simultaneously to maintain the $\Delta k = 0$ phase-matching condition and to satisfy the condition $\Delta m = 0$. Numerically this is done by setting $\Delta k = 0$ and $\Delta m = 0$ in Eqs. (20) and (21) and solving for T and ω_p with V and ω_s held constant. Next three parameters are adjusted simultaneously by solving Eqs. (21) - (23) for T, ω_p and V with ω_s again held constant, and Δk, Δm, and Δm_s set to zero.

In practice this would be analogous to setting temperature to a value calculated for phase matching and observing the location of the cluster curve nearest the phase-matched signal frequency. Next, temperature and pump frequency are adjusted simultaneously to move that cluster curve to intersect the desired frequency at phase matching. At this point oscillation is on the resonance nearest the specified frequency. Finally, temperature, pump frequency, and voltage are adjusted simultaneous to bring the cavity resonance to the desired frequency while maintaining coincidence of the signal and idler modes and phase matching.

The second method of three parameter tuning considers a situation in which oscillation has been achieved with optimum phase matching and coincidence of the modes in satisfying the conservation of energy condition. Continuous output frequency tuning is possible over a limited range while maintaining optimum DRO operating conditions. One parameter can be changed arbitrarily, but the other parameters must be changed in a prescribed manner. This prescription for this change is again obtained by differentiating Eqs. (21) - (23) and this time setting the all total derivatives equal to zero. The pump frequency ω_p is chosen as the independent parameter, and the differentiation yields

$$\frac{d\Delta k}{d\omega_p} = 0 = \left(\frac{\partial \Delta k}{\partial \omega_s}\right)_{\omega_p} \frac{d\omega_s}{d\omega_p} + \frac{\partial \Delta k}{\partial \omega_p} + \frac{\partial \Delta k}{\partial T}\frac{dT}{d\omega_p} + \frac{\partial \Delta k}{\partial V}\frac{dV}{d\omega_p}, \tag{43a}$$

$$\frac{dm}{d\omega_p} = 0 = \left(\frac{\partial m}{\partial \omega_s}\right)_{\omega_p} \frac{d\omega_s}{d\omega_p} + \frac{\partial m}{\partial \omega_p} + \frac{\partial m}{\partial T}\frac{dT}{d\omega_p} + \frac{\partial m}{\partial V}\frac{dV}{d\omega_p}, \tag{43b}$$

and

$$\frac{dm_s}{d\omega_p} = 0 = \frac{\partial m_s}{\partial \omega_s}\frac{d\omega_s}{d\omega_p} + \frac{\partial m_s}{\partial \omega_p} + \frac{\partial m_s}{\partial T}\frac{dT}{d\omega_p} + \frac{\partial m_s}{\partial V}\frac{dV}{d\omega_p}. \tag{43c}$$

Again, only the first partial derivatives evaluated in the region of consideration are required. All of the partial derivatives are determined by material characteristics and DRO configuration resulting in three linear equations with three unknowns, which are solved by the usual methods. Continuous frequency coverage can be obtained with an incremental series of continuous frequency sweeps. A calculation of tuning in this manor is shown in Fig. 19. The extent of tuning for the individual sections will be limited by the range of parameter adjustment. For example, there may be a maximum voltage that can be applied or the extent of pump frequency tuning may be limited. A limit of ± 1000 V was used in the figure.

The calculations of two and three parameter tuning show that a DRO can be tuned to any frequency in its operating range [3] with reasonable adjustment of the tuning parameters. Continuous tuning is possible over spectral ranges of approximately the extent of a free spectral range. Complete coverage of larger spectral regions has to be done by scanning a series of smaller regions. The control of individual parameters, particularly temperature, require difficult tolerances. The control problem can be shifted to another more easily controlled parameter such as voltage with multiple parameter control of the DRO. The degree of correction required on the second parameter can then be used as an error signal to control the first parameter. Fortunately, the oscillating frequencies of the monolithic DRO exclusive of mode hops are relatively insensitive to voltage and temperature changes. If mode hops and cluster jumps are avoided, the frequency change of the DRO is approximately one half the frequency change of the pump.

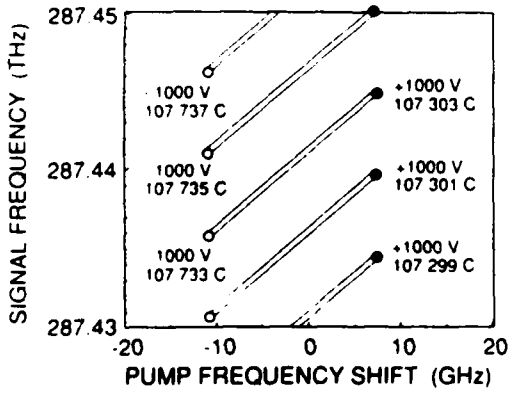

Fig. 19. Calculated tuning for varying voltage, pump frequency, and temperature simultaneously in a way to maintain $\Delta m = 0$, $\Delta m_s = 0$, and $\Delta k = 0$.

VI. Summary

The theory used to model tuning of the DRO is verified at many stages. The first order threshold approximation agrees well with more general calculations in the limit of low cavity loss. The theory accurately models observed cluster curves for two monolithic MgO:$LiNbO_3$ DROs. The modeling includes temperature dependent dispersions, thermal expansion, and the electro-optic and piezoelectric effects in the nonlinear material. The effect of DRO cavity finesse on the fine details of tuning gives a reasonable explanation of observed cluster jumps. Further substantiation of the model in the fine details of tuning is provided by the accurate prediction of the axial-mode-hop rate for tuning parameter change.

An understanding of DRO tuning is important for controlled stable operation. Continuous tuning rates were calculated for single and multiple parameter adjustment. Tolerances for stable operation were estimated. The results of these calculations will be useful for DRO design optimization. Multiple parameter tuning including pump frequency adjustment will be required to reach any arbitrary frequency in the OPO operating range. With appropriate control the DRO will be able to produce stable outputs with frequency stability as good as that available in the pump source.

The DRO should find application in the generation of stable fixed-frequency radiation. Incremental tuning in controlled mode hops or cluster jumps will have applications in spectroscopy and differential absorption LIDAR. Slow, high-resolution tuning will be possible over limited frequency ranges for spectroscopic applications.

The theory presented here could easily be extended to DRO configurations other than monolithic devices. Other degrees of freedom such as direct length control in a discrete component DRO would provide greater versatility in operation. Independent control of signal and idler cavity lengths would be useful in providing greatly extended ranges of continuous tuning. The development of stable DRO operation is now possible through the combination of improved nonlinear optical materials and frequency stable laser development such as diode-pumped solid-state lasers. Optical parametric oscillators again appear to be on the threshold of achieving a potential that was first understood twenty-five years ago.

Appendix A. Material properties of MgO:$LiNbO_3$ related to DRO tuning

A. Temperature Dependent Dispersion

Edwards and Lawrence [26] have developed temperature dependent dispersion equations for congruently grown $LiNbO_3$ based on data reported by D. F. Nelson and R. M. Mikulyak [27] and Smith, Riccius and Edwin.[28] They use dispersion equations of the form

$$n^2 = A_1 + \frac{A_2 + B_1 F}{\lambda^2 - (A_3 - B_2 F)^2} + B_3 F - A_4 \lambda^2 \quad , \tag{A1}$$

where

$$F = (T - T_0)(T + T_0 + 546) \quad , \tag{A2}$$

λ is wavelength in μm, and T is temperature in °C. Coefficients for congruent $LiNbO_3$ are as follows:

	Ordinary	Extraordinary
A_1	4.9048	4.5820
A_2	0.11775	0.09921
A_3	0.21802	0.21090
A_4	0.027153	0.021940
B_1	2.2314×10^{-8}	5.2716×10^{-8}
B_2	-2.9671×10^{-8}	-4.9143×10^{-8}
B_3	2.1429×10^{-8}	2.2971×10^{-7}
T_0	25	25

The material used in this work is not congruent $LiNbO_3$; rather, it is 5%MgO:$LiNbO_3$. There is little refractometric data available for the second material. To obtain an approximate set of equations for 5%MgO:$LiNbO_3$, the extraordinary index was adjusted by changing A_{1E} from 4.5820 to 4.55207. This has the effect of increasing the calculated noncritical phasematching temperature for 1064- to 532-nm second harmonic generation from −19.4 °C to 107.04 °C. The measured value for the MgO doped material is 107 °C.[29] This modification to the congruent dispersion equations accurately reproduces the observed tuning curve for a singly resonant OPO that was tuned between 0.85 and 1.48 μm by varying temperature between 122 and 190 °C.[30] This modification also predicts parametric florescence pumped at 514.5 and 488 nm when the crystal is tuned between 100 and 450 °C (Table A1).

TABLE A1. Comparison of measured and calculated values for parametric fluorescence in MgO:$LiNbO_3$.

514.5-nm pump wavelength			488-nm pump wavelength	
experimental temperature setting	observed fluorescence wavelength	calculated temperature	observed fluorescence wavelength	calculated temperature
148 °C	777.1 nm	146.70 °C	673.3 nm	143.17 °C
198	741.2	196.21	653.1	194.93
248	710.8	245.26	634.5	245.18
298	684.5	293.38	617.3	294.12
318	674.8	312.52		
348	660.8	341.50	601.3	341.86
398	639.2	389.31	585.7	390.38
448	619.2	436.60		

B. Electro-Optic Effect

Electro-optical, piezoelectric, and thermal expansion characterization of $LiNbO_3$ are reviewed by Räuber.[31] A somewhat more extensive tabulation of electro-optical coefficient measurements is given by Yariv and Yeh.[32] Their treatment of electro-optical effect is followed here. The index ellipsoid in a principle coordinate system is given by

$$\frac{x^2}{n_x^2} + \frac{y^2}{n_y^2} + \frac{z^2}{n_z^2} = 1 \, . \tag{A3}$$

When an electric field is applied, the electro-optical effect is described by the modified index ellipsoid

$$\left(\frac{1}{n_x^2} + r_{1k}E_k\right)x^2 + \left(\frac{1}{n_y^2} + r_{2k}E_k\right)y^2 + \left(\frac{1}{n_z^2} + r_{3k}E_k\right) + 2r_{4k}E_k yz + 2r_{5k}E_k xz + 2r_{6k}E_k xy = 1 \, , \tag{A4}$$

where $r_{ik}E_k = \sum_{k=1}^{3} r_{ik}E_k$, $i = 1, \cdots 6$.

For point group $3m$, to which $LiNbO_3$ belongs, the following relationships apply:

$n_x = n_y = n_o$, $n_z = n_e$, and

$$(r_{ik}) = \begin{bmatrix} 0 & -r_{22} & r_{13} \\ 0 & r_{22} & r_{13} \\ 0 & 0 & r_{33} \\ 0 & r_{51} & 0 \\ r_{51} & 0 & 0 \\ -r_{22} & 0 & 0 \end{bmatrix} . \tag{A5}$$

There are only four independent electro-optical coefficients. We consider only application of an electric field along the y axis ($E = E_y$) which further simplifies the index ellipsoid to

$$\left(\frac{1}{n_o^2} - r_{22}E_y\right)x^2 + \left(\frac{1}{n_o^2} + r_{22}E_y\right) + \frac{z^2}{n_e^2} + 2r_{51}E_y yz = 1 \, . \tag{A6}$$

The presence of the yz -cross term shows that the electro-optical effect results in a slight rotation of the principle axes. This is a small effect that accounts for less than 1% of the refractive index change even at the highest fields that are considered here; therefore, this rotation is ignored. For propagation in the x-direction we have

$$n_y = \left(\frac{1}{n_o^2} + r_{22} E_y \right)^{-1/2} \approx n_o - \frac{n_o^3 r_{22} E_y}{2} \qquad \text{(A7)}$$

and $n_z = n_e$.

Yariv and Yeh[32] list three values for r_{22} of $LiNbO_3$ measured with low-frequency applied electric field for different optical wavelengths:

$r_{22}(633\ \text{nm}) = 6.8 \times 10^{-12}$ m/V,

$r_{22}(1.15\ \mu\text{m}) = 5.4 \times 10^{-12}$ m/V, and

$r_{22}(3.39\ \mu\text{m}) = 3.1 \times 10^{-12}$ m/V.

These values suggest that we use $r_{22} = 5.5 \times 10^{-12}$ m/V near the wavelength 1.06 μm, the wavelength region at which our 5%MgO:$LiNbO_3$ DRO was operated. The value 6.8×10^{-12} m/V is from a measurement reported in 1967.[33] Note that this measurement was made even before the growth of congruent $LiNbO_3$ was reported.[34,35] We are working with a yet slightly different material 5%MgO:$LiNbO_3$, [24,25] and caution is required in applying these values.

C. Thermal Expansion

Thermal expansion measurement to second order in temperature for $LiNbO_3$ have been reported by Kim and Smith.[36] They express the fractional change of length with the quadratic function

$$\frac{\Delta l}{l} = \alpha (T - T_R) + \beta (T - T_R)^2 \ , \qquad \text{(A8)}$$

where l is length, Δl is change in length, T is temperature in °C, and $T_R = 25$ °C is a reference temperature. The DRO length is measured along the crystal x-axis. One set of coefficients,

$$\alpha_{11} = 1.54 \times 10^{-5}\ ^\circ\text{C}^{-1}$$

and $$\beta_{11} = 5.3 \times 10^{-9}\ ^\circ\text{C}^{-2},$$

apply to expansion in the xy -plane, and a second set to expansion in the z -direction. The spread in measurements reported by Kim and Smith suggest an accuracy of about 10% in the two coefficients.

D. Piezoelectric Effect

The direct piezoelectric effect describes the electric polarization P that results when a stress T is applied to a material by the relationship

$$P_i = d_{ijk} T_{jk} \ , \qquad \text{(A9)}$$

where d_{ijk} are the piezoelectric moduli. The converse piezoelectric effect describes the strain S that results when an electric field is applied to a piezoelectric material by the relationship [37]

$$S_{jk} = d_{ijk} E_i \ . \qquad \text{(A10)}$$

Summation of the repeated indices is implied in both of the above equations, and the moduli d_{ijk} are the same in both equations. The elongation of the DRO cavity is given by S_{11}, the x-component of change of a vector that lies in the x-direction. For these measurements electric field is applied in the y-direction E_y, and he modulus d_{211} is required for the calculation of strain. The symmetry of the stress tensor allows the use of a contracted subscript notation in which the modulus d_{211} is expressed as d_{21}. The $3m$ symmetry of the lithium niobate crystal reduces the number of independent moduli to 4. The reduced matrix of piezoelectric moduli for point group $3m$ is

$$(d_{jm}) = \begin{bmatrix} 0 & 0 & 0 & 0 & d_{15} & -2d_{22} \\ -d_{22} & d_{22} & 0 & d_{15} & 0 & 0 \\ d_{31} & d_{31} & d_{33} & 0 & 0 & 0 \end{bmatrix} . \qquad \text{(A11)}$$

Using the relationships between the moduli, it follows that strain is given by

$$S_{11} = d_{211} E_{11} = d_{21} E_{11} = -d_{22} E_y \ . \qquad \text{(A12)}$$

The value of piezoelectric modulus reported by Smith and Welsh,[38] $d_{22} = 2.08 \times 10^{-11}$ Coulombs per Newton, is used. They identify the $LiNbO_3$ which they used as commercially grown with a Curie point of 1165 °C. Sound propagation measurements were used to determine the piezoelectric moduli.

The derivatives used in Eqs, (20), (21), and (22) are expanded in Eqs. (18) and Table I. Evaluation for the experimental conditions described in Section IV using the material properties described above is given in Table II. Derivatives involving the electro-optic and piezoelectric effects are given with respect to voltage applied to the electrodes on the crystal surfaces perpendicular to the y-axis. An effective crystal thickness between the electrodes t is used, and these derivatives are given by

$$\frac{\partial \Delta k}{\partial V} = \left(\omega_s n_s^3 + \omega_i n_i^3 \right) \frac{r_{22}}{2 c t} \ , \qquad \text{(A13)}$$

$$\frac{\partial m}{\partial V} = -\frac{l}{\pi c t} \left\{ \left(n_s \omega_s + n_i \omega_i \right) d_{22} + \left(\omega_s n_s^3 + \omega_i n_i^3 \right) \frac{r_{22}}{2} \right\} \qquad \text{(A14)}$$

and

$$\frac{\partial m_s}{\partial V} = -\frac{l}{\pi c t} \left\{ n_s \omega_s d_{22} + \omega_s n_s^3 \frac{r_{22}}{2} \right\} \ . \qquad \text{(A15)}$$

Acknowledgements

This work was supported by the Office of Naval Research through contracts N00014-88-K-0576 and N00014-88-K-0701 and by NASA through grant NAGW-1760. C. D. Nabors and W. J. Kozlovsky are grateful to the Fannie and John Hertz Foundation for support of their graduate studies. The authors express their appreciation to Crystal Technology of Palo Alto, CA for supplying the MgO:$LiNbO_3$ material. Our appreciation is also extended to

many individuals who helped in a number of ways. Martin Fejer and Eric Gustafson provided many helpful discussions and suggestions in the course of this work. Dieter Jundt performed the parametric fluorescence measurements of phase matching for MgO:$LiNbO_3$. Stephen Yang operated the apparatus for the measurements shown in Fig. 10. The help of Janet Okagaki in formating and preparing the figures and the optical fabrication of the monolithic DROs by Joe Vrhel are especially appreciated.

* Present address, MIT Lincoln Laboratory, 244 Wood St., Lexington, MA 02173

† Present address, IBM Almaden Research Center, 650 Harry Rd., San Jose, CA 95120

References

1. J. A. Giordmaine and R. C. Miller, "Tunable coherent parametric oscillation in $LiNbO_3$ at optical frequencies," Phys. Rev. Lett. **14**, pp. 973-976 (1965).
2. J. A. Giordmaine and R. C. Miller, "Optical parametric oscillation in $LiNbO_3$," in *Physics of Quantum Electronics*, P. L. Kelley, B. Lax and P. E. Tannenwald, eds. (McGraw, New York, 1966), pp. 31-42.
3. G. D. Boyd and A. Ashkin, "Theory of parametric oscillator threshold with single-mode optical masers and observation of amplification in $LiNbO_3$," Phys. Rev. **146**, pp. 187-198 (1966).
4. R. G. Smith, "A study of factors affecting the performance of a continuously pumped doubly resonant optical parametric oscillator," IEEE J. Quantum Electron. **QE-9**, pp.530-540 (1973).
5. S. E. Harris, "Tunable optical parametric oscillators," Proc. IEEE **57**, pp. 2096-2113 (1969)
6. R. G. Smith, "Optical parametric oscillators," in *Advances in Lasers*, vol. 4, A. K. Levine and A. J. DeMaria, eds. (Dekker, New York, 1976), pp. 189-307.
7. R. L. Byer, "Parametric oscillators and nonlinear materials," in *Nonlinear Optics*, P. G. Harper and B. S. Wherrett, eds. (Academic, San Francisco, 1977), pp. 47-159;
   R. L. Byer, "Optical parametric oscillators," in *Quantum Electronics: A Treatise*, vol. 1, part B, H. Rabin and C. L. Tang, eds. (Academic, New York, 1975), pp. 587-702.
8. for example see A. Yariv, *Quantum Electronics*, 3rd. ed. (Wiley, New York, 1989), chapter 17, or Y. R. Shen, *The Principles of Nonlinear Optics* (Wiley, New York, 1984), chapter 9.
9. R. Graham and H. Haken, "The Quantum-Fluctuations of the Optical Parametric Oscillator. I," Z. Phys. **210**, pp. 276-302, (1968).
10. C. D. Nabors, S. T. Yang, T. Day, and R. L. Byer, "Coherence properties of a doubly-resonant monolithic optical parametric oscillator," to be published in J. Opt. Soc. Am. B.
11. J. E. Bjorkholm, "Analysis of the doubly resonant optical parametric oscillator without power-dependent reflections," IEEE J. Quantum Electron. **QE-5**, pp.293-295, (1969).
12. J. Falk, "Instabilities in the doubly resonant parametric oscillator: a theoretical analysis," IEEE J. Quantum Electron. **QE-7**, pp. 230-235 (1971).
13. J. A. Armstrong, N. Bloembergen, J. Ducuing, and S. Pershan, "Interactions between light waves in a nonlinear dielectric," Phys. Rev. **127**, pp. 1918-1939 (1962).
14. M. Born and E. Wolf, *Principles of Optics, 3rd ed.* (Pergamon, Oxford, 1965), pp.323-329.
15. A. Siegman, *Lasers* (University Science Books, Mill Valley, CA, 1986), pp. 435-436.
16. G. D. Boyd and D. A. Kleinman, "Parametric interaction of focused Gaussian light beams," J. Appl. Phys. **39**, pp. 3597-3639 (1968).
17. W. J. Kozlovsky, C. D. Nabors, R. C. Eckardt and R. L Byer, "Monolithic MgO:LiNbO3 doubly resonant optical parametric oscillator pumped by a frequency-doubled diode-laser-pumped Nd:YAG laser," Opt. Lett. **14**, pp. 66-68 (Jan. 1, 1989).
18. C. D. Nabors, R. C. Eckardt, W. J. Kozlovsky, and R. L. Byer, "Efficient, single-axial-mode operation of a monolithic MgO:$LiNbO_3$ optical parametric oscillator," Opt. Lett. **14**, 1134-1136 (Oct. 15, 1989).
19. T. Kane and R. L. Byer, "Monolithic, unidirectional, single-mode Nd:YAG ring laser," Opt. Lett. **10**, pp. 65-67 (Feb. 1985).
20. A. Nilsson, E. Gustafson, and R. L. Byer, "Eigenpolarization theory of monolithic nonplanar ring oscillators," IEEE J. Quantum Electron. **25**, pp. 767-790, (April 1989).
21. W. J. Kozlovsky, C. D. Nabors and R. L. Byer, "Efficient second harmonic generation of a diode-laser-pumped cw Nd:YAG laser using monolithic MgO:$LiNbO_3$ external resonant cavities," IEEE J. Quantum Electron. **24**, pp. 913-919 (June, 1988).
22. B.-K. Zhou, T. J. Kane, G. J. Dixon and R. L. Byer, "Efficient, frequency-stable laser-diode-pumped Nd:YAG lasers," Opt. Lett. **10**, pp. 62-64 (Feb. 1985).
23. T. J. Kane, A. C. Nilsson and R. L. Byer, "Frequency stability and offset locking of a laser-diode-pumped Nd;YAG monolithic nonplanar ring oscillator", Opt. Lett. **12**, pp. 175-177 (March 1987).
24. Gi-Guo Zhong, Lin Jian and Zhong-Kang Wu, 11th International Quantum Electronics Conference, (IEEE, New York, Cat. No. 80 CH 1561-0, 1980), p. 631.
25. D. A. Bryan, R. R. Rice, R. Gerson, H. E. Tomaschke, K. L. Sweeney and L. E. Halliburton, "Magnesium-doped lithium niobate for higher optical power applications," Opt. Eng. **24**, pp. 138-143 (1985).
26. G. J. Edwards and M. Lawrence, "A temperature-dependent dispersion equation for congruently grown lithium niobate," Opt. Quantum Electron. **16**, pp. 373-375 (1984).
27. D. F. Nelson and R. M. Mikulyak, "Refractive indices of congruently melting lithium niobate," J. Appl. Phys. **45**, pp. 3688-3689, (1974).
28. D. S. Smith, H, D. Riccius and R. P. Edwin, "Refractive indices of lithium niobate," Opt. Commun. **17**, pp. 332-335 (1976); errata, **20**, p. 188 (1977).
29. J. L. Nightingale, W. J. Silva, G. E. Reade, A Rybicki, W. J. Kozlovsky and R. L. Byer, "Fifty percent conversion efficiency second harmonic generation in magnesium oxide doped lithium niobate," Proc. SPIE **681**, *Lasers and Nonlinear Optical Materials*, pp.20-24 (1986).
30. W. J. Kozlovsky, E. K. Gustafson, R. C. Eckardt and R. L. Byer, "OPO performance with a long pulse length, single frequency Nd:YAG laser pump," Proc. SPIE **912**, *Pulsed Single-Frequency Lasers: Technology and Applications*, pp. 50-53 (June, 1988).
31. A. Räuber, "Chemistry and Physics of Lithium Niobate," in *Current Topics in Materials Science*," vol. 1, E. Kaldis, ed. (North-Holland, Amsterdam, 1978), pp. 481-601.
32. A. Yariv and P. Yeh, *Optical Waves in Crystals*, (Wiley, New York, 1984), ch. 7.
33. J. D. Zook, D. Chen, and G. N. Otto, "Temperature dependence and model of the electro-optic effect in $LiNbO_3$," Appl. Phys. Lett. **11**, pp. 159-161 (1967).
34. R. L. Byer, J. F. Young, and R. S. Feigelson, "Growth of high-quality $LiNbO_3$ crystals from the congruent melt," J. Appl. Phys. **41**, pp. 2320 (1970).

35. F. R. Nash, G. D. Boyd, M. Sargent III and P. M. Bridenbaugh, "Effect of optical inhomogeneities on phase matching in nonlinear crystals," J. Appl. Phys. 41, pp. 2564-2575 (1970).
36. Y. S. Kim and R. T. Smith, "Thermal expansion of lithium tantalate and lithium niobate single crystals," J. Appl. Phys. 40, pp. 4637-4641 (1969).
37. J. F. Nye, *Physical Properties of Crystals* (Oxford, London, 1985), ch.7.
38. R. T. Smith and F. S. Welsh, "Temperature dependence of the elastic, piezoelectric, and dielectric constants of lithium tantalate and lithium niobate," J. Appl. Phys. 42, pp. 2219-2230 (1971).